Search for Supersymmetry Production Signals in Events with Two Leptons with the Same Sign using the CMS Detector

Ph.D. Thesis in Physics.

DEPARTMENT OF PHYSICS
UNIVERSIDAD DE LOS ANDES, BOGOTÁ, COLOMBIA.

Presented by:

Alberto Andrés Ocampo Rios.[1]

Advisor:
Prof. Bernardo Gomez Moreno[2].
Departamento de Física
Universidad de los Andes Bogotá Colombia.

co-Advisor:
Dr. Marcello Maggi[3].
INFN Bari, Italy.

Bogotá, Junio 1, 2011

[1] aocampor@cern.ch
[2] bgomez@uniandes.edu.co
[3] marcello.maggi@cern.ch

Contents

List of Figures

List of Tables

Acknowledgments

This thesis would not have been possible without the help, economic support, and intellectual contributions done by many people. I would like to specially thank Colciencias, the HELEN program, and the physics department of *Universidad de los Andes* for their economic support during all the work. I would also like to thank professors Juan C. Sanabria, Carlos Avila, and Bernardo Gomez for their constant help during the entire duration of the PhD program. Special thanks are also given for all the intellectual contributions done by Dr. Marcello Maggi, and Dr. Michelle Pioppi., and in general a lot of people working within the CMS collaboration that helped me to developed as a scientist. This document is not only my work, it is actually the work of a lot of people during many years.

Chapter 1

Introduction

CERN is the home of the Large Hadron Collider or LHC. The LHC is the largest proton-proton accelerator constructed up to date, with the aim to search for new physics. On March of 2010 the LHC started to collide the first protons, this date was the starting point for the first physics run of the accelerator. During 2010 the data obtained from the collisions was collected at a centre of mass energy of 7 TeV. This energy is the highest obtained by a man made accelerator so far.
The data collected by the LHC and its experiments: ATLAS, CMS, LHCb, and ALICE; is expected to give insights about fundamental questions related to the Standard Model of particles (SM). The three main scientific goals of the LHC program are: to understand the electroweak symmetry breaking mechanism present in the SM, through the search for the Higgs Boson; to understand the quark-gluon plasma face of matter; and to search for any physics beyond the SM, in particular for supersymmetric matter.
Supersymmetry (SUSY) is considered the most plausible extension of the SM, since it is a generalisation of the fundamental space time symmetry. It establishes a symmetry between fermions and bosons duplicating the spectrum of known particles, since for each fermion of the SM model there will be a supersymmetric boson partner (sboson), and for each boson of the SM there will be a supersymmetric fermion partner (sfermion). The SUSY extension of the SM solves many problems at the Quantum Field level when extending the theory to the very high energy scales, like the Grand Unification Theory scale (GUT, 10^{16} GeV). This is the main reason for which SUSY continues to be searched for, in spite of 30 years with no experimental evidences.
In this thesis the data collected with the Compact Muon Solenoid experi-

ment (CMS) was used to search for signals of production of SUSY matter at energies below 7 TeV, and above the exclusion limits set by LEP and Tevatron experiments.
Since SUSY models have a large number of unknown parameters, the initial searches were guided by parametrisations based on mSUGRA that allowed to reduce drastically the space of unknown parameters. For this purpose the CMS and ATLAS collaborations have chosen a set of theoretical benchmark points to be used in the preparation of the initial analyses. Due to the reduced energy and statistics of the data used in this first search only the low-mass part of the SUSY spectrum was scanned.
The main problem in the early searches for SUSY signals is how to distinguish them from SM signals. SUSY is supposed to have several phenomenological signals that can statistically discriminate it from SM processes. The topology of these signatures depends on the events selected for a specific search. In this thesis only events with two leptons carrying the same sign, Missing Transverse Energy, and Several Jets; were used to search for a significant statistical deviation from the SM yield, as an evidence of physics beyond SM and perhaps SUSY. This channel was used due to its clean signal with a very low level of SM background according to model predictions.
As it is expected from the theory, events with two leptons of the same sign are expected to be produced with higher cross sections in SUSY models than in the SM. If in addition to the lepton pair one requires also a big amount of Missing Transverse Energy or MET, and a high deposit of energy in the calorimeters, very few events resulting from SM processes can be accepted, therefore any significant signal could be associated with new physics consistent with SUSY. The distinction between SM signals and any new signals is a very delicate experimental issue, and will be the main focus of this work.
In this document, after this brief introduction a chapter describing theoretical basic aspects of SUSY is presented. The phenomenological aspects associated with SUSY and in particular with the Minimal Standard Supersymmetric Model (MSSM) are discussed, as well as some implications of the different SUSY breaking mechanisms.
Since the initial CMS searches are guided by mSUGRA, a section describing the main features of this model is included. Once all the theory has been introduced, a discussion of the basic experimental signals that a detector like CMS would observe are described in detail. The chapter finishes with a presentation of the previous searches performed at the experiments at LEP and Tevatron.
In the third chapter a description of the LHC and the CMS detector is presented, making an emphasis on the detector variables that are relevant for

SUSY searches. This chapter is followed by a complementary chapter that describes the CMS reconstruction.
Chapter five gives a description of how initial SUSY searches are being done in the CMS experiment. It describes the treatment given to possible SUSY signature within the CMS analysis groups.
The sixth chapter describes the same-sign double lepton analysis. In this chapter descriptions about: the backgrounds, data driven methods to estimate the backgrounds, event selection, and a small study of the SM background; can be found.
Chapter seven presents the analysis done with the 2010 data, making special emphasis on the Data Driven technics developed to determine the SM signal at this new energy range, so that any deviation from it can be identified in the most impartial way. In the last chapter the results of the searches are presented, together with the conclusions. Several appendices were added to describe the work done during the PhD and to complement the analysis when needed.

Chapter 2

Supersymmetry

The subject of the present work is the search for signals of Supersymmetry (SUSY) in nature. Until now no experimental evidence of any phenomena associated with SUSY has been discovered, however there are several theoretical reasons related with particle physics and with field theory that make this extension of the Standard Model (SM) very plausible and worth exploring. In this chapter the general theoretical aspects of SUSY are going to be described.
The SUSY extension of the SM results in a large set of free parameters whose values are not known, resulting in a large space of possibilities for SUSY models. Therefore to perform initial experimental searches for SUSY signals, particular models and parameter space configurations have been consider by the CMS experiment. The choice of these models and parameter configurations have been done in order to provide a diverse set of final state signals in order to prepare software that is as flexible as possible for possible discoveries.
In this chapter a description of some theoretical scenarios used by CMS will be presented, and some of the phenomenology resulting from them will be discussed. Finally a summary of the previous searches done by other experiments is going to be presented.

2.1 What is supersymmetry?

The Standard Model of particles is composed by 3 generations of fermions and a set of bosons that mediate the interactions between particles. The fermions are divided in two families called quarks and leptons, all of them with spin 1/2.

The mediating particles are vector bosons with spin 1, these particles are γ, $W^{\pm}$, Z, and 8 gluons. Besides of the fermions and the vector bosons there is an extra scalar field, the Higgs (still not discovered), that provides mass to the other particles through the interaction of its vacuum expectation value with the other fields.
SUSY is a symmetry that can be implemented into field theories. It was discovered at the beginning of 1970's as a symmetry transformation that involves and mixes fermionic and bosonic degrees of freedom, putting them on the same footing[1]. It also constitutes an extension of the Poincarè's space-time symmetry.
SUSY field theories can be written in an elegant way by including anti-commutative variables, Grassman variables, extending the space-time, that has four commutative degrees of freedom, into a "Superspace" that involves four extra anti-commutative variables. Within this formalism fermion and boson fields become part of single "Superfields" that have the same number of fermionic and bosonic degrees of freedom.
The fermions and bosons within a superfield or "supermutiplet" have the same mass term, therefore, a pure SUSY theory predicts that each particle has a "Superpartner" that differs in spin by 1/2, but that otherwise has the same mass, in contradiction with particle physics phenomenology.
By the end of 1970's important progress had been done in this field, and it had been proven that SUSY-breaking mechanisms could be implemented in such a way that most of the good field-theory features were preserved while mass gaps between the fermions and bosons belonging to a superfield would be generated.
Under SUSY-breaking, the particle spectrum would be divided into light particles and heavy superparticles, allowing to construct SUSY extensions of the SM. In this extensions all the SM states correspond to the light sector of the mass spectrum, and a new set of heavy-superpartner states is predicted[1].

SUSY is a global symmetry transformation written in terms of transformation parameters that are constants. If those parameters are given an arbitrary dependence on the space-time variables, SUSY is promoted into a local symmetry. To achieve this, a new gauge superfield has to be introduced. The spin content of the gauge superfield is (3/2,2). The presence of a spin 2 boson field brings gravity into the theory as a SUSY-gauge field, at the prize of including a "gravitino" with spin 3/2. This local version of SUSY is called "Supergravity" or SUGRA[1].

The most economical extension of the SM into a SUSY theory is called the Minimal Standard Supersymmetric Model, or MSSM. Since there are

not any empirical evidences of SUSY until now, the initial experimental searches that are being performed in experiments like CMS, are guided by the predictions and constrains based on the MSSM model. In order to reduce the parameter space, the searches have resorted to GUT schemes, like for example SUGRA-GUTs[1].

2.2 Why to look for SUSY?

There are several reason that motivate the search for experimental evidences of SUSY. Some of the most important are:

- SUSY provides a possible solution to the Hierarchy problem.
- The theory may give a candidate for cold dark matter (if R parity is conserved).
- SUSY allows the existence of a light Higgs boson in agreement with electroweak constraints.
- SUSY allows Gauge couplings to be unified.

The way in which SUSY addresses the previous problems will be described in the following subsections.

2.2.1 The Hierarchy Problem

The fermion loop contribution to the self-energy correction for the mass of the Higgs boson(scalar field) is of the form:

$$\pi^f_{\phi\phi} = -2N(f)\lambda_f^2 \int \frac{d^4k}{(2\pi)^4} \left[\frac{1}{k^2 - m_f^2} + \frac{2m_f^2}{(k^2 - m_f^2)^2} \right]. \qquad (2.1)$$

In this equation the first term is quadratically divergent. If one takes k up to the planck mass ($M_{Pl} \approx 10^{-19}$ GeV plank mass), the self energy corrections would be 30 orders of magnitude larger than the expected Higgs mass ($m_\phi \leq 1$ TeV).
In the case of the fermion fields, this divergence is logarithmic, so that even at the plank scale the correction is of the same order of magnitude of the mass of the state.
The scalar field quadratic divergence when renormalised, leaves a finite correction of the order of $N(f)m_f^2\lambda_f^2/8\pi$ which would be small even for the SM top quark contribution.

It is plausible that at some very high energy scale more fermions could be found, and the corrections due to those particles would need to be fine-tuned in order to leave unaffected the Higgs mass value.
This problem is known as the Hierarchy problem of the SM, and becomes very important when extending the theory to higher energy scales.
In SUSY theories this problem is solved since the Higgs mass self energy corrections has additional contributions coming from sfermions partners (bosons). The new contributions cancel exactly the quadratic divergences, providing therefore a solution to the Hierarchy problem, and predicting a Higgs mass range in agreement with electroweak constrains[2], that is another of the standing problems of the SM.

2.2.2 Dark Matter Candidate

The dark matter problem is another reason to search for experimental evidence of SUSY, since it may provide a candidate. In SUSY theories a new parity called R-parity is included in order to extend to this realm barion and lepton number conservation, avoiding undesirable scenarios like proton decay. This parity is defined as

$$R = (-1)^{3B+L+2S}, \tag{2.2}$$

where B is the baryon number, L the lepton number, and S the spin of the particle being considered. R is a multiplicative quantum number that separates SM particles from SUSY partners; it does it in such a way that all the standard model known particles have R-parity equal to 1 and all the SUSY companions have R-parity equal to -1.
If R parity is conserved, SUSY particles would be produced in pairs and the decay of each of them should include another SUSY particle. This implies that the Lightest SUSY Particle (LSP) would be stable, since it has no other SUSY particles to decay into. In most SUSY parametrisations the LSP is neutral and weakly interacting like for example the neutralino $\tilde{\chi}_1^0$.
Cold dark matter should be neutral massive and at most weakly interacting, therefore the neutralinos become a good candidate since they are massive and stable and should have been produced copiously in the early stages of the universe. Charged candidates for LSP are not favoured by cosmological constraints, and therefore the LSP should be neutral. In the cases in which the R-Parity is non conserved, SUSY does not longer provides a dark matter candidate.

2.2.3 Gauge Couplings

Once SUSY particles are considered, the re-normalisations of the gauge couplings for the fundamental interactions within the framework of Grand Unification Theories (GUT) are affected. This happens in such a way that the extrapolation of this new couplings to higher energies brings them together to a common point if SUSY is included(see figure 2.1).
All characteristics discussed in this sections are included in the Minimal Supersymmetrical Standard Model or MSSM, the following section presents a description of this model.

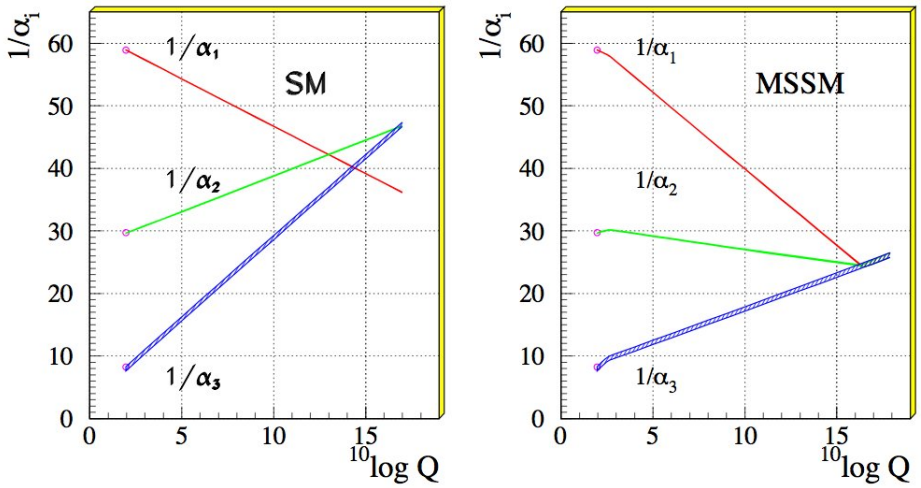

Figure 2.1: The left plot, shows the extrapolation of the SM coupling constants without considering SUSY. The right plot, shows the same extrapolation after including the Minimal Supersymmetrical Standard Model (MSSM)[3].

2.3 Minimal Supersymmetrical Standard Model

In SUSY models the space time is extended into a "Super-space" by including anti-conmutative grassman variables. The minimum extension involves four grassmanian degrees of freedom and is often called $N = 1$ SUSY[1]. If this model is tuned to reproduce the SM phenomenology, via an appropriate SUSY-breaking mechanism it results in the simplest possible SUSY extension of the SM called Minimal Supersymmetrical Standard Model or MSSM.

Table 2.1: Standard Model and Minimal Supersymmetric model spectrums.

SM	**MSSM**
leptons $\rightarrow l^{\pm}$	s-leptons $\rightarrow \tilde{l}^{\pm}$
neutrinos $\rightarrow \nu_l$	s-neutrinos $\rightarrow \tilde{\nu}_l$
quark $\rightarrow q$	s-quark $\rightarrow \tilde{q}$
Charged vectorial boson $\rightarrow W^{\pm}$	Winos $\rightarrow \tilde{W}^{\pm}$
Neutral vectorial boson $\rightarrow \gamma, Z^0$	fotino, Zino $\rightarrow \tilde{\gamma}, \tilde{Z}$
gluons $\rightarrow g$	gluinos $\rightarrow \tilde{g}$
Higgs $\rightarrow H$	Higgs doublet $\rightarrow h_1, h_2$

This model includes the entire SM, as it is known today, and in addition it predicts a whole spectrum of new SUSY partners. The particle spectrum of the SM and MSSM is shown on table 2.1.
The implementation of the SM electroweak breaking in the SUSY extension results on a mixing of the gaugino sector (SUSY partners of the SM gauge bosons), so that the actual observable states are four charged fermions or charginos, four neutral fermions or neutralinos, and five higgses, as shown in table 2.2.

Even though the MSSM is able to reproduce the phenomenology of the SM, there are no theoretical predictions for the actual values of parameters such as the Higgs masses, the SUSY-companion masses, and coupling constants; resulting in more than 100 unknowns that can only be fixed by experimental results.
Constraints in the SM electroweak region give hints about the Higgs mass value, however those clues are not enough to make a measurable prediction. Calculations done including SUSY allow physicist to impose constraints on the upper mass limit of the lightest MSSM neutral Higgs boson. As it is known this boson should have a mass in the electroweak scale so that naturalness of this parameter holds[2].
The lack of theoretical predictions for the masses of the MSSM particles, is due to the huge number of unknown parameters and depends on the SUSY breaking mechanism used. Therefore the way in which SUSY is broken has important phenomenological consequences.

Table 2.2: MSSM Electroweak mixing.

Winos $\rightarrow \tilde{W}^{\pm}$ fotino, Zino $\rightarrow \tilde{\gamma}\tilde{Z}$ gluinos $\rightarrow \tilde{g}$ higgs doublets $\rightarrow h_1, h_2$	Mixes to $\rightarrow$	Charginos $\rightarrow$	light $\rightarrow \tilde{\chi}_1^{\pm}$ heavy $\rightarrow \tilde{\chi}_2^{\pm}$
		Neutralinos $\rightarrow$	$\tilde{\chi}_1^0 \leftarrow$ lightest $\tilde{\chi}_2^0$ $\tilde{\chi}_3^0$ $\tilde{\chi}_4^0 \leftarrow$ heavier
		Higgses $\rightarrow$	h H A $H^{\pm}$

2.4 SUSY Breaking

SUSY can be broken explicitly by including symmetry-breaking terms directly in the lagrangian, or it could be spontaneously broken by the presence of a non-SUSY vacuum state. The first scenario is called "hard SUSY breaking" and the second one is called "soft SUSY breaking". There are several important reasons related with field theory to favour the soft breaking mechanisms[4].
In global SUSY models (without gravity), spontaneous SUSY breaking results in a positive vacuum energy, which makes the breaking mechanism not fully satisfactory, since it would require the inclusion of new fields in order to cancel triangle anomalies and etc.
In local SUSY, or SUGRA, the symmetry can be broken in a similar way as in the SM. This is some times called "super-Higgs" effect. Similarly to the Higgs case, in this scenario, the two polarization degrees of freedom associated with the massless Goldstone fermion (Goldstino) that mediates the breaking, are absorbed by the gravitino, giving it four polarization states, and therefore making it massive, as opposed to its SUSY partner the graviton. The resulting mass gap breaks SUSY.
At this level, the MSSM is considered as a "low energy" approximation to an underlying fundamental theory in which SUSY is spontaneously broken by some unknown dynamics. The source of this breaking dynamics comes from a "hidden sector". This hidden sector couples very weakly and indirectly

to the "observable sector", composed by the SM particles and their SUSY partners. Since at the moment there is no way to know anything about the nature of the hidden sector, what is relevant is the "agent" that couples to the observable sector, mediating the SUSY breaking.
Since the gravitational interaction couples universally to energy, it becomes a candidate to couple with the hidden sector, mediating the SUSY breaking, in what is called Gravity-Mediated SUSY Breaking. Another possibility is that SM gauge interactions couple with the hidden sector to break SUSY, in what is known as Gauge-Mediated SUSY Breaking (GMSB)[5].

2.5 Supergravity Grand Unification, SUGRA-GUTs

The gauge symmetry group of the SM, $SU(3)_C \times SU(2)_L \times U(1)_Y$, can be included into more complex symmetry groups, like for example the $SU(4)_C \times SU(2)_L \times SU(2)_R$ group in the Pati-Salam model, or the $SU(5)$ group in the Georgi-Glashow model, or the $SO(10)$ group. Through an adequate symmetry breaking one can get back to the SM symmetry group, making the SM a low-energy effective theory. One of the goals of this theories, called Grand Unified Theories (GUTs), is to unify the fundamental interactions at a higher energy scale.
The Supersymmetric Grand Unified Theories (SUSY-GUTs) are an extension of the GUTs idea, in which the effective low-energy theory is SUSY instead of the SM. Since SUSY breaking can only be implemented in a consistent fashion within the framework of Supergravity, the most well-behaved version of GUT models is SUGRA-GUTs. In this model, grand unification of interactions is achieved at an energy scale of 10^{16} GeV (the GUTs scale), something that would not happen in SM-GUTs theories, making SUSY a necessary element in the Grand Unification ideal.
From the experimental point of view, SUGRA-GUTs allows a drastic reduction of the unknown parameter space, since at the GUTs scale all free parameters of the theory unify into five[2]. These are the mSUGRA-GUTs parameters:

- m_0 : universal scalar mass.
- $m_{1/2}$: unified gaugino mass.

- A_0 : universal tri-linear scalar coupling.

- $\tan\beta$: ratio of vacuum expectation values of the two Higgs doublets.

- sign(μ) : sign of the Higgs mass parameter.

If a point is given in the mSUGRA-GUTs parameter space, the values of all MSSM parameters at the TeV scale can be calculated; parameters like: masses, coupling factors, decay widths, etc.
In order to prepare software analysis tools and Monte Carlo simulated data for the early searches for SUSY, the CMS experiment has defined a set of benchmark points. These benchmark points are presented in table 2.3. They have been chosen to provide a wide variety of phenomenological scenarios, so that the initial inclusive searches will be as flexible as possible when it comes to the expected final-state signals. Similarly, in a GMSB scenario, a set of unified parameters was also defined. The benchmarks used in CMS for these type of SUSY are described in table 2.4.

2.6 SUSY Production at Colliders

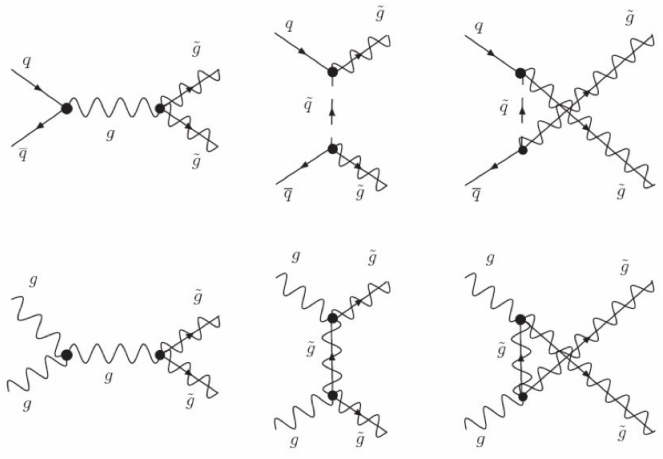

Figure 2.2: Feynman first order diagrams for the gluino gluino production at hadron colliders.

At the Tevatron and at the LHC, SUSY matter could be produced mostly

Table 2.3: Benchmarks for mSUGRA.

Benchmarck	m_0	$m_{1/2}$	A_0	$\tan\beta$	sign(μ)
LM0	200	160	-400	10	+
LM1	60	250	0	10	+
LM2	185	350	0	35	+
LM2 mhf 360	185	360	0	35	+
LM3	330	240	0	20	+
LM4	210	285	0	10	+
LM5	230	360	0	10	+
LM6	85	400	0	10	+
LM7	3000	230	0	10	+
LM8	500	300	-300	10	+
LM9	1450	175	0	50	+
LM9p	1450	230	0	10	+
LM9 top mass 175	1450	175	0	50	+
LM10	3000	500	0	10	+
LM11	250	325	0	35	+
LM12	2544.58	246.564	-865.752	47.5897	+
LM13	270	218	-553	40	+
HM1	180	850	0	10	+
HM2	350	800	0	35	+
HM3	700	800	0	10	+
HM4	1350	600	0	10	+

Table 2.4: Benchmarks for GMSB

Benchmarck	λ	m_{mess}	N_5	C_{Grav}	$\tan\beta$	sign(μ)
GM1b	80	160	1	1	15	+
GM1c	100	200	1	1	15	+
GM1d	120	240	1	1	15	+
GM1b	140	280	1	1	15	+
GM1b	160	320	1	1	15	+
GM1b	180	360	1	1	15	+

in the form of squarks and gluinos. This is because at hadron colliders strong interactions dominate the production cross sections.

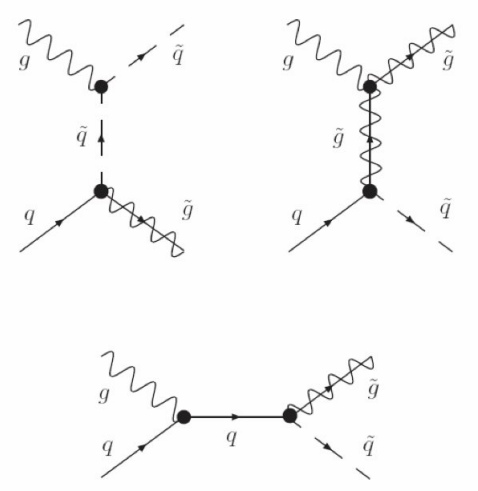

Figure 2.3: Feynman first order diagrams for the gluino s-quark production at hadron colliders.

In a proton-proton collision at the LHC energies, s-particles are produced as a result of parton-parton interactions. Since the partons carry a fraction of the proton momentum, the effective energy available for the production of new particles will be less than the total energy available in the CM frame. Also, due to the same reasons the parton-parton CM frame is not known. In figures 2.2, 2.3, and 2.4 the processes that lead to the production of s-quarks and gluinos are shown. These particles could decay into different SUSY particles, but the decay modes depend on the mass difference between them. The table 2.5 shows the decays for both options: the case in which the gluinos have a bigger mass, and the opposite case.
Neutralinos and Charginos are produced mostly as the decay of heavier particles (see table 2.5). Their decay modes characterize the SUSY final state topologies, this modes are depicted in figures 2.5, and 2.6.
In summary, the most likely experimental signals resulting from the proton-proton collisions at the LHC will be those resulting from the decays of s-quarks and gluinos. In the case of R-parity conserving SUSY two LSP's will be part of the final state, typically $\tilde{\chi}_1^0$, as well as other products of the decay chains like high P_T partons or quarks, and leptons.

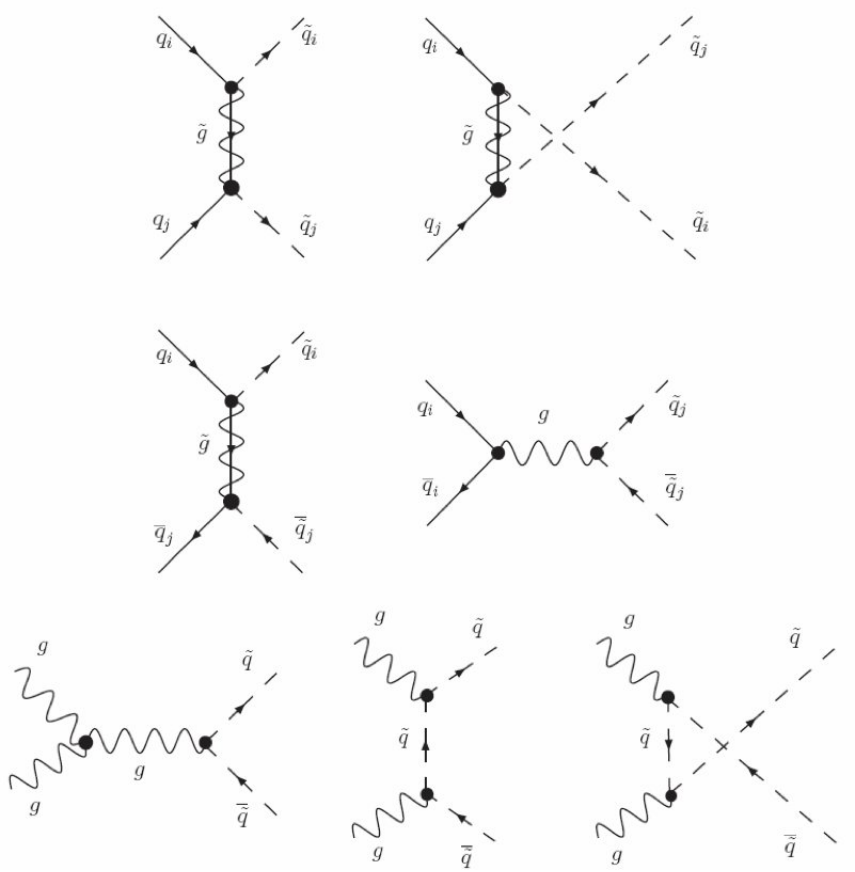

Figure 2.4: Feynman first order diagrams for the s-quark s-quark production at hadron colliders.

Table 2.5: Squarks and Gluino decays

S-Particles	Decays
gluinos and squarks:	
If $m_{\tilde{q}} < M_{\tilde{g}}$	
$\tilde{g}$	$\rightarrow q + \tilde{q}$
$\tilde{q}$	$\rightarrow q + \tilde{\chi}_l^0$ $\rightarrow q' + \tilde{\chi}_k^{\pm}$ $\rightarrow q + \bar{b}\tilde{b} + q\bar{b}b$
If $m_{\tilde{q}} > M_{\tilde{g}}$	
$\tilde{g}$	$\rightarrow q + \bar{q} + \tilde{\chi}_l^0$ $\rightarrow q + \bar{q}' + \tilde{\chi}_k^{\pm}$ $\rightarrow \bar{t}\tilde{t} + \bar{t}t$ $\rightarrow \bar{b}\tilde{b} + \bar{b}b$
$\tilde{q}$	$\rightarrow q + \bar{g}$ $\rightarrow q + \tilde{\chi}_l^0$ $\rightarrow q' + \tilde{\chi}_k^{\pm}$

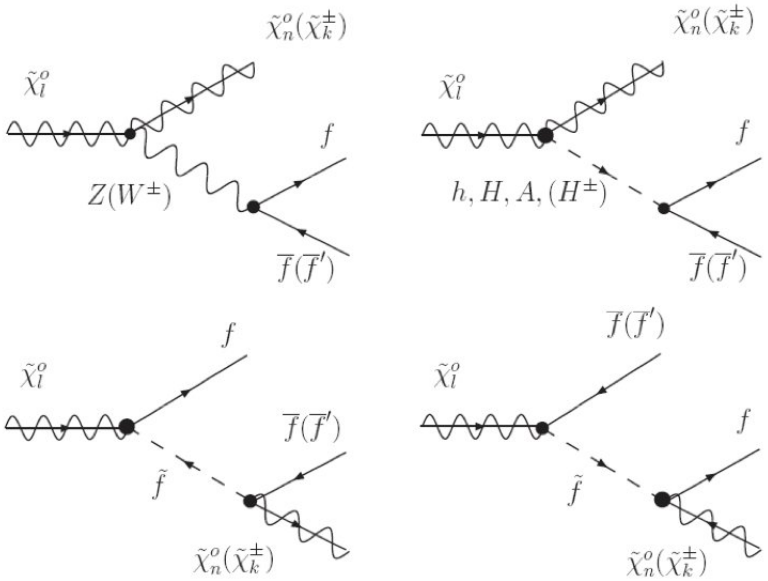

Figure 2.5: Feynman first order diagrams for the Neutralino decays.

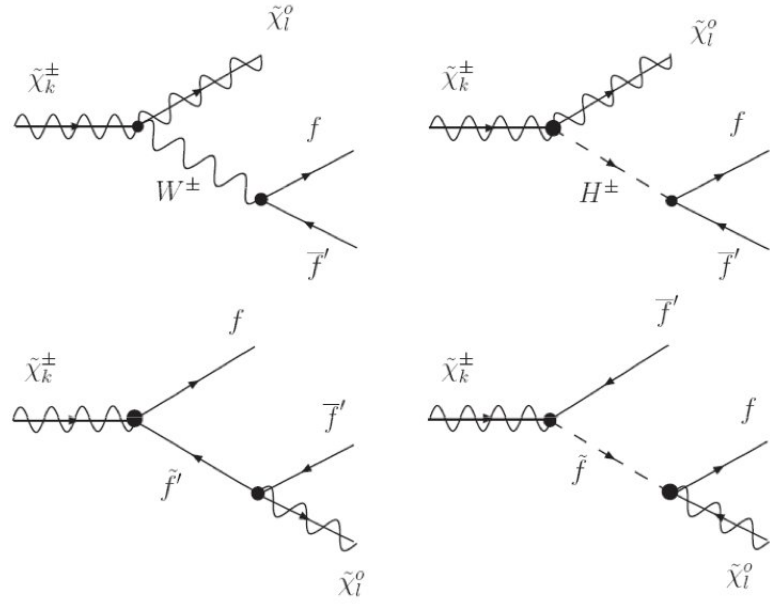

Figure 2.6: Feynman first order diagrams for the Chargino decays.

2.7 Experimental Signals of SUSY

Processes like those shown in the previous section characterize the final state topologies in SUSY searches at the LHC. These topologies are quite complex by themselves and they are convoluted with similar signals produced by SM processes, therefore a good knowledge of these processes is mandatory to successfully distinguish SUSY from SM signals (that constitute the "background").
Even though a good reduction of the SM background can be done by applying intelligent cuts, there will always be an irreducible remanent that can be distinguished only through statistical distributions.
As it was described previously, SUSY is a broken symmetry. Therefore due to the mass gap expected between SM particles and their SUSY companions, all SUSY particles are expected to be massive (hundreds of GeV/c^2), and short lived. This implies that experimental searches should look initially for events with high amounts of energy deposited in the calorimeters.
The SUSY models can be grouped in two kinds: R-Parity conserving, or non R-Parity conserving. The difference between them result in significant differences in the experimental signatures. In the case in which R-Parity is conserved, one massive neutral particle usually called the Lightest SUSY Particle (LSP), is expected to be stable. This LSP should be neutral, otherwise its existence should have been detected due to its electromagnetic interactions. Cosmological arguments related with dark matter reinforce this expectation.
Because the LSP is expected to be heavy and only weakly interacting, its experimental signature is a large amount of Missing Transverse Energy (MET) in events in which SUSY matter is produced. Since each event will have two LSP in the final state that will not deposit energy in any detector there will be a deficit in the energy balance of the collision.
In models in which R-Parity is not conserved, the LSP will not be stable, and this will change the experimental signature. The R-parity is an extension of the conservation of L and B in the SM, therefore the R-parity violation should be small. In this scenario single sparticle production is allowed as well as charged LSP's that decay into SM particles. One of the experimental signals in the search for this kind of SUSY is an excess in the production of SM particles specially leptons.
Even in the case of R-parity conservation, there are theoretical scenarios in which the next particle to the LSP (NLSP) is long-lived, and therefore able to go through the detector before it decays. In this work neither R-parity violating SUSY nor R-Parity conserving SUSY with long-lived NLSP will

be considered, the search will be motivated by signals with high amounts of MET.
In the SM most of the MET produced comes from neutrinos created after weak interactions, however statistically the SM-MET is smaller than the MET produced by SUSY. The amount of MET produced by a SUSY process can still be faked by $t\bar{t}$ processes, however MET on its own is still an excellent variable to separate SUSY from QCD and even Electroweak backgrounds.
SUSY events could result in final state signals with or without leptons, the first ones are referred as "leptonic signals" and the second ones as "hadronic signals". In the leptonic cases the leptons present in the final states are isolated, meaning that they are produced away from hadrons. Events with non-isolated leptons are treated as background.
Leptonic topologies may have several leptons in the final state, these leptons may come in any flavour combination. An example of this is the production of a neutralino and a chargino that decay into three leptons, with one or two different flavours; such a signal is hard to find within SM processes.
In the pure hadronic case, acoplanarity in the jets, together with a high amount of MET, could be a signal of SUSY production. In this case, searches can be done for two or more jets together with MET.
In summary, the leptonic SUSY searches look for events with at least one isolated lepton, high amounts of MET, high amounts of energy deposited in the calorimeters, and several jets.

2.8 Previous Searches

SUSY has been searched in collider experiments mostly in three accelerators, those accelerators are: SPS and LEP at CERN, and Tevatron at Fermilab.
The first accelerator that searched for SUSY was the Super Proton Synchrotron (SPS). The two experiments that were collecting data at that moment were UA1 and UA2. These experiments set some exclusions limits for the squark and gluino masses. The results of these searches are summarised in figure 2.7 together with results of later searches.
The second accelerator that searched for SUSY at CERN was the Large Electron-Positron collider (LEP). This accelerator was able to make very precise measurements of SM parameters, however it only provided exclusion limits for SUSY searches mostly due to the low CM energy available. The searches were done with an integrated luminosity of 3.6 fb^{-1}. These data

were collected by the detectors ALEPH, DELPHI, L3, and OPAL, at an $\sqrt{s}$ between 90 GeV and 208 GeV. Several topologies were used to search for SUSY, but no signal of its production was found[6].
The third accelerator searching for SUSY is the Tevatron with the two collider detectors CDF and D0. At the moment of the preparation of this document, this search is still underway. The Tevatron collides protons with anti-protons at a center-of-mass energy of 1.96 TeV.
In part b of figure 2.7 the results of the exclusion limit for gluino and squark masses obtained by CDF and D0 with the most recent data are presented. The main conclusions of these searches will be discussed in detail in this section[7].
SUSY models that conserve R-Parity, as well as models that do not, have been tested with both Tevatron and LEP data. To look for SUSY in these data, signals of production of: squarks, gluinos, charginos, and neutralinos have been searched with very similar topologies in all the experiments mentioned above. Until today no SUSY signal has been found.

2.8.1 Searches for Squarks and Gluinos

In the case in which R-Parity is conserved, searches have been done in the topologies formed by one, two, three or more jets; and missing transverse energy. These type of topologies could result from processes such as $\tilde{q} \rightarrow q\tilde{\chi}^0$, and $\tilde{g} \rightarrow q\bar{q}\tilde{\chi}^0$, were the quarks and antiquarks will result in high P_T jets and the neutralinos will result in MET. Some exclusion plots for this kind of inclusive searches done by the experiments at LEP and Tevatron are presented in figure 2.7[10, 6, 7]. These results show that in the case of mSUGRA the masses of squarks and gluinos should be higher than about 400 GeV/c^2, in the case of the non mSUGRA scenarios masses of the squarks should be lighter.
More exclusive searches have been done also. In figure 2.8(a) the exclusion limit set by CDF on the stop mass and the neutralino mass, done with a 95 % confidence level are presented. This plot came out from a two jet topology analysis in which a stop is produced and later decays into a charm and a neutralino, $\tilde{t} \rightarrow c\tilde{\chi}^0$ [8]. A very similar analysis, but this time looking for the decay $\tilde{b} \rightarrow b\tilde{\chi}^0$ yields the limits shown in figure 2.8(b) [9].
These channels only included hadrons in the final signal (hadronic channels). Exclusive channels in which there are leptons in the final state can also be searched for in the case of squark and gluino production. Even though the production of squarks and gluinos is common for all channels in which SUSY

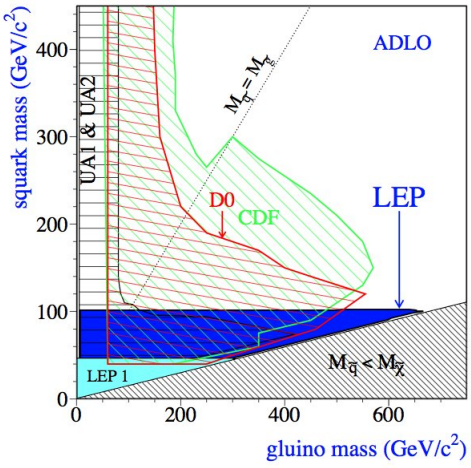

(a)

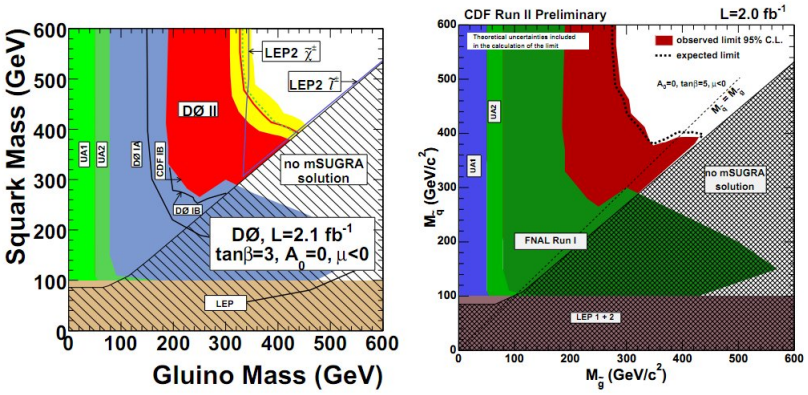

(b)

Figure 2.7: In part (a) the excluded region for squark and gluinos masses, as obtained by LEP is shown (taken from reference [6]). In part (b) the same plot is shown for the SUSY searches done by D0 and CDF experiments at the Tevatron (taken from reference[7]).

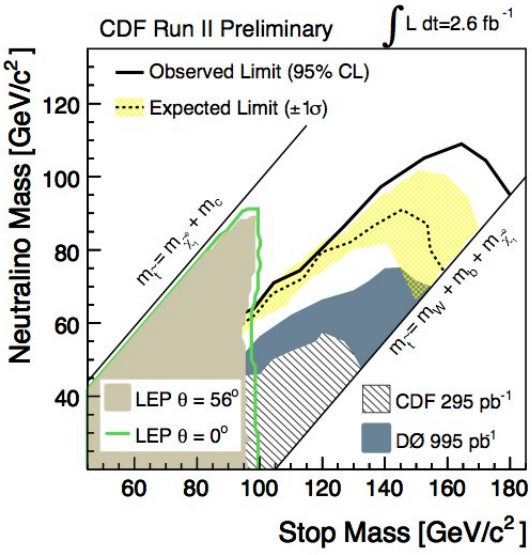

(a)

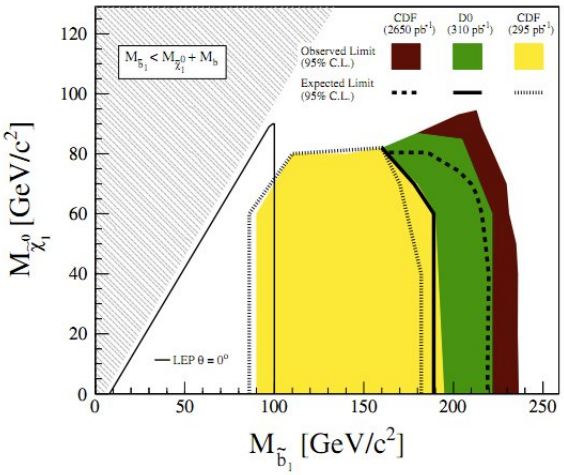

(b)

Figure 2.8: In plot (a) the 95 %-confidence-level exclusion region for the stop mass and the neutralino mass obtained by CDF is shown (integrated luminosity of 2.6 fb^{-1}, taken from reference [8]). In plot (b) a very similar result but this time for sbottom is shown. Results from previous experiments are also included in the plots (taken from reference [9]).

can be seen, there are also other channels in which SUSY has been searched. Signals of production of SUSY with one, two, three or more leptons in all combination of flavours and electric charges plus jets and MET are very important also. The primary s-particles produced as a result of the collisions, will generate decay chains mediated by weak interactions resulting in different topologies with lepton production. The study of these "leptonic channels" has constituted a very important part of the searches performed at LEP and Tevatron. In the next sub-sections these searches are going to be discussed.

2.8.2 Searches for s-leptons

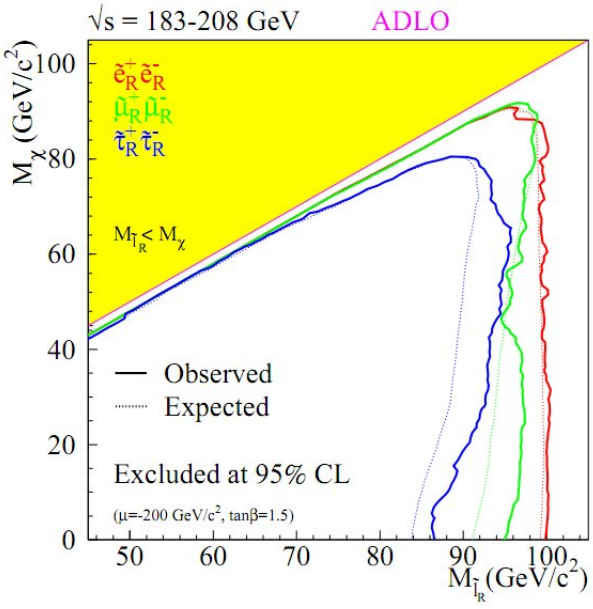

Figure 2.9: The excluded region for pair-produced s-leptons resulting from LEP experiment (taken from reference [11]).)

Searches with a leptonic final state signature give another possible scenario in which SUSY could be discovered. A natural channel to perform a leptonic search is $\tilde{l} \rightarrow l\tilde{\chi}_0$. This kind of studies have been performed at LEP and Tevatron. The specific experimental signature is: isolated leptons and MET. In the mSUGRA case, when the parameter m_0 is small, the s-leptons are theoretically allowed to be light, making this kind of search important.

The exclusion limits set on the s-lepton masses by the LEP experiments can be seen in figure 2.9 [11]. The yellow region is excluded for the s-lepton decay into neutralinos since neutralinos in this region are heavier than s-leptons. The plot also shows that the mass of s-leptons should be higher than about 95 GeV.

2.8.3 Search for Charginos and Neutralinos

In the chargino searches performed at LEP, two theoretical cases yielding different decay topologies were considered. The first case is characterized by a large m_0; In this case the decay $\tilde{\chi}^{\pm} \rightarrow \tilde{\chi}_0 W^{\pm}$ would be dominant, yielding a final state topology composed by MET and all the possible W-decay scenarios. In the second case, m_0 has a small value, this implies that the s-leptons have a light mass. In this case the decay $\tilde{\chi}^{\pm} \rightarrow \tilde{l}\nu \rightarrow \tilde{\chi}^0 l\nu$ would be dominant. Figure 2.10(a) shows the LEP exclusion limit for this search. In figure 2.10(b) the exclusion limit plot is shown for a case in which the chargino and the neutralino have a very similar mass. From these plots it can be concluded that the chargino masses should be higher than about 103 GeV/c^2 while the neutralinos should have masses higher than about 40 to 45 GeV/c^2.
Searches for neutralinos at LEP, in the cMSSM framework, were also performed. They profit from the fact that in this theoretical scenario the stau mass could be between the neutralino and the chargino masses. This possibility was studied mostly by ALEPH, in which the following searches were performed:

- $e^+e^- \rightarrow \tilde{\chi}^+\tilde{\chi}^- \rightarrow \tilde{\tau}\nu\tilde{\tau}\nu \rightarrow \tau\nu\tilde{\chi}^0\tau\nu\tilde{\chi}^0$,
- $e^+e^- \rightarrow \tilde{\chi}^0_2\tilde{\chi}^0_1 \rightarrow \tilde{\tau}\tau\tilde{\chi}^0_1 \rightarrow \tau\tilde{\chi}^0_1\tau\tilde{\chi}^0_1$, and
- $e^+e^- \rightarrow \tilde{\chi}^0_2\tilde{\chi}^0_2 \rightarrow \tilde{\tau}\tau\tilde{\tau}\tau \rightarrow \tau\tau\tilde{\chi}^0_1\tau\tau\tilde{\chi}^0_1$.

All final topologies coincide in the presence of taus and missing energy. The limits established for these topologies can be seen in figure 2.10(c)[11].
Tevatron has also searched for charginos and neutralinos, the most recent and precise measurement come from this accelerator. An example of such a search is the case in which a chargino and a neutralino result from the decay of a heavier SUSY particle produced after a proton anti-proton collision ($p\bar{p} \rightarrow \tilde{\chi}^{\pm}\tilde{\chi}^0 X$). This case can produce a three lepton signature that has a very small probability to be produced by SM processes. As a results of these searches, limits on the chargino-neutralino production cross sections

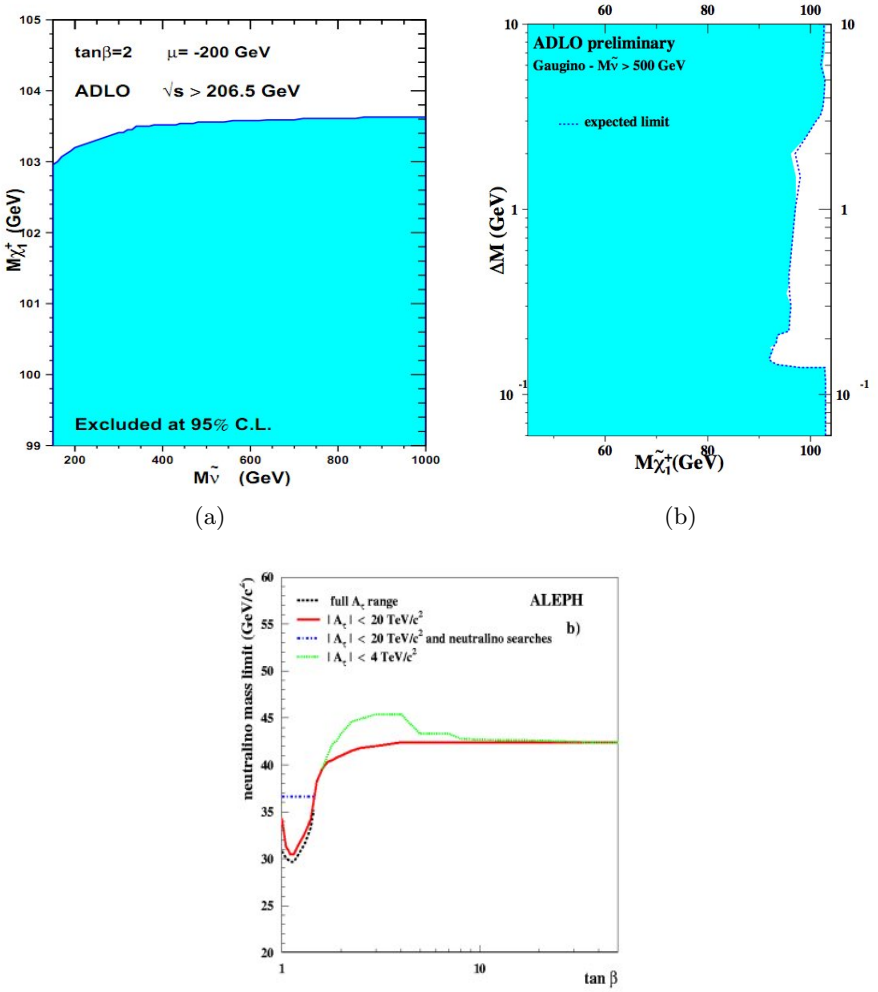

(a) (b)

(c)

Figure 2.10: LEP results for chargino and neutralino searches. Plot (a) shows the excluded region for charginos at large m_0. Plot (b) shows the excluded region for charginos masses at low $\Delta M = M(\tilde{\chi}^+) - M(\tilde{\chi}^0)$. Plot (c) shows the excluded region for neutralino masses as set by ALEPH detector (taken from reference [11]).

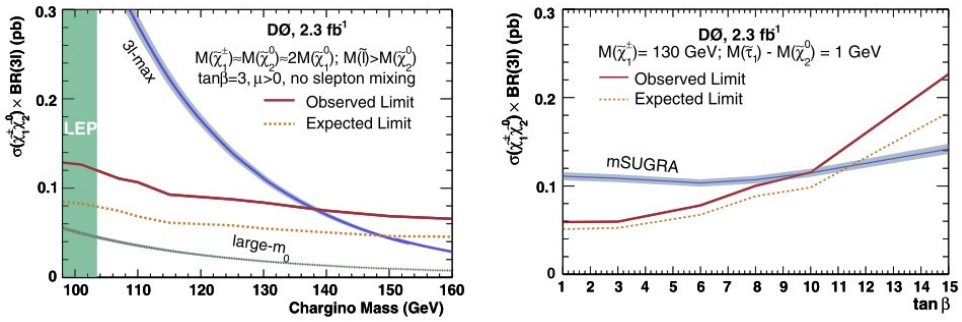

Figure 2.11: Cross sections upper limits at 95 % confidence level for chargino-neutralino production at Tevatron (taken from reference [12]).

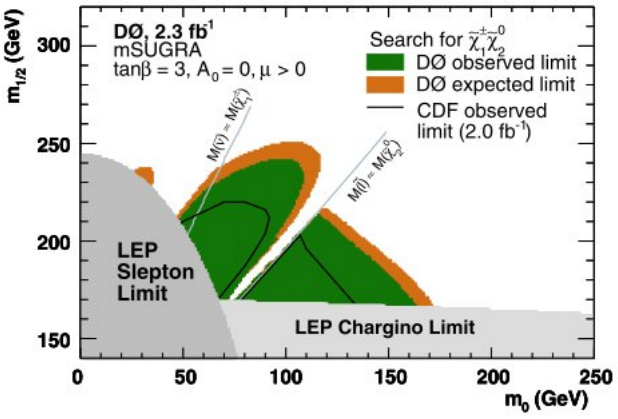

Figure 2.12: mSUGRA parameter plane plot with the 95 % C.L. excluded region resulting from the cross section plots of figure 2.11 (taken from reference [12]).

going into 3 leptons have been set, as presented in figure 2.11. When one considers mSUGRA, these limits could be translated into excluded regions in the parameter space plane (m_0, $m_{1/2}$). The excluded region in the mSUGRA plot can be seen in figure 2.12 (details can be found in reference [12]).

2.8.4 Higgs Boson and SUSY Searches

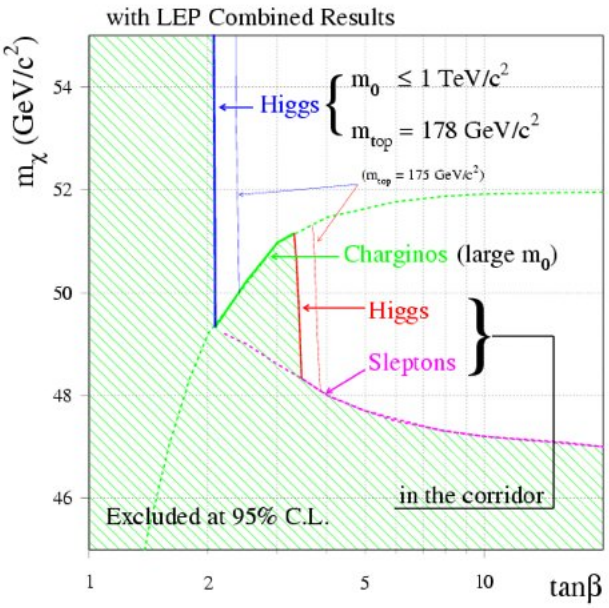

Figure 2.13: The combination of all the searches done under the cMSSM framework give these exclusion regions (taken from reference [11]).

For some values of the cMSSM parameters, the lightest MSSM neutral higgs boson behaves as in the standard model, and therefore the lowest mass of the SUSY higgs can be compared with the actual limits set for the SM higgs. These limits constrict some theoretical parameters (M_2 in cMSSM) such that limits can be set for the mass of the LSP. LEP SUSY searches combined gave an exclusion limit plot for the LSP masses using this method. In figure 2.13 [11] two cases defined by the value of m_0 were considered. In the first one in which m_0 has a large value (bigger than 1 TeV/c^2) and the top mass is considered to be 178 GeV/c^2, approximately all the possible values of $\tan\beta$ smaller than 3 are excluded, and therefore the LSP mass is expected to be bigger than about 50 GeV/c^2. In the second case for low m_0

masses, the $\tan\beta$ values smaller than 4 are also excluded, and therefore the LSP mass is expected to be bigger than about 47 GeV. These values are in agreement with other searches.

2.8.5 R-Hadrons Searches

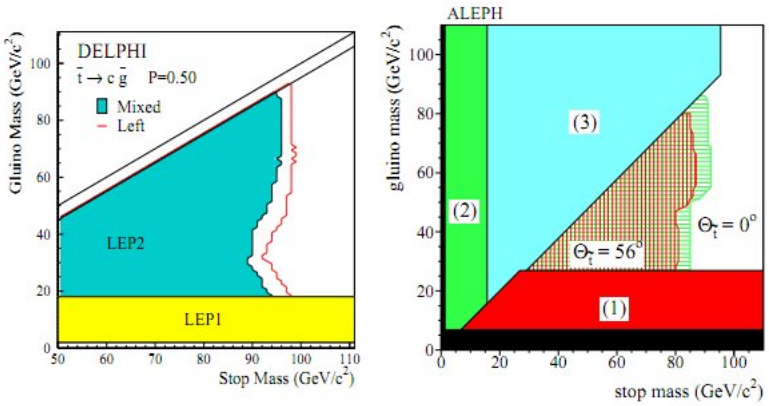

Figure 2.14: In the left plot the excluded regions for the decay $\tilde{b} \to b + \tilde{\chi}^0$ made by DELPHI are shown. In the right plot an ALEPH result is shown with the excluded regions in the plane ($m_{\tilde{t}}$,$m_{\tilde{g}}$). In the plot the black area shows the excluded region by the Z-lineshape. The region label as 1 was excluded by LEP 1 searches for $e^+e \to q\bar{q}\tilde{g}\tilde{g}$ decays The second region shows the exclusion done with LEP 1 for the $e^+e \to q\bar{q}\tilde{q}\tilde{q}$ decay. The third region shows the exclusion done with the LEP 2 searches for squarks (taken from reference [11]).

SUSY signals can also be searched by looking for heavy long lived charged particles. These particles are predicted in SUSY models in which the gluino is the LSP. This type of LSP would hadronize into stable charged and neutral particles called R-Hadrons. In these kind of models the MET signal may not be always present. In the case in which the produced R-Hadron is neutral it will have a low energy to interact with the calorimeter and therefore it will escape from detection as MET. In the case in which the R-Hadron is charged the particles created may behave similar to a heavy muon[13].These final states were searched mostly by DELPHI and ALEPH, the results are shown in figure 2.14 [11].

2.8.6 Other Searches

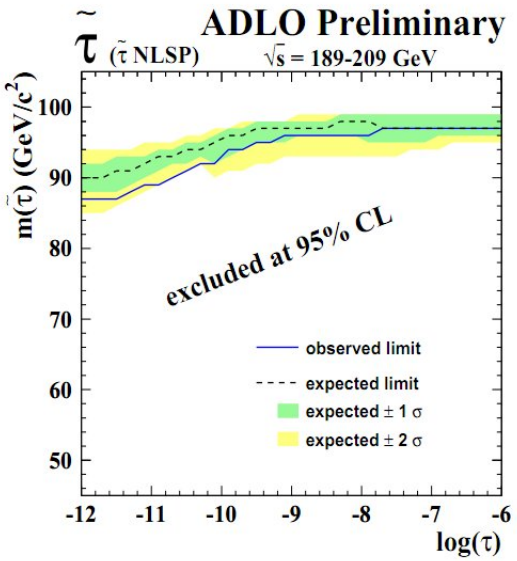

Figure 2.15: The exclusion limit for a s-tau NLSP in the GSMB framework (taken from reference [11]).

Another flavour of SUSY searched at LEP and at Tevatron is the one with gauge mediated SUSY breaking usually referred as GMSB, with the gravitino as the LSP. In this case the neutralino, together with a s-lepton, are expected to be the next to the lightest SUSY particle (NLSP). In figure 2.15 the LEP exclusion limit for s-tau NLSP is presented[11][6].
Similar searches have been done at Tevatron using different channels. As an example, GMSB has been searched in the channel in which two photons and MET is present. Only exclusion limits on the production cross section for these processes have been set with no evidence of SUSY production. The complete study can be found in reference [14]. The plot that shows the exclusion limit set by this search can be seen at figure 2.16.
Searches for R-Parity violating SUSY have been done at LEP and at Tevatron. R-Parity violating SUSY has important phenomenogical consequences such as the production of a single SUSY particle, or the decay of the LSP into SM particles. These changes imply a higher fermion multiplicity, and probably less or no MET in the final state.
An example of these kind of searches is the one done at CDF [15], in which

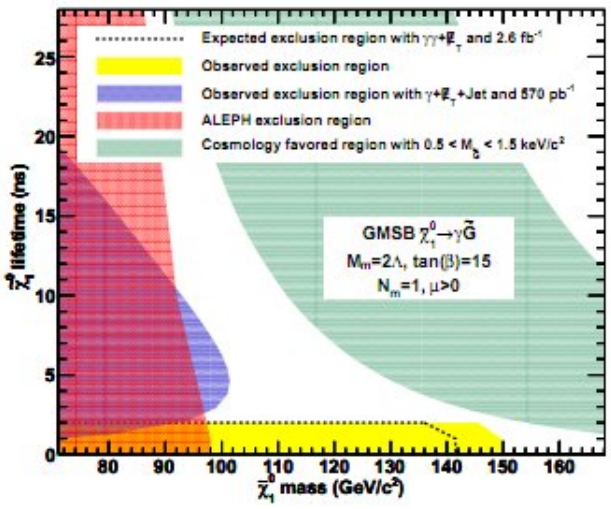

Figure 2.16: The exclusion limit set to the lightest neutralino lifetime and mass with 95 % C.L, this limit is the current world best limit set by CDF at Tevatron (taken from reference [14]).

a tau s-neutrino could decay into two different flavour leptons. The results were summarized as a 95% C.L. upper limit plot of the cross section multiplied by the branching ratio of the decay (figure 2.17).
Several other topologies that may result from SUSY processes have been searched, but so far non of them have given any excess when compared to SM processes. Even though no experimental evidence of SUSY has been found, upper limits have been set for the particles that could exist. Until today not all the possible SUSY parameter space has been scanned, therefore there is still a lot of work to be done.

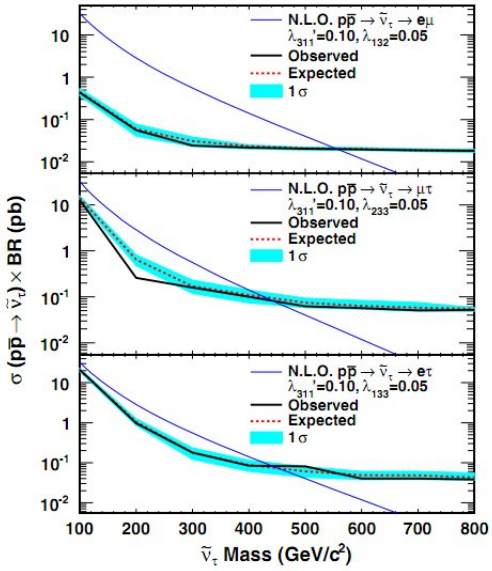

Figure 2.17: The expected and observed 95 % C.L. upper limits on $\sigma(p\bar{p} \rightarrow \tilde{\nu}_\tau) \times BR(\tilde{\nu}_\tau \rightarrow e\mu, \mu\tau, e\tau)$ as a function of $M_{\tilde{\nu}_\tau}$(taken from reference [15])

Chapter 3

The CMS Detector

The search for SUSY signals that is the subject of this thesis, has been performed with the Compact Muon Solenoid (CMS), one of the four large experiments located at the CERN LHC. CMS together with ATLAS, are the two multipurpose detectors designed to search and discovery new physics in the energy range of the TeV; new physics like for instance SUSY.
As it was discussed in the previous chapter, the experimental signals of SUSY demand excellent performance of all sub-detection systems of an experiment like CMS: excellent tracking and calorimetry for jet reconstruction, high degree of energy hermeticity, and high efficiency in lepton reconstruction.
In this chapter, a brief description of the LHC and the CMS detector is presented. In this description, the emphasis will be made on those features of the detector that are crucial for SUSY searches.

3.1 The Large Hadron Collider (LHC)

The Large Hadron Collider or LHC is a particle accelerator located at CERN in the border line between France and Switzerland. It is installed inside a tunnel buried at a depth that varies from 50 to 175 m. This tunnel, original build for the LEP accelerator, has a circumference of 26.7 km (see figure 3.1).

The LHC was designed to accelerate and collide two circulating beams of hadrons, these beams could be made out of protons or lead ions. In this thesis only the data coming from proton collisions was used, therefore only the LHC parameters that describe the proton beams are presented.
Each beam in the accelerator was designed to reach an energy of 7 TeV, this is equivalent to a Center-of-Mass (CM) energy of 14 TeV for every collision,

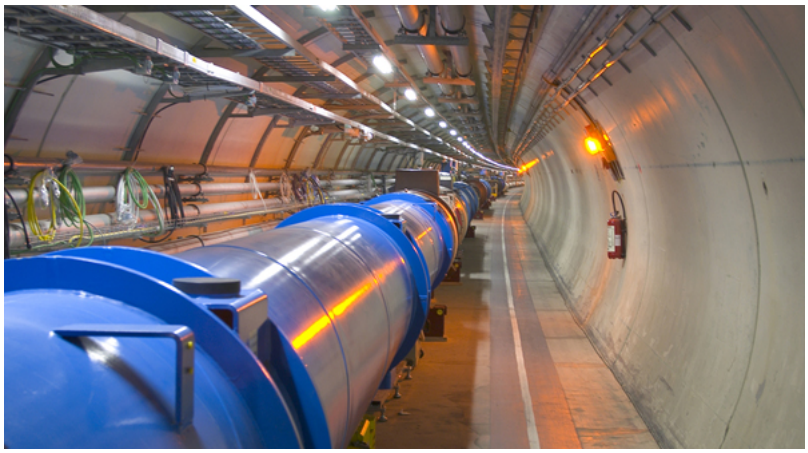

(a)

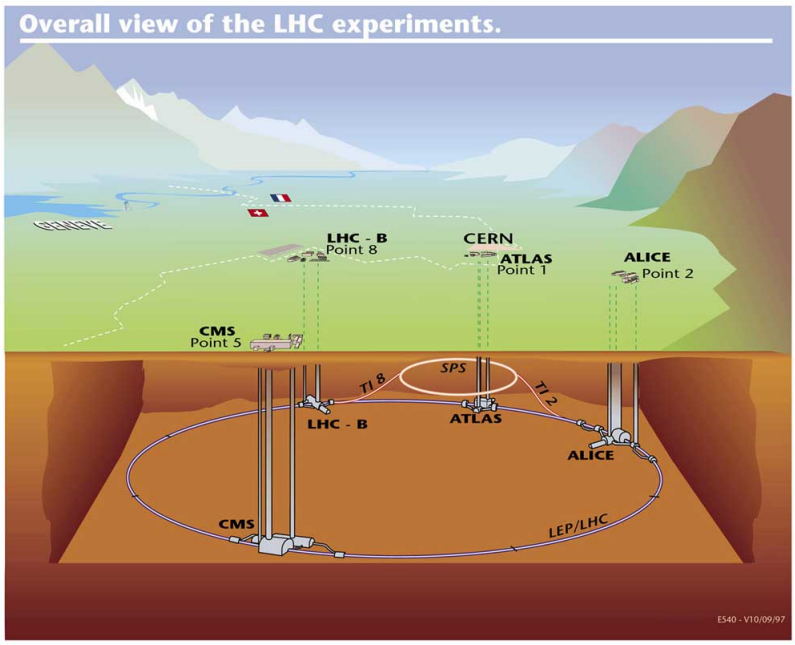

(b)

Figure 3.1: Figure (a) shows an actuall picture of the LHC inside the tunnel, each of the blue tubes is a main dipole magnet. In figure (b) a geographical representation of the LHC and its main experiments is shown.

however during the first year of LHC running the energy per beam was set to 3.5 TeV, this was done to protect the magnets in the starting phase of the accelerator. In conclusion, the CM energy at which the search presented in this work was done corresponds to 7 TeV.
Each proton beam is designed to be made of up to 2808 bunches, with every bunch made out of approximately 1.15×10^{11} particles; however in the early days of the LHC commissioning these parameters were lower than these values.
The first collisions at the LHC took place on March 30 of 2010, with just two bunches in the accelerator. Very fast progress allowed the LHC operators to reach a 3 bunch configuration four days later, with a luminosity of 1.1×10^{28} $\mathrm{cm}^{-2}\mathrm{s}^{-1}$ in all the experiments. By May 19th 2010 the experiments were already collecting data with the purpose of physics analysis.
In September, the distance between two consecutive bunches was 150 ns, and it decreased up to 50 ns during the last week of the LHC proton run for 2010, by the end of November. The number of bunches reached 368 per beam. All these achievements allowed a luminosity peak of 2×10^{32} $\mathrm{cm}^{-2}\mathrm{s}^{-1}$, during the last days of running (see table 3.1). The 2010 run finished with a recorded integrated luminosity of 48 pb^{-1} by most of the LHC experiments.

Table 3.1: LHC relevant parameters for the 2010 run.

Energy per proton	3500 GeV
Number of particles per bunch	1.15×10^{11}
Maximum number of bunches per beam	368
Stored energy in the beams	25 MJ
RMS bunch length	7.55 cm
Crossing angle	285 μ rad
Total cross section	100 mb
Average events per bunch crossing	17.9
Luminosity lifetime	14.9 hours
Energy loss per turn	6.71×10^3 eV
Distance between two proton bunches	50 ns
Maximum reached Instantaneous luminosity	2×10^{32} $\mathrm{cm}^{-2}\mathrm{s}^{-1}$

The LHC has four interaction points in which the four large experiments CMS, ATLAS, ALICE, and LHCb, are located. In addition to these experiments, there are two small detectors designed to measure scattering in the forward region at very small angles, with the main purpose of determine the

proton-proton total cross section, these experiments are called TOTEM and LHCf.
All the LHC experiments were designed aiming at different physics programs, in particular ATLAS and CMS are both multi-purpose detectors whose main physics goals are: Search for the Higgs boson, and exploration of any possible new physics in the new energy ranges provided by the LHC. ALICE was designed to study the physics of heavy ion collisions, specially the quark gluon plasma. LHCb was designed to study CP violation in B meson systems. Besides of measuring total cross sections LHCf uses the proton-proton collisions as a way to simulate cosmic rays in laboratory collisions. TOTEM will explore the kinematical region were the strong interaction between protons can not be described with pQCD.
The instantaneous luminosity given by the accelerator is different at each of these detectors, it has a maximum at CMS and ATLAS with a designed optimal value of $L = 10^{34}$ cm^{-2}s^{-1}, and a minimum at ALICE with a luminosity of $L = 10^{27}$ cm^{-2}s^{-1}, this values have not been reached yet.
To reach the described performance, the LHC uses superconductive magnets. These magnets have a working temperature of 1.9 K, which is the lowest temperature of any superconducting accelerator up to date.
The main dipoles of the LHC can produce a magnetic field of approximately 8.4 Tesla at a current of about 11700 A. Each one of these magnets has a length of 14.3 m. To construct the entire accelerator 1232 of these dipoles were needed (see figure 3.1(a), and 3.2).

3.2 The Compact Muon Solenoid

The LHC tunnel is divided in 8 points. Each of these points was built to contain a detector either during the LEP or the LHC period. The CMS detector is located at the point number 5 as can be seen in figure 3.1(b). This point is located at Cessy, France, in the northern most point of the accelerator.
The CMS is called the Compact Muon Solenoid because:

- It is very heavy for its actual size (Compact), and almost all geometrical regions are covered by the detector.
- It is optimized to detect and trigger on muons.
- Its central magnet is a very large superconductive solenoid that encases the tracker and the calorimeters.

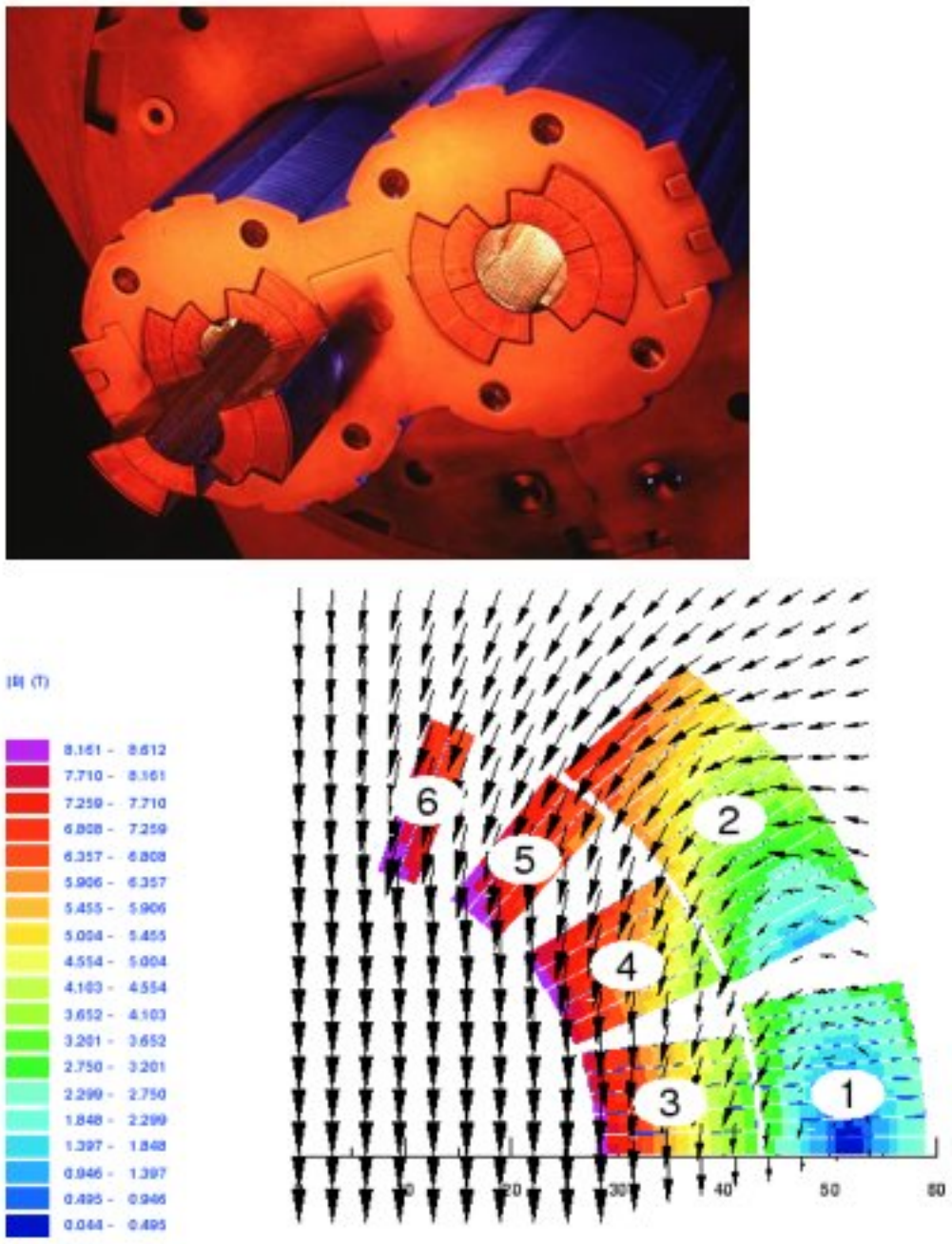

Figure 3.2: In the upper part a picture of the cross section of a dipole magnet from the LHC is presented, and the lower part a graph with the magnetic field lines produced are shown [16].

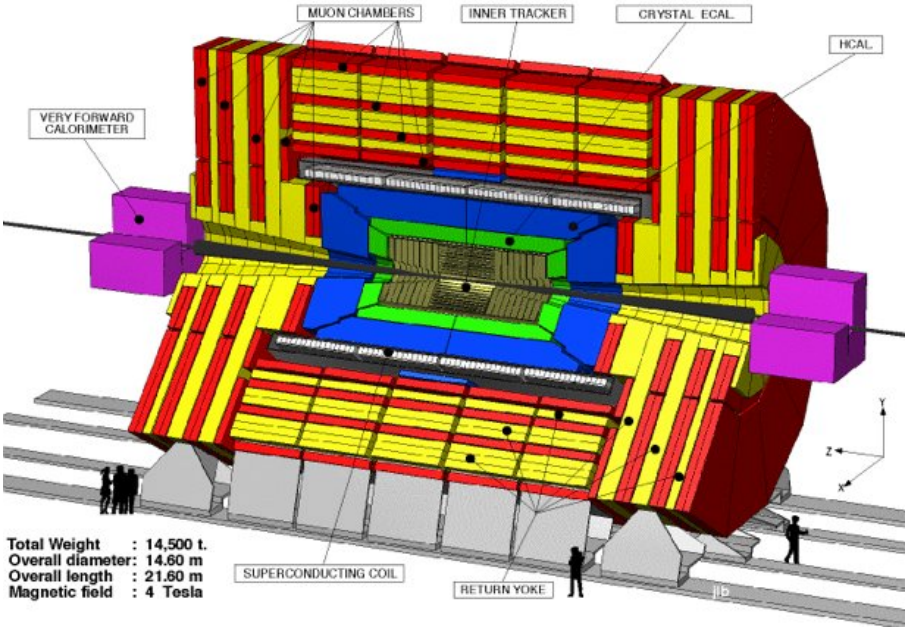

Figure 3.3: The CMS detector.

The CMS was designed to reach the following physics milestones:

- To study physics at the TeV scale which was so far unexplored.
- To search for the Higgs boson, and therefore provide a better understanding of the electroweak symmetry breaking of the SM.
- To discover new physics that could exist in the unexplored TeV region, as for example Supersymmetry or Extra-dimensions.

The CMS detector is made out of 4 big sub-detector systems, these systems are:

- a central tracking system,
- a calorimetry system,
- the solenoid magnet with its return yoke,
- and a muon tracking system.

The CMS has a cylindrical shape (see figure 3.3) along the beam line with a radius of 7.3 m, a length of 21.6 m, and a total weight of 12500 t. The different detection systems are geometrically distributed into 3 regions, those regions are a forward end-cap, a backward end-cap, and a central barrel (see figure 3.3). The description of these systems is going to be presented in the following sections.

3.2.1 Tracker System

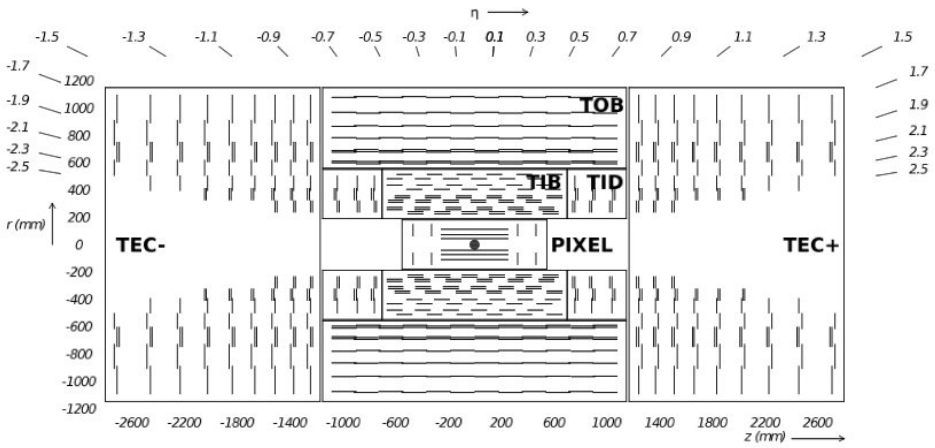

Figure 3.4: This figure shows a transverse view of the central tracker[17].

An excellent tracker performance is very important to achieve the CMS physics goals, because every possible discovery will rely on the reconstruction of more fundamental basic objects such as: leptons, jets, or any other charged physical object. The charged objects will interact with the tracker and the magnetic field producing curved tracks, these tracks will provide important information for particle identification.
In the specific case of this thesis a good resolution in the tracker is vital to distinguish isolated tracks from non-isolated ones (tracks that are kinematically separated from reconstructed jets). This is important because SUSY is expected to produce isolated leptons such as those resulting from the decay of Z and $W^{\pm}$. Non-isolated leptons can be the result of the decay of heavy flavours which are not directly related with SUSY signals.
The tracker plays an important role in b-tagging, tau reconstruction, and momentum determination of the charged particles that traverse it. The tracker will be able to create 3D images of the collision vertex and any sec-

ondary vertex like in the case of b-tagging, with the exception of the neutral particles.
The CMS tracker was designed to record the path of the charged particles that will traverse the detector after every collision, to do so this system was built using two different technologies which are: pixel detectors, and silicon strip detector.
In figure 3.4, a transversal cut of the CMS tracker is shown. In this picture the different parts of the tracker can be seen. These tracker parts are discussed in the next sections.

Pixel Detector

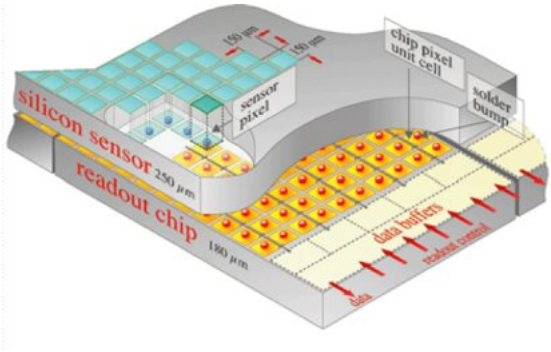

Figure 3.5: This figure shows a representation of a few tiles inside the Pixel detector. Each tile has the same width of two human hairs.

The pixel detector is the closest one to the beam pipe, therefore it is exposed to very high levels of radiation coming from the collisions. The radiation at a distance of 8 cm from the beam pipe will be of about 10 million particles per square cm per second. This number is very high and demanded a careful design for this system. The radiation hardness achieved in the pixel detector system will allow it to operate for about 10 years.
The Pixel detector has three cylindrical layers at a radius of 4, 7 and 11 cm from the beam pipe. It also has a disk at either end. Each one of the three layers of pixels is divided into little 100 μm by 150 μm tiles. Each one of these tiles is a tiny silicon sensor sensible to charged particles (see figure 3.5). There are approximately 66 million of these tiles, all of them cover an active area of 1.1 m^2. When a charged particle passes through any of those sensors, the electrons in the silicon get enough energy to create electron-hole

pairs and therefore a small electrical current, this current is read out by the electronics attached to each tile. The pixel readout allows the experimentalist to know a charged particle trajectory with a space resolution of one tile (100 μm by 150 μm).
Because the pixel detector has 66 million channels and each of them generates an output power of 50 micro-watts, it needs a cooling system that prevents the detector from overheating. With this aim the system is mounted on a frame of aluminium cooling tubes that serve as support for the pixel structure[18][19], some of these tubes are laser welded to an aluminium container that distributes liquid C_6F_{14} to cool down the detector to about -10 C°.

Silicon Strip Detectors

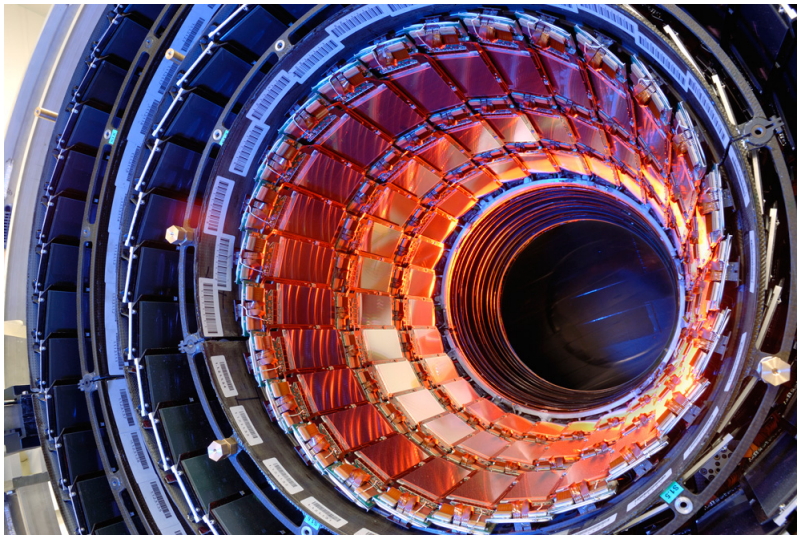

Figure 3.6: A picture of the barrel region of the silicon strip detector. Some of the modules can be seen without the pixel detector installed.

Once the particles leave the pixel detector, they pass through ten layers of Silicon Strip Detectors (SSD) (see figure 3.6). These detectors surround the pixel system and they go out until a radius of 130 cm completing the central part of the CMS tracker.
The SSD contains 15148 sensitive modules with a total of 9.3 million strips. All the information produced is read by 80000 microelectronic chips. Each

one of these modules is made out of a set of sensors, a mechanical support structure, and the electronics for the readout.
The SSD has an active area of 200 m^2 and consist of four inner barrel layers assembled in shells (TIB); two inner end-caps, each one composed of three small discs (TID); an outer barrel formed by six layers of detectors (TOB); and two outer end-caps that close the tracker (TEC)(see figure 3.4).
Both TIB, and TID use 320 μm thick silicon-micro-strips sensors. This sensors are oriented so that the strips are parallel to the beam axis in the TIB and in a radial direction in the TID. In the TIB, the strip pitch is 80 μm for the two inner layers and 120 μm for the two outer ones; on the other hand in the TID the mean pitch varies between 100 μm and 141 μm.
The TOB has an outer most radius of 116 cm. It consists on a barrel with 6 layers of 500 μm thick micro-strip sensor. In this case the strip pitches are 183 μm on the first 4 layers, and 122 μm on the two outer layers. The TOB covers the geometrical region of $|z| < 118$ cm (where z is the direction parallel to the beam). Beyond this range the forward and backward TECs are located, covering the regions 124 cm $< |z| <$ 282 cm, and 22.5 cm $< r <$ 113.5 cm.
Each of the two TEC is composed of 9 disks, and each disk has a different number of silicon micro-strips detector rings, going from 4 rings for the outer-most disk to 7 for the inner-most. The silicon micro-strips detectors have a thickness of 320 μm on the four inner rings, and 500 μm on the 3 rings that follow, they have radial strips with an average pitch going from 97 μm to 184 μm.
The modules located in the two inner-most layers of the TIB, the two inner-most layers of the TOB, rings one and two of the TID, and rings one, two, and five of the TECs, have a second micro-strip detector module mounted back to back; this module provides a measurement of the coordinate z in the barrel and r in the end-caps[20].
A schematic of the complete tracker system can be seen at figure 3.4[17].

3.2.2 The CMS Calorimeters

The CMS Calorimeter system shown in figure 3.3 in green and blue, is composed by a electromagnetic calorimeter (ECAL) and a hadronic calorimeter (HCAL), both of these calorimeters are enclosed in the magnetic solenoid, increasing the resolution of the system since the particles do not have to go across the solenoid. The two calorimeters are designed to detect electrons, photons, charged hadrons, and neutral hadrons. To do so the two systems

are made out of several layers of heavy material that stops the particles, and sensitive material that measures the energy released by the particles being stopped. The detection and identification of these particles is very important, for instance there are decay channels either in SUSY and in Higgs physics that produce photons, electrons, and jets in the final states. In the SUSY searches, the s-particles are expected to be heavy and therefore they will leave large amounts of energy deposited in the calorimeters. In fact, important and relevant SUSY triggers are based on the calorimeter performances such as the H_T and MET triggers, these quantities are going to be defined on a later chapter.

ECAL

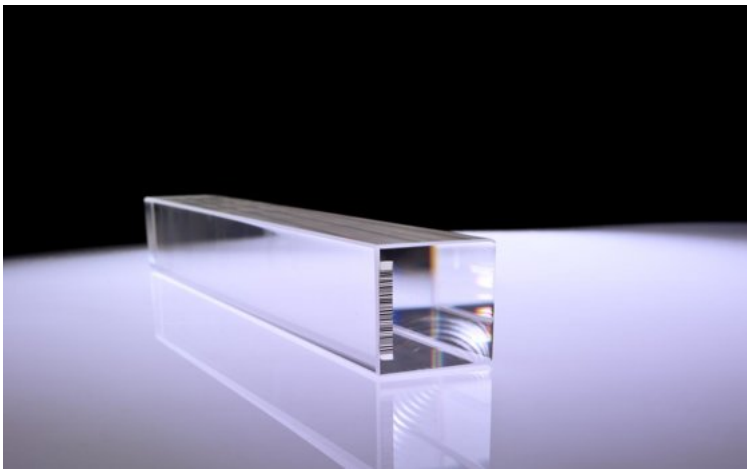

Figure 3.7: A picture of one of the crystals used in the ECAL.

The electromagnetic calorimeter or ECAL is located just after the tracker inside the CMS solenoid. It is designed to stop electrons and photons produced in the LHC collisions.
The ECAL is composed by a barrel and two end-caps. The barrel consist of 61200 crystals arranged into 36 super-modules, each one of which contains 1700 crystals. On the other hand, the end-caps are made out of approximately 15000 crystals.
The exact amount of crystals for the entire ECAL is 75848. Each crystal in the barrel has the dimensions: 2.2 cm $\times$ 2.2 cm $\times$ 23 cm, and in the end-caps 3 cm $\times$ 3 cm $\times$ 22 cm.

Each crystal is made out of lead tungstate (PbWO4). This material is as heavy as stainless steel, but with a small percentage of oxygen in its crystalline phase. The lead tungstate is highly transparent and scintillates when electrons and photons pass through it. Photodetectors are added at the end of each crystal to collect this scintillation light and convert it into an electrical amplified signal (see figure 3.7)[18].

ECAL Preshower

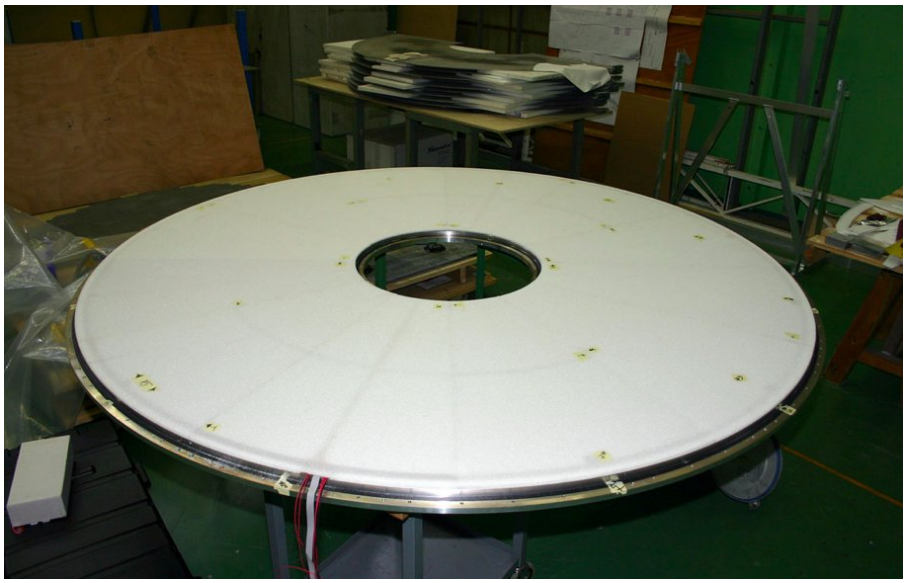

Figure 3.8: A picture of one of the preshower disks ready for installation.

One of the important Higgs boson decay channels produces two high energy photons. This signal can be faked by a π^0 that decays into two photons that are close enough to each other, so that they are reconstructed as one high energetic photon. To prevent that from happening, a small calorimeter called the Preshower detector was installed before the ECAL end-caps, since in this region this kind of effect is expected to be more frequent. The preshower is a silicon strips detector with the form of a disk that provides a better granularity than the ECAL due to their 2 mm wide strips, compared with the 3 cm $\times$ 3 cm ECAL crystals.
The preshower is made out of two planes of lead, followed by silicon detectors similar to those used in the tracker. When the photons cross the

lead layers, they produce an electromagnetic shower made out basically of electron-positron pairs. This shower is later on detected by the silicon sensors. The fact that there are two layers of lead and detectors present, allows the preshower to make an estimation of the photon incident direction.
The silicon sensors in the preshower are divided into 32 strips and have approximate dimensions of 6.3 cm $\times$ 6.3 cm $\times$ 0.3 mm, arranged in a grid that forms an almost circular shape covering the ECAL-end-cap crystals (see figure 3.8). The preshower has a temperature control system because it has to work at a temperature of approximately -10°C, while the operational temperature of the ECAL is higher.
The preshower system forms a disk of 2.5 m in circumference, it has a hole of 50 cm in diameter located in the middle where the beam pipe passes through. This disk is 20 cm thick and contains inside it the cooling and heating system, the two lead layers, and the silicon sensors[18].

HCAL

The HCAL is a calorimeter designed to stop the hadrons produced in the LHC collisions. It also closes the detector hermetically to grant a measurement of the complete transverse energy produced after every collision (of course with the exception of the beam pipes).
A hermetical experiment is needed to detect neutrinos and new physics such as SUSY, since any unbalance on transverse energy is a signal of neutral weakly interacting particles escaping. Missing energy can be a signal of new physics if it is statistically incompatible with the missing energy produced by SM neutrinos and any other systematical effect.
The HCAL is a sampling calorimeter, this means it has contiguous layers of absorbing and active materials. It is divided into a barrel (HB) and a couple of end-caps (HE). In the barrel the system is composed of 5 cm thick copper absorber plates followed by 4 mm thick plastic scintillator tiles. In the end-caps the copper plates are 8 cm thick. In the copper layers hadron showers are produced and a sample of their energy is registered by the scintillators. The scintillator tiles are connected to wavelength-shifting plastic fibres that are in-charge of the read-out of the light signal. The HB is about 79 cm thick, this distance corresponds to about 5.15 nuclear interaction lengths[18].
To extend the hermeticity of the calorimeters and to improve the measurement of the missing energy, CMS has two separate forward calorimeter (HF) located at 10.9 m in each side from the interaction point. These calorime-

ters cover the region $3 < |\eta| < 5$. They use quartz fibres as active material embedded in copper[21].

3.2.3 The CMS Magnet

The CMS magnet is located right after the calorimeters, it is a superconductive solenoid with 6 m in diameter and 12.5 m in length. The tracker and the calorimeter are fit inside the solenoid while the muon chambers are located outside inserted in a steel return yoke.

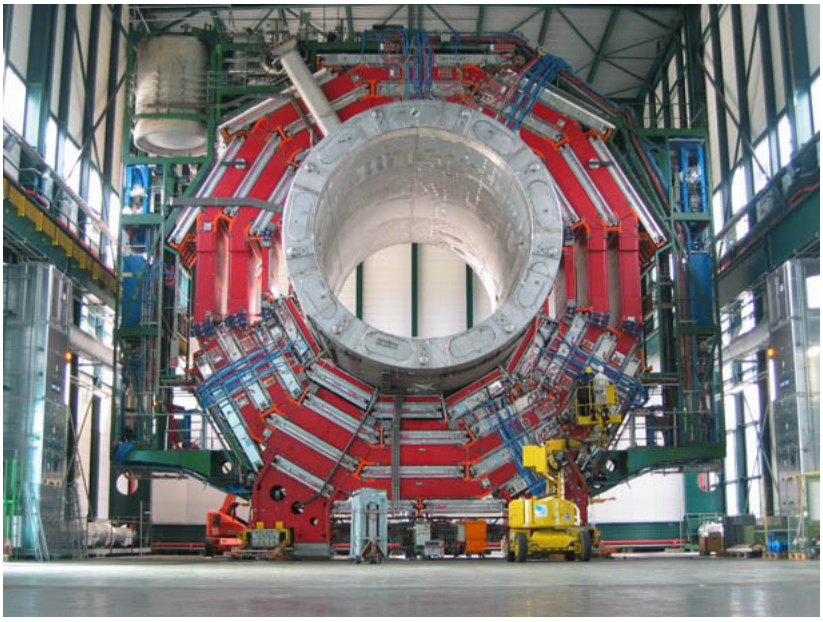

Figure 3.9: Picture of the CMS solenoid magnet together one of the barrel yoke "wheels".

The CMS solenoid produces an inner magnetic field of 3.8 Tesla where the tracker and calorimeters are located. Its purpose is to bend the charged particles so that their momentum and charge can be measured. The magnetic field is strong enough so that the curvature of the particles with high momentum is still significant.
The CMS solenoid is made out of a superconductive coil working at a temperature of -268.5 °C. In the barrel region, an iron yoke gives support to the muon chambers and prevents the magnetic field from spreading out providing a compactified return. In the barrel region the yoke is composed of

Figure 3.10: Picture of one of the end-cap yoke disks.

five sections or "wheels" with a dodecagonal shape and a diameter of 14 m. Each section is composed by three concentric layers of iron[18], with gaps in between to fit the muons chambers (see figure 3.9).
In the end-caps the yoke is formed by disks of approximately the same diameter. In this case the muon chambers are not inside the yoke, but they are sticked to the surface (see figure 3.10). The magnet and its yoke have an overall weight of 12000 tonnes.

3.2.4 Muon System

The Muon System is located outside the magnet, it is composed of chambers installed inside the yoke wheels in the barrel and between the yoke disks in the end-caps. The CMS muon system was designed to detect and trigger on muons coming from LHC collisions, and to reconstruct the tracks with high momentum resolution.
This system is the result of the use of three different detector technologies: Drift Tubes (DT), Resistive Plate Chambers (RPC), and Cathode Strip Chambers (CSC). The DT's are located in the barrel region, the CSC's are located in the end-caps, and the RPC's are located in both the barrel and the end-caps (see figure 3.11). The DT's and CSC's are high space resolution tracking detectors while the RPC's are high time resolution triggering detectors.

One of the signatures of high P_T physics is the presence of high momentum muons in the final state. These muons play a very important role in the search for new physics, for example in several SUSY and Higgs searches whose signals contain muons in their final states. This characteristic makes the muons protagonist of the design of triggers for the CMS detector.
Having a muon detector as big as the one of CMS, underlines the importance of identifying muons properly. Due to its high mass, muons do not interact with matter as much as lighter particles, and therefore they leave small deposits of energy in the calorimeters. Even thought the tracker system can reconstruct the muon's tracks clearly, this information is not enough to unambiguously identify them, therefore a muon system outside the central detector is required.
Muons have a long life time, allowing to locate their detectors far away from the interaction point, resulting in a high precision in the momentum and charge measurement. A description of the muon subsystems will be presented next.

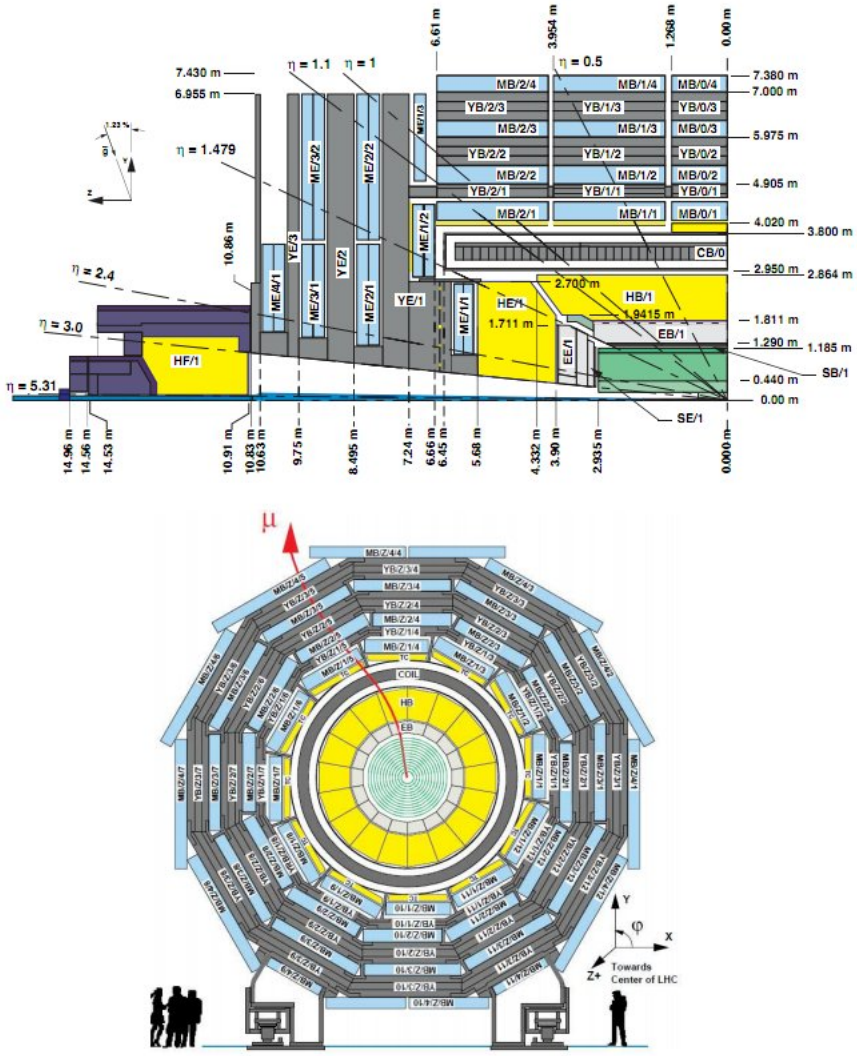

Figure 3.11: A schematic view of the end-cap and barrel regions of the CMS detector. The muon chambers are represented in light blue, the eta coverage is also shown[22].

Drift Tubes

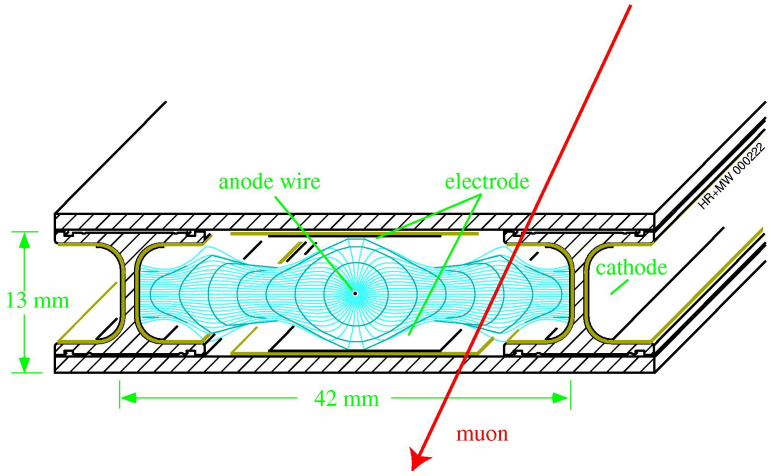

Figure 3.12: A schematic representation of a DT and its detection of a muon.

The DTs are used for triggering and tracking on muons. Each DT chamber has an average size of 2 m $\times$ 2.5 m, and consists of 12 aluminium layers arranged in groups of four. Each group has up to 60 tubes of 4 cm wide filled with gas. In the middle of each tube a stretched wire is located. The wire collects all the electrons produced as a result of the ionisation left by a passing charged particle, like a muon.
When a charged particle passes through the tubes, it interacts with the gas knocking electrons out of the atoms, these electrons drift until they reach the positively charged wires in the tube. This interaction creates an electrical current that is read out as a sign of a particle passing near by the wire(see figure 3.12). From this signal plus drift time information two coordinates can be measured for every detected particle: the position in the wire where the electrons hit, and the distance that those electrons travel before hitting the wire (determined using the knowledge of the electron drift velocity in the gas).
The CMS barrel is divided in 5 wheels named YB0, YB$\pm$1, and YB$\pm$2. There are 250 DT chambers in the barrel wheels. Each wheel is divided into 12 sectors, each one covering an angle of 30 degrees. There are four layers of chambers per sector, named MB1 to MB4, going from the inner-most one to the outer-most one[22][18].

Cathode Strip Chambers

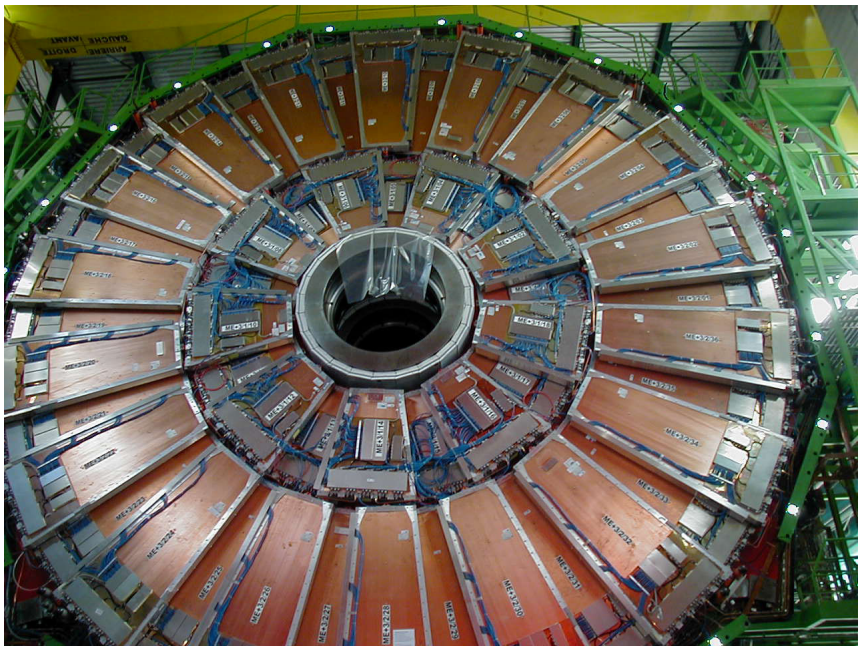

Figure 3.13: A picture of a muon end-cap disk with all the CSC mounted on it.

The CSC's are designed to trigger and register muons only in the end-caps. They consist on positively-charged anodes wires crossed with negatively-charged cathode strips made out of copper. This grid is located inside a chamber filled with an ionising gas.
When muons pass through a CSC chamber, they knock out electrons from the gas atoms. These electrons drift until they reach the anode wires, leaving behind positive ions that move to the copper cathode. This process creates two currents that can be measured, giving the CSC a very good spatial resolution in two coordinates.
The end-caps have a non uniform magnetic field, therefore a detector with a good space resolution in two dimensions, such as the CSC is needed there. The CSC system is composed by rings of trapezoidal chambers mounted on four disks on each end-cap. Each disk has rings of CSC chambers with 18 or 36 chambers per disk. There are 468 chambers in total, located in modules that contain six layers of chambers each. This arrangement allows for accurate identification of muon tracks, and a match with tracks reported in

the inner tracker. An example of how CSC are installed in the end-caps can be seen in figure 3.13[18][23].

Resistive Plate Chambers

The RPC detectors complete the muon system. They are present in the barrel and the end-caps providing redundant information both for triggering and tracking. In the barrel they are located together with the DTs, providing a tool to cross-check triggering and track reconstruction. RPC's together with the CSCs provide a similar tool in the end-caps.

The basic detection element in this system is the RPC strip. These strips

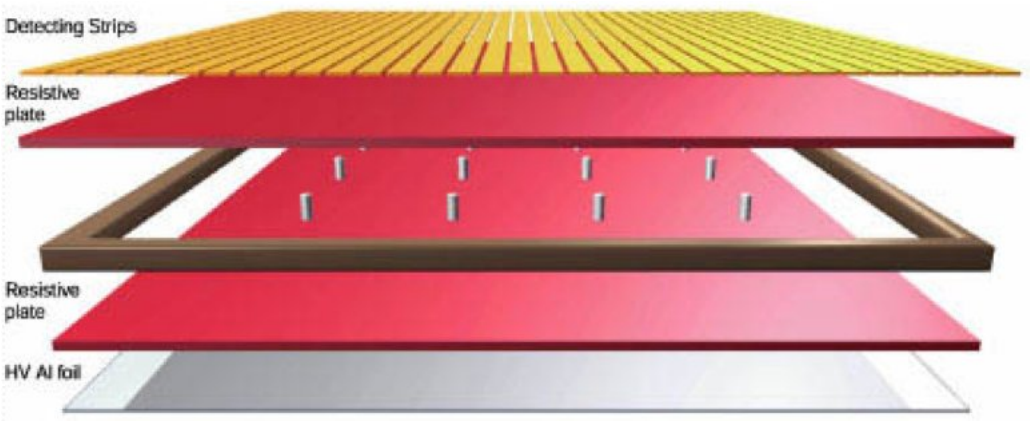

Figure 3.14: A schematic of a RPC roll.

are organised in rolls that consist of two separate parallel resistive plates, one of them being a positively-charged anode, and the other one being a negatively-charged cathode. These plates create a volume that is filled with gas that gets ionised when a charged particle traverses it. On the surface of one of the resistive plates the metallic detecting strips are located, as can be seen in figure 3.14.

A RPC chamber consist of one or several rolls of strips equipped with the same gas system. These chambers are installed fit next to the DT in the barrel yoke gaps, or are installed next to the CSCs in the endcap disks.

When a muon passes through the RPC gas produces ionisation that results in an avalanche of current, that induces a signal in one or several strips. The information of strip hits on different layers plus the information of DTs or CSCs segments is used to reconstruct Muon tracks with high space and

time resolution.
The RPC's in the barrel are distributed by sectors. There are 5 wheels called W±1, W±2, and W0. Each wheel is divided in 12 sectors each one covering an azimuthal angle of 30 degrees. Moving outwards in each sector there are 6 layers of RPC's, this layers are used to reconstruct a muon track and assign a quality value to it. A perfect track would leave 6 hits, in 6 different aligned strips, in 6 different rolls. A low quality track would only leave three hits in three different aligned rolls. Less than three hits in the RPC rolls are not considered as muons candidates.
In the end-caps the RPC's are located in a similar way as the CSC chambers. They are distributed in 6 disks called RE±1, RE±2, and RE±3. There are two rings per disk, each one with 36 rolls on it, each of these rolls covers an azimuthal angle of 10 degrees, so that the complete circumference is covered.
As a PhD student and a member of the CMS collaboration, I performed different tasks that are not directly related with my physics research but that are very important to fulfill the scientific goals of CMS. These tasks are considered service work for the collaboration. Most of my service work was done developing software tools for monitoring data quality for this subdetector. A summary of all this work is presented in the appendix A.

3.3 Trigger System

At full luminosity approximately one billion of proton-proton interactions occur per second in the interaction point of the CMS detector. The amount of data resulting from these interactions can not be recorded with the present technology, also most of these interactions are not interesting for the scientific program of the experiment; therefore a system is required to selects automatically only the interesting events. Such as system is provided by the CMS Trigger.
The trigger is designed to reduce the rate of collisions and select only the important events out of them, it is divided into a Level-1 trigger (L1 Trigger), and a High Level Trigger (HLT) which have also subdivisions on their own. In the next section a description of these systems is presented.

3.3.1 L1 Trigger

The very first step of the CMS trigger is executed by very fast electronic cards, these cards are specially designed to select events that match with physical patterns that suggest high P_T physics. This task is executed by the

L1 trigger (L1), that reduces the amount of data to be analysed from a rate of approximately one billion of interactions per second to one hundred thousand interactions per second. This is achieved by selecting only the events that may contain interesting physics, these events are potentially formed by physical objects such as for example: muons, electrons, jets, photons, or taus. The L1 is divided in sub-systems in charge of detecting these basic objects. This trigger is programmed directly on electronics, and it does not relies on normal CPU's as the High Level Trigger does.

Due to natural constraints as the speed of the electronics and the size of

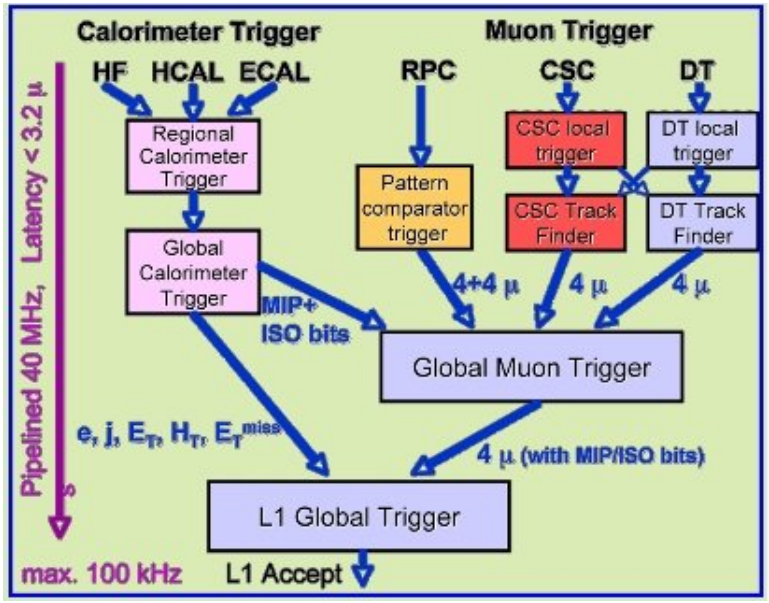

Figure 3.15: CMS L1 Trigger schematic

the cavern, the L1 trigger is forced to readout a signal, make a decision, and send the accepted events to a buffer for the HLT to analyse them in approximately 3.2 μs[24]. This time corresponds to 128 bunch crossings each one of 25 ns; time in which a very simple algorithms is required to decide which events are saved and which ones are rejected. Every operation in the L1 trigger should be repeated every 25 ns, therefore a pipeline organisation is implemented such that there are no dead times in the system.

The L1 trigger is divided in three subsystems which are the L1 Global Calorimeter Trigger, the L1 Global Muon Trigger, and the L1 Global Trigger. The description of these triggers follows.

3.3.2 Global Muon Trigger

The Global Muon Trigger (GMT) is a combination of the muon triggers that come from three detectors which are DT, RPC, and CSC. The GMT is in charge of selecting the best four muon candidates for each event and sort them by their quality. These muon candidates are sent to the Global Trigger which is in charge of making the final decision before the High Level Trigger is reached.
To select the best four muon candidates per event, the GMT has to synchronise the incoming muons and merge or suppress the duplications. It also has to give an isolation value to the muons based on the calorimeter information. More information about the GMT can be found in reference [25].
Full efficiency ($\epsilon > 95$ %) of this trigger is very important in the region of $\eta < 2.5$, because any inefficiency will affect the physics searches and results of the experiment. This trigger alone is not enough to select all possible types of interesting events, therefore other triggers based on other subdetectors are necessary, such as calorimeter triggers.

3.3.3 Global Calorimeter Trigger

The Global Calorimeter Trigger (GCT) is designed to detect signatures of isolated and non-isolated particles, such as electrons, photons, jets, and taus. It is also in charge of selecting events with high amounts of MET and total transverse energy.
The GCT chain starts at the calorimeter level with the ECAL and the HCAL. Deposits of energy on these two subdetectors are added up in the so called trigger towers, these towers are regions in the $\eta \times \phi$ plane with a size of $\Delta\eta \times \Delta\phi = 0.087 \times 0.087$. They are analysed by the Regional Calorimeter Trigger (RCT) which identifies isolated and non-isolated candidates for photons and electrons, and adds up the trigger towers to form trigger regions.
The GCT receives the information coming from the RCT to identify and classify jets, calculate the missing and the total transverse energy of an event, and sort the events by its transverse energy. The four better candidates of each category (isolated and non-isolated electrons and photons, central jets, forward jets, and tau jets) are sent to the global trigger to make the final decision. More information about this trigger can be found in reference [26]

3.3.4 Global Trigger

After the GMT and the GCT have selected the best four candidates of each category, they send the selected objects to the Global Trigger (GT). The L1 GT divides the information coming from the GMT and the GCT into 128 channels called trigger bits, each one corresponding to a trigger algorithm based in most of the cases on a physical object, for instance MET, H_T, Jets, etc. These bits are used as input for the High Level Trigger, which receives the information and has the last decision on when this event is saved or not. In addition to the 128 trigger bits, there are 64 more technical triggers bits which are used to perform tasks like for instance record cosmic muons during collisions, which are used to calibrate the geometry of the central tracker. More information about the GT can be found in reference [27].
An schematic with the complete L1 trigger workflow can be seen in figure 3.15

3.3.5 High Level Trigger

The second big step in the reduction of the data rate is performed by the High Level Trigger (HLT), that reduces the trigger rate from one hundred thousand to only one hundred events per second. The HLT is implemented on a computer farm of more than a thousand processors, this computers run very fast algorithms to select the interesting events in about a tenth of a second. This information is saved and stored in the global Grid to be analysed later. The criteria of the HLT algorithms are more sophisticated than the ones used by the L1 trigger.
The HLT must have a high efficiency to successfully fulfill the CMS physics program. The reconstruction of the objects in the HLT should be as close as possible to the off-line reconstruction, so that no big differences between the reconstructed objects and the triggered ones exist. The LHC reaches an energy that has never been reached before, therefore the HLT trigger should be as inclusive as possible so that unknown phenomena are not lost in the process. More information about the HLT can be found in reference [28].
Once the HLT has accepted events, it splits them into datasets depending on the triggers paths they followed. These datasets are sets of triggers that have something in common, for example a muon dataset will include all triggers based on muons. These datasets are sent to be stored at CERN computer centre and immediately distributed to the computing structure of the CMS, so that all the accepted events are available via GRID.

3.3.6 CMS Computing Model

In order to provide CMS and the other LHC experiments with the needed computing capabilities, CERN implemented a world wide computer network called GRID in order to share CPU and storage capabilities in real time. The GRID is a world-wide-net of computers connected together in a hierarchical organisation so that the users around the world can all share data and computational power. The GRID is divided by clusters of computers called "Tiers" which are classified depending on its computational power, storage capacity, and internet speed connection (see figure 3.16).

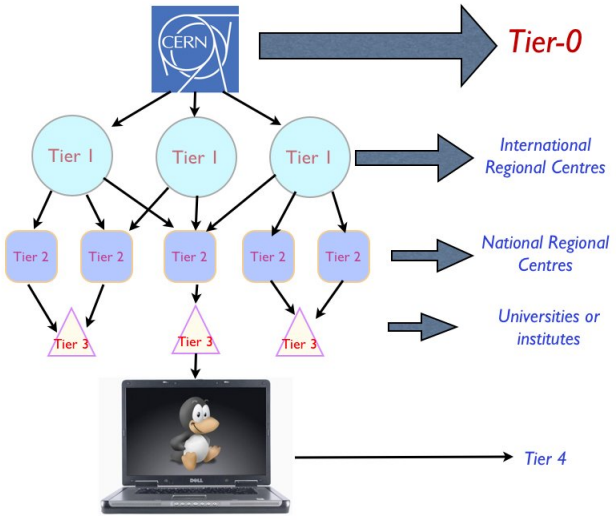

Figure 3.16: The tier structure of CMS GRID is shown.

- The first tier is called Tier 0, it must have enough space to store all data collected by the experiment. It is here where all raw information coming from the detector is saved, reconstructed, and later on transmitted to the rest of the chain.
- The second type of cluster is the Tier 1. There are several of these Tiers around the world, organised in international regional centres. In these Tiers further reconstruction and analysis, together with production of simulated data is done, stored, and distributed to smaller Tiers.
- The third type of tier is the Tier 2. there are several of them located basically at national centres. These Tiers are used for local data

analysis and simulation.

- The fourth of the Tiers is the Tier 3, which is basically a small cluster of computers installed at an institute in order to provide local analysis capabilities and access to the GRID resources.
- The last Tier is the Tier 4 which are the desktops and laptops of the users involved in the experiment.

The complete Tier structure can be seen in figure 3.16.
Next chapter presents a description of how the data taken with the CMS detector is reconstructed. This reconstruction uses all the subsystems mentioned in this chapter.

Chapter 4

Event Reconstruction in CMS

The events saved by the CMS trigger are initially stored in a raw format (RAW) that contains only detector information. To produce events that contain physical objects, a reconstruction is needed. The reconstructed data (RECO) is produced by processing the RAW data with software that implements algorithms in order to obtain objects like electron, photons, muons, jets, and missing energy. The output of this process is a RECO dataset that includes all physical objects on it, this type of data is sent to the Tiers 2 where it is accessible to CMS users.
Currently there are two ways to reconstruct a physical object for a given event. The first reconstruction framework which is the most used in the collaboration is called in this thesis Standard Reconstruction (SR). The second framework which is based in more detailed algorithms is called Particle Flow (PF). A description of these two frameworks is presented in the following sections.

4.1 Standard Reconstruction

The SR is the way in which all CMS objects are reconstructed at both off-line and trigger levels. The SR algorithms reconstruct particles by optimising the computational and time resources available. More complex and accurate reconstructions are often possible but they require more time and computational power.
The SR objects in CMS are widely used and have been commissioned with good results, however in this type of reconstruction not all event information

is used. SR does not reconstruct the complete set of particles present in an event.

4.2 Particle Flow Reconstruction

A second type of reconstruction is done by the PF algorithms. These algorithms are designed to reconstruct all particles of an event including hadron candidates. This reconstruction relies on a compact detector that does not have energy losses and therefore allows a complete measurement of the energy deposited by each particle in all subdetectors. PF optimises every particle reconstruction using the complete set of subdetectors that may include information about it. The RECO process in CMS produces both kind of particles: SR and PF, therefore every analysis can be made in both ways[29].

4.3 Experimental Reconstructed Physical Objects

All CMS subdetectors contribute with a specific task in the particle detection, however the information collected by them would be meaningless without the appropriate reconstruction algorithms. A description of how each particle or physical object is reconstructed by the CMS detector in both frameworks, SR and PF, together with a description of the important experimental variables used in a SUSY search is presented in the following sections.

4.3.1 Photons

The main instrument for photon detection is the ECAL. In this subdetector these particles are reconstructed using the energy deposits leaved in the crystals. When a photon is produced it crosses the tracker detector basically without any interaction, being detected only when it arrives at the ECAL. There, its detection is possible due to the interaction with the dense material of the PbWO4 crystals. From this interaction an electromagnetic shower of electron-positron pairs and bremsstrahlung photons is created. Due to the strong magnetic field inside the calorimeter, the showers spread in the ϕ coordinate as they move away from the collision point, leaving a wider energy deposition pattern in the ECAL.
The deposits in the ECAL are collected together to form clusters. These clusters can be added up with neighbour ones to form Super Clusters (SC)

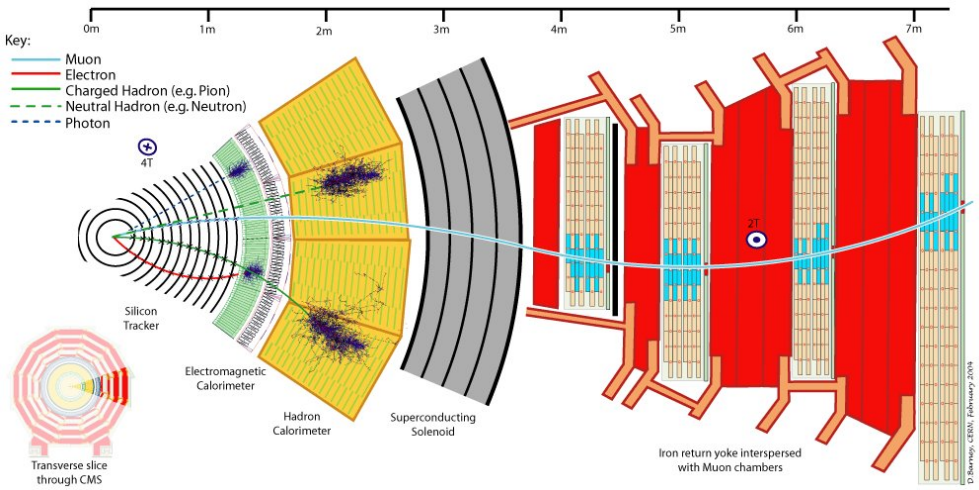

Figure 4.1: A representation of how the particles are detected in the CMS experiment.

extended in ϕ. These SC are the seeds for the electrons and the photons reconstructed in the calorimeter.
To distinguish if the clusters belong to electrons or photons, the basic difference in detection between these two particles is used. Since the electrons are charged, they do interact with the tracker leaving a track that can be matched to a SC. On the other hand, when a photon is reconstructed no track is expected to match the SC (see figure 4.1). Other identification cuts are required for photons, such as isolation. These cuts were not required in this analysis and therefore they are not described, however they can be found in reference[30].

4.3.2 Electrons

The electron reconstruction uses the same SCs used in the photon reconstruction. In the case of electrons these SCs are preselected choosing only those with energy deposition above 4 GeV. The selected SCs are matched with a pair or a triplet of hits in the inner tracker or in the tracker end-caps. When a matching is found, the complete object (SC + hits) is taken as a seed for the electron reconstruction.
As part of the electron identification a veto on high values of the ratio between the energy deposited in the HCAL over the energy deposited in the ECAL (H/E) in the same direction is applied. This veto is there to guaran-

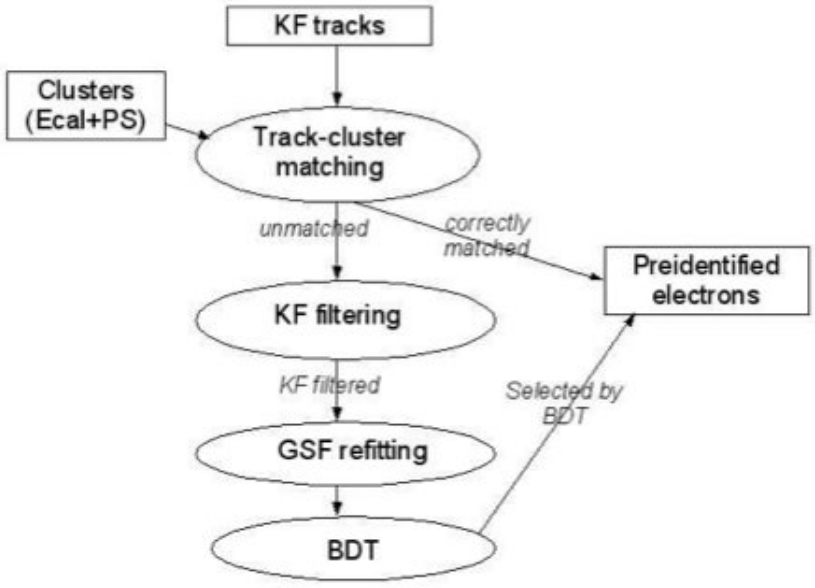

(a)

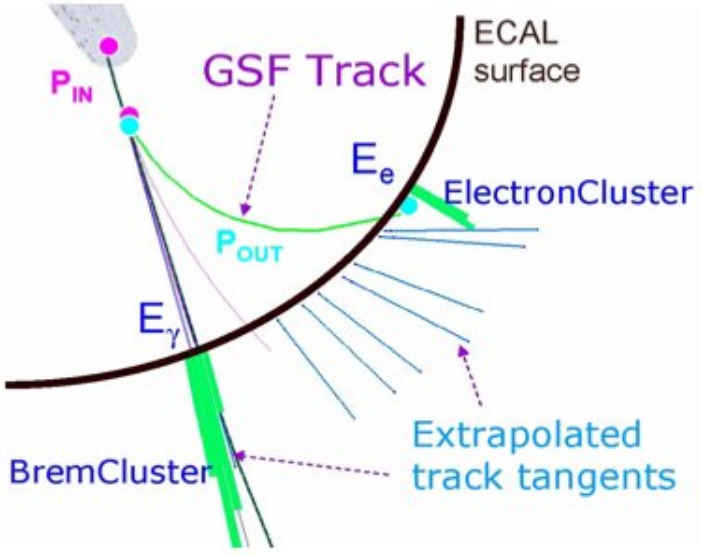

(b)

Figure 4.2: The graph 4.2(a) shows a representation of how the electron reconstruction algorithm works, the graph 4.2(b) shows how an electron track looks when a photon has been radiated[31].

tee low hadronic contributions to the electron candidates.

There are cases in which the SC seed does not contains all the information of an electron, as for example the case in which an electron radiates a photon before it reaches the calorimeter. In these cases there are two SC in the calorimeter, one corresponding to the electron after radiation, and the other one corresponding to the radiated photon. To account for this kind of cases properly, algorithms that use the tracker information have been implemented.

The SR algorithm uses a Kalman Filter (KF) algorithm to reconstruct the electron tracks [32]. The KF algorithm works well when an electron does not radiate. In this case the tracks can be reconstructed easily, because they are usually located inside a cone in the tracker that points to the SC. However, there are cases in which the real track of the electron is too curved, and the KF algorithm fails to reconstruct it, for these cases more considerations are needed to properly distinguish electron tracks.

There is another algorithm used to reconstruct tracks, this one requires more computational time but it can follow the curve of the tracks in the case where radiation is present. This algorithm is called Gaussian Sum Filter (GSF) and is the one used by the PF electron reconstruction. This algorithm is more precise than the KF, and leads to better reconstructed trajectories. A graphical representation of how the electron reconstruction algorithm works, and how the electrons that have a radiated photon are reconstructed is shown in figure 4.2.

Besides tracks and SC matching, other quantities are considered to identify electrons correctly, these quantities are:

- the ratio between the electron energy and the electron momentum (E/P). This cut guarantees that the reconstructed particle has a small mass if the ratio is required to be close to unity,
- the output of a Multi-Variable Analysis (MVA) using a Boosted Decision Tree (BDT) (for more details see references [33][31][34]). It helps to discriminate pions from electrons,
- the $\Delta\eta$ cut that measures how much different are the η extrapolated from the track of the electron to the calorimeter, and the η of the electron SC after being weighted in energy,
- and a similar cut in $\Delta\phi$[33][31].

The plots showing the performance of the E/P and the BDT cuts are shown in figure 4.3. From the plots one can see how these criteria rejects most of

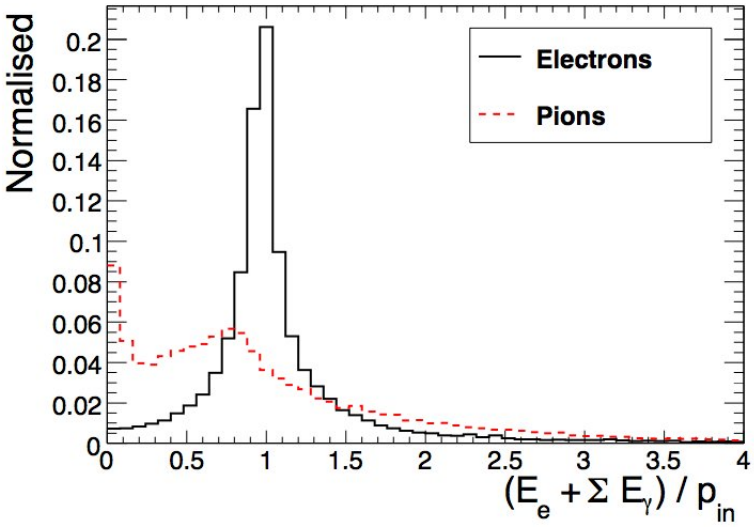

(a)

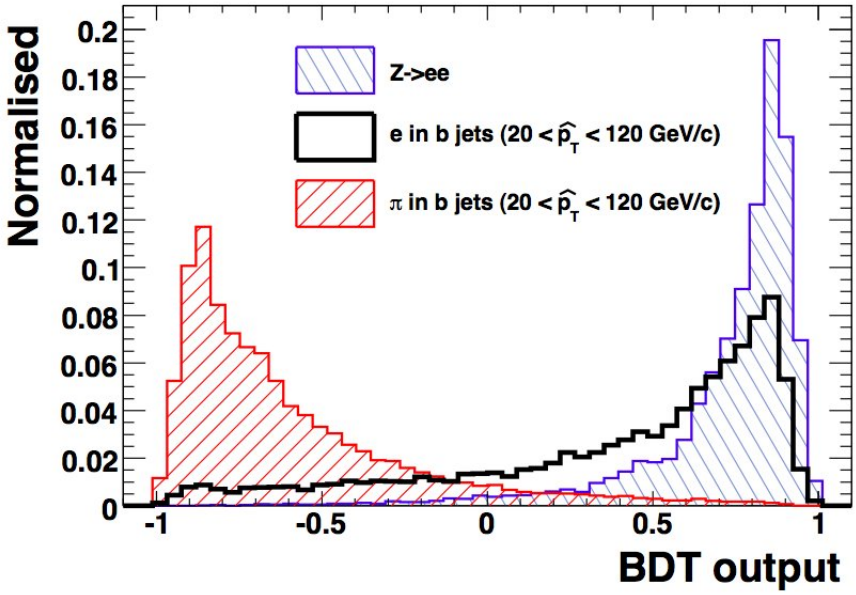

(b)

Figure 4.3: The plot 4.3(a) shows the distribution of E/P for electrons and for pions used in the electron identification. The plot 4.3(b) shows the distribution of the boosted decision tree output for PF electrons[31].

the pions present within the electron candidate sample.

4.3.3 Muons

When a high P_T muon is produced in CMS, it traverses the entire detector without being stopped. Muons interact with the entire detector leaving signals that can be used for their identification in all subsystems, therefore their reconstruction algorithm uses the entire CMS.
The first step needed to identify muons is to find a seed in the muon system. This seed is taken from the DT or CSC segments. DT segments when the muon passes through the barrel, and CSC segments when it passes through the end-caps.
The kinematical variables of the muon seeds are estimated using the segments produced in the DT or CSC chambers. These segments together with the RPC hits can reconstruct what is called a "Stand-Alone muon" (SA), which is basically a muon candidate reconstructed using only the muon system.
These muon candidates are reconstructed using segments as seeds coming from specific chambers. These seeds are extrapolated to the next chambers looking for matching segments or hits. If there is a match, the seed is updated with the next segment and a new extrapolation is done until all muon system is scanned. This process is done by steps, propagating from one layer to the next one the hits and the segments in the muon chambers. There are several algorithms to make these extrapolations, however the most used method is the one that extrapolates the next step with a helix parametrisations of the track. This extrapolation includes all effects produced by the interaction of the muons with the detector material.
Muons are also reconstructed in the tracker. This kind of muon candidates are called tracker muons and are basically isolated tracks. Tracker muons can be matched with the calorimeter information, so that tracks that leave small deposits in the calorimeters can be identified as "calorimeter muons" or CaloMuons. Tracker muons can also be propagated and matched to SA muons to produce muon candidates that use information from the complete detector. This kind of muon candidates are called "Global Muons" and are the ones that have the best estimation of the complete track and momentum[35]. In case of ambiguities in the track reconstruction and matching, the best muon candidate is chosen based on a best χ^2 criteria.

4.3.4 Jets

There are four kind of jets that CMS defines, these jets are born from the different combinations of the subdetector information used to reconstruct them. These jets are classified as:

- Calorimeter jets (CALO-Jets): Constructed using only the information coming from the CMS calorimeters. Particles that traverse the calorimeter leave energy deposits on the calorimeter cells, these cells are added up to construct clusters of cells which are interpreted as jets.

- Track jets: Produced by clustering the tracks in the tracker detector and associating them with a jet.

- Calorimeter-plus-track jets (Jets Plus Track jets or JPT): These jets combine the information of the calorimeters and the tracker. These jets are created using the clusters of energy formed by the calorimeter cells exactly as in the case of the CALO-Jets. Once the CALO-Jets are formed, the tracks are associated with a cluster based on a spatial separation in the η, ϕ plane, between the CALO-Jet and the track being considered. Tracks are then classified as inside-tracks or outside-tracks, this classification depends on the direction where the tracks are pointing, if they are pointing to the corresponding CALO-Jet they are called inside-tracks, if they are pointing outside the jet they are called outside-tracks. The JPT jets are later on corrected with the information of the tracks, the momentum of the tracks is added up to the associated jet energy, and the direction of the jet is also corrected.

- Particle Flow jets (PF Jets): These jets are constructed using a collection of previously identified particle candidates. The first step of the PF algorithm is to identify all particles of an event as leptons, charged hadrons, neutral hadrons, or photons. After these identifications PF jets are formed using these particles as input. Schemes representing these four type of jets in the detector can be seen in figure 4.4 [36].

CMS jets can be classified depending on the detectors that were used to construct them, however to obtain a collection of jets, a clustering algorithm is needed. CMS supports four types of algorithms that create jets with different topologies, these topologies are different depending on how the constituent particles of a jet are clustered. The basic topology consists in a cone of a radius defined as $R = \sqrt{\Delta\phi^2 + \Delta\eta^2}$, however some cases are different. The algorithms supported by CMS are described below:

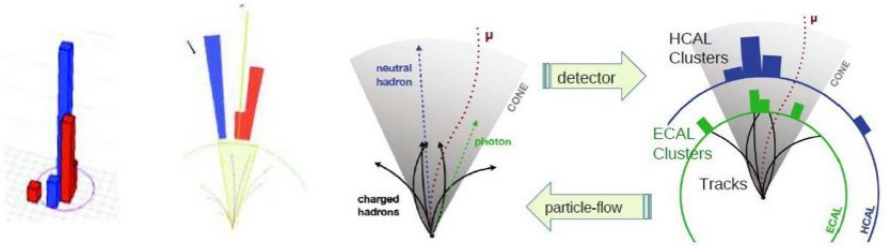

Figure 4.4: The picture of the left shows a representation of how the calorimeter jets are reconstructed. In this case the red and the blue columns represent energy deposits in the ECAL and the HCAL respectively. The second picture shows a JPT jet reconstruction; the third picture shows PF candidates clustered as a jet; and the right most picture shows the same PF jet from a detector point of view.

- Iterative Cone: In this algorithm a list of objects ordered by P_T is given as input. From these objects the first one is taken as a seed for a proto-jet, then all objects within a cone of a determined radius around the seed are taken as constituents of this proto-jet. From this subset a new jet axis is re-calculated and used as a new seed. This process is repeated until the jet axis is stable. Once the jet axis reaches stability all the objects that constitute the jet are taken out of the initial list of objects and assigned to the identified jet. Then, with the reduced list of ordered jets, the process is started again until the list is exhausted. This algorithm is not infrared-safe, nor collinear-safe (this is an important issue that will be discussed in detail later).

- Midpoint Cone: This algorithm works similar to the Iterative cone algorithm, however in this case the constituents of the proto-jets are not removed from the original input list of particles. This fact allows the proto-jets to be overlapped. Once a proto-jets list is created, for each pair of jets laying in a cone radius closer than R, the midpoint is used as an additional seed and therefore some proto-jets are merged. The Midpoint cone algorithm is not infrared-safe, and nor collinear-safe.

- Seedless Infrared-Safe Cone (**SIS** cone):This algorithm first looks for all possible stable cones of radius R from the total number of particles in an event. For each stable cone a proto-jet is created and removed

from the initial list of particles. The difference between this algorithm and the previously described ones lies in the definition of a stable cone. For the SIS algorithm a stable cone is defined as the cone that is invariant under a second algorithm that checks for the possible other cones formed by the particles inside a 2R distance in the $\eta\phi$ plane. If there are not any particles, then the initial cone is immediately selected as a proto-jet, declared stable, and the constituent particles are taken out of the initial list of particles and assigned to the cone. A complete description of this algorithm can be found at reference [37]. This algorithm is both collinear and infrared safe.

- Clustering algorithm ($\mathbf{K_T}$), and anti-clustering algorithm ($a\mathbf{K_T}$): These algorithms are based in a different metric that relies on the transverse energy of the constituent particles. Initially all input particles are taken in any order, each particle is taken as a proto-jet. For each proto-jet a distance value is assigned, defined as $d_i = E^2_{T,i}$. This proto-jet is compared with all other proto-jets present in the event, so that a distance between each pair of proto-jets is defined as $d_{ij} = min(E^2_{T,i}, E^2_{T,j})[(\eta_i - \eta_j)^2 + (\phi_i - \phi_j)^2]/R^2$, where R is the value previously defined. Afterwards the smallest d_i and d_{ij} are found and compared, if the smallest value is d_i, this jet cannot be merged, and is taken out of the list of available proto-jets. If on the contrary, d_{ij} is the smallest value then both jets are merged. The entire procedure is repeated until all jets are stable. This algorithm is known as $\mathbf{K_T}$, the other algorithm $a\mathbf{K_T}$ is basically obtained by multiplying the distances by (-1). These algorithms are both infrared-safe and collinear-safe[38].

CMS supports the algorithms: $a\mathbf{K_T}$ with a radius of 0.5, and 0.7; SIS cone with a radius of 0.5, and 0.7; and $\mathbf{K_T}$ with a radius of 0.4, and 0.6. These algorithms are both infrared and collinear safe which are important requirements for a jet reconstruction. Some jet algorithms need a seed as input to produce a final collection of jets, this seed may have a threshold in energy resulting in a energy dependence of the final jets. When such an algorithm is applied to the case in which a single energetic particle produces two collinear particles, of which one may be below the threshold, the algorithm will fail to reconstruct correctly the jet. An algorithm is called collinear-safe if it is protected from such cases[39].
The second case appears when production cross-sections are calculated at parton level, these cross-sections should be finite despite the infrared divergences present in the Feynman diagrams, these divergencies are presented when infrared photons are radiated from a particle as a product of a large

distance interaction. An algorithm that clusters jets without being affected by these type of processes is called infrared-safe[38].
As it has been presented, there are several algorithms to reconstruct jets in CMS. This obeys to the complexity of identify them. First of all, in every bunch crossing there are more than 10 proton-proton interactions, and each of these interactions produces several particles and jets. Only one out of these interactions is produced at high P_T, otherwise the L1-trigger would have rejected the event (bunch crossings with more than one high P_T interaction is highly improbable). Second, given a proton-proton interaction at high P_T, only a couple of partons would participate of it, and the expectator partons will hadronize producing more particles and jets. As a consequence, there is a huge amount of particles and jets in every high P_T bunch crossing. Of course the signal of the parton-parton high P_T interaction can be cleaned by making suitable P_T cuts on the different physics objects including the jets. However, where to establish that cut is a matter of choice, and affects the sample of accepted particles. Under these conditions, which are the jets present in the final sample, which tracks belong to one jet, and which tracks belong to another jet may vary when using one algorithm or another.
The algorithms used by CMS (mentioned above) can be used in conjunction and they serve as double check of each other. The most used algorithm in this work is the $a\mathbf{K_T}0.5$, even though cross-checks have been done with other algorithms.

4.3.5 Taus

The reconstruction of tau leptons is more difficult than that of muons or electrons, because taus are much heavier and unstable, decaying very fast and in many more modes than for example the muons. Actually approximately two thirds of the decay modes of the taus are purely hadronic, and have final state signatures very similar to those that quark-gluon, or QCD processes produce. This implies an experimental challenge because the production cross sections for the processes that can fake a tau are generally orders of magnitude higher than the tau production cross section, therefore, identifying them implies a very good rejection of fakes.
There are several tau reconstruction algorithms in CMS, they can be listed as:

- Track Corrected Tau algorithm (TCTau): This algorithm aims to identify the taus that decay into leptons. It does so by considering the tracks and the energy deposits in the calorimeters. First a jet candidate for a tau is selected, and a leading track associated to this jet is

chosen. This track is the one with the highest momentum bigger than 5 GeV/c, it should have also a transverse impact parameter less than 1 mm. All other tracks in between a tight cone are considered as decay products of the tau if they differ in the z-impact parameter no more than 10 mm. An isolation requirement is also included to complete the identification.
To calculate the energy and momentum of the tau, jets reconstructed with the $a\mathbf{K_T}$ algorithm with a radius of 0.5 are taken. After all track corrections are applied, an estimation of the tau momentum is done, the details can be found in reference[40].

- Cut based particle-flow fixed and shrinking cone: In these algorithms the taus are identified by adding up all four-momentum vectors of the particles associated with a jet candidate of a tau. Particles are considered if the momentum is bigger than 0.5 GeV/c, and are located inside a $R < 0.15$ cone around the leading track. This track is selected inside a cone of $R < 0.1$ around the jet direction, and is required to have a momentum bigger than 5 GeV.
There are two possibilities for the particle-flow isolation cuts used in the tau identification, both of them consider the same radius $R < 0.5$ for the isolation of the tau, however the cone in which the tau is expected to be contained varies. The first possibility is a fixed cone in which all photons at a distance $R < 0.15$ from the leading track, and all charged hadrons at a distance $R < 0.07$ are considered part of the signal. In the shrinking cone algorithm the photons inside a fixed cone of $R < 0.15$ are considered part of the signal, but for the charged hadrons the cone is defined as $R < 0.5/E_T$, where E_T is the transverse energy of the PF tau jet. The details of the algorithm can be found in references[40].

- Tau Neural Classifier (TaNC): This algorithm was created to improve the isolated based tau identification algorithms, it considers the different hadronic decay modes of the taus individually. The dominant tau hadronic decays have one or three $\pi^{\pm}$ and up to two π^0 mesons, these decays proceed through intermediate resonances that can be mapped to a tau initial state. This approach is used by the Tau Neural Classifier algorithm implementing two complementary technics which are: a method to reconstruct the decay mode, and an ensemble of neural network classifiers used to identify each decay mode resonance and to reject the background produced by quarks and gluons. The details can

be found in references[40, 41].

Since taus produce jet like signatures, their reconstruction has the same kind of complexities of the jet reconstruction, but even more the algorithms have to be able to differentiate between taus and jets with a fairly good efficiency. The analysis that includes taus uses a combination of different algorithms that serve as cross-check of the reconstruction.
When all events have been reconstructed, and their constituents have been identified, physics analysis can be done with the reconstructed data. Next chapter presents a description of how SUSY is being searched in the CMS experiment. These type of searches are based in all what has been described in this chapter.

Chapter 5

Search for SUSY Signals in the CMS Experiment

SUSY can produce many different final topologies in the LHC collisions, therefore several kinds of analysis have been designed to perform a comprehensive search. These analyses must be inclusive so that no new physics is wiped out by very exigent cuts. Besides, since no experimental signature of SUSY has ever been discovered, there is a complete ignorance about which topologies to expect.
Even though there is no phenomenological information about SUSY, the early searches must be based on predictions of theoretical models. In these sense, theoretical benchmarks are important as examples of possible topologies used to design SUSY analysis strategies. These benchmarks are chosen to provide a wide variety of possible signals so that the analysis tools are as general as they can be. It is not the goal of the initial analysis to confirm or rule out the theoretical model from which the benchmarks were chosen, but to do a complete scan of the energy region not yet explored. In the following sections a brief description of the CMS strategy for SUSY searches is presented.

5.1 SUSY Search Benchmarks

The CMS collaboration has chosen a set of theoretical benchmark points in order to design the search strategies and the software tools to look for SUSY signatures. Most of these benchmarks are based on the mSUGRA model. The choice of this particular model obeys to the reduced parameter space that it provides in the GUT scenario. The main purpose of the particular

benchmark points was to provide examples of topologies to search for, trying not to miss any. They serve as guides for the design of analysis that do not adhere strictly to the details of the specific model.
As it was presented in chapter 2, there are some official mSUGRA benchmark points chosen by CMS divided in low mass (LM), high mass (HM), and some other combinations. These points were chosen thinking on a long term in which the LHC will reach the 14 TeV center of mass energy and a very high luminosity accumulating data over a period of several years. However at this early stage the reduced center of mass energy and luminosity, only allows to scan a low mass region.
The most inclusive signal of production of SUSY that one can search for includes, energetic jets pointing to a high P_T process, and a large amount of missing transverse energy pointing to the production of a couple of LSPs. A possible next step when moving to a more exclusive analysis, is to require the presence of isolated leptons. From the SM it is known that most of the isolated leptons come from electroweak processes which are kinematically well known. Any kinematic difference, or any difference in the production cross section for a certain number of leptons would be a signal of new physics. If these isolated leptons come together with high P_T jets and missing transverse energy, they could point towards production of SUSY matter. Therefore, final states with isolated leptons are a good scenario to discover new physics including SUSY.
The CMS SUSY searches have been divided into hadronic and leptonic searches in view of the possibilities mentioned above. A short description of both type of searches is given in the next sections.

5.2 Hadronic Searches

The cases in which SUSY decays only in hadronic channels are considered by the CMS SUSY group and divided in three cases which are: the case in which an exclusive search is done for several number of jets (2,3 or more jets); the case of an inclusive analysis that requires 3 or more jets; and a third case based on the presence of isolated photons and MET in the final state. Even though all these cases demand the presence of missing transverse energy, other experimental variables related with SUSY may play an important role too. These variables will be discussed in detail in the next sections.

5.3 Leptonic Searches

The CMS SUSY group divided the leptonic analysis based on the number of leptons produced in the final state. The most basic search is based on events with a single isolated lepton in the final state (plus jets and missing transverse energy), this final lepton can be either an electron, a muon, or a tau. This analysis has the highest statistics of all leptonic cases, however it also has the highest background coming from the SM.
The single lepton analysis is based on selecting events with MET, several number of jets, high H_T, and one lepton (these variables will be defined in the following sections). This signal is easily faked by top anti-top production, and electroweak processes such as W production.
The second option for a leptonic analysis is the case in which there are two leptons in the final state. This topology can be divided in two analysis which are: same sign leptons, and opposite sign leptons.
The double lepton analysis consist on a final signature that can mix all lepton flavours. The analysis is based in a high MET and a dense jet environment, together with the presence of two isolated leptons. In this case the signal to background significance increases in comparison with the single lepton case, where the significance is defined as:

$$Sig = \frac{N_Signal}{\sqrt{N_{Background}}}.$$

In the double lepton case, when the leptons have the same electric charge, the number of background events is highly reduced because SM processes do not have high production cross-sections for these kind of final states. The counterpart comes from the reduced statistics for this channel.
The third case that is being considered by the CMS SUSY group has three leptons in the final state with all possible combinations of flavour and electric charges. The fourth and last case is the case in which there are two leptons and an isolated photon present.
All these analyses represent the initial effort that CMS is doing in the search for SUSY. The present work is focused on the same-sign leptonic channel.

5.4 Reference Analyses

Within the hadronic and leptonic searches described in the previous section, the CMS SUSY group has defined eight different reference analyses (RA). The hadronic RAs are:

- RA1, Exclusive n-jet analysis.
- RA2, Inclusive 3 or more jets analysis.
- RA3, Photons plus MET analysis.

The leptonic RAs are:

- RA4, Single lepton analysis.
- RA5, Same-sign double lepton analysis.
- RA6, Opposite-sign double lepton analysis.
- RA7, Triple lepton analysis.
- RA8, Double lepton plus photon analysis.

This thesis is focused on the leptonic RA5 analysis that studies the same sign double lepton signal. This signal also includes cuts in MET and HT besides of some other demanding cuts. Since this search is leptonic, only that kind of signals are going to be considered.

5.5 Experimental Variables

Even though the final topology for each RA is different, some of the cuts used are common to all of them. These cuts are defined based on a set of experimental variables that are either specifically designed for a SUSY analysis or very important for this kind of analysis. In the next sections a description of all important and widely used variables is presented.

5.5.1 MET

In the SM the only particles that can escape from detection by a hermetic detector like CMS are the neutrinos. These almost massless particles only interact weakly and therefore detecting them is very difficult. In the search for new physics, specially SUSY, the production of massive weakly interacting particles is expected. These particles will escape detection by CMS in the same way as the neutrinos do (like the neutralinos). The experimental signature of these particles in the CMS experiment would be a directional

unbalance in the transverse energy measured by the detector. This quantity is called Missing Transverse Energy (MET) and it is defined as:

$$MET = |-\sum_{i=0}^{N_T} \vec{E}_{T,i}| = \sum_{i=0}^{N_T} E_i(sin(\theta_i)cos(\phi_i)\hat{i} + sin(\theta_i)sin(\phi_i)\hat{j}), \quad (5.1)$$

where N_T is the total number of particles in an event, and $\vec{E}_{T,i}$ are all the energy deposits present in the detector in a specific direction. CMS has defined three different versions of MET which are:

- CaloMET: This MET is formed by the energy deposited in the calorimeters of the CMS. It is corrected when muons are detected, so that the total energy of the event is included in the calculation.

- tcMET: This MET takes the CaloMET as input, but is later on corrected using the tracking information present in the event.

- pfMET: The particle-flow MET is constructed after the entire set of particles of the event is reconstructed. Once that is achieved the total four-momentum of the event is found, the transverse energy of this final vector is taken as the negative of the particle-flow MET[42].

MET is one of the most promising variables in the search for new physics. It has a discriminating power between QCD and SUSY processes. In SUSY, the most important background for this variable is due to top anti-top quarks decay which may produce two energetic neutrinos.

5.5.2 H_T

SUSY is expected to be produced in very dense environments, because most of the s-particles are expected to be heavy (heavier than a hundred GeV). This implies that the calorimeters will have large amounts of energy deposited on them. This energy will come from jets produced in the decay of gluinos or squarks, as well as high momentum lepton deposits produced by electrons and taus.
To measure such effect a scalar variable called H_T is used. This variable is defined as the sum of the transverse momentum of the jets involved in the event.

$$H_T = \sum_{i=0}^{N_J} |\vec{P}_{T,i}|, \quad (5.2)$$

where N_J is the total number of jets in the event. This variable is used as a necessary requirement in most SUSY analyses, and also as a trigger for a SUSY signal. A large value of H_T is a signature of energetic jets production.

5.5.3 MHT

H_T is expected to be high (some hundreds of GeV) in SUSY events, however, in some cases it could happen that an unbalance in the total transverse jet energies is present. This unbalance is assigned to a variable called Missing HT or MHT. This variable is useful in a purely hadronic environment to discriminate events of new physics such as SUSY. MHT is defined as:

$$MHT = |-\sum_{i=0}^{N_J} \vec{P}_{T,i}|, \tag{5.3}$$

this variable is similar to MET, but it contains the information of the jets only.

5.5.4 $\alpha_{\mathbf{T}}$

Another important variable in the hadronic SUSY searches is called α_T. This variable measures the asymmetry present in events with 2 or more jets.
In normal QCD events with two jets are expected to be back to back and its total transverse momentum is expected to cancel out. Any deviation from this behaviour will be a signature of MET. Some analysis rely on this property to define a variable called α_T as an alternative or a complement to MET.
In the case of events with two jets, α_T is defined as:

$$\alpha_T = \frac{P_{T2}}{M_T} = \sqrt{\frac{P_{T2}}{2P_{T1}(1-\cos\Delta\phi)}}, \tag{5.4}$$

where: P_{T1} and P_{T2} are the transverse momentum of the jets one and two, $\Delta\phi$ is the angular separation between the two jets, and M_T stands for the transverse mass of the two jets. If the angular separation of the two jets is 180°, M_T is a maximum and α_T is peaked at 0.5, which is the case of pure QCD events. α_T is expected to have a pronounced tail when MET is present.

In the case were n-jets are present, this variable is defined as:

$$\alpha_T = \frac{H_T - \Delta H_T}{2M_T} = \frac{H_T - \Delta H_T}{2\sqrt{H_T^2 - MHT^2}}. \tag{5.5}$$

In this case all jets must be merged until two final pseudo-jets are formed. From these two final objects ΔH_T is calculated to obtain a value for α_T. There are several ways to create the two pseudo-jets needed to calculate ΔH_T, so far the most used consist in calculate the combination of pseudo-jets that minimise this variable.
This α_T definition has a maximum when ΔH_T, and MHT are both zero. This implies that the transverse momentum of the jets is balanced and there is no missing energy present due to a missing jet. In the case in which SUSY is present, this definition of α_T presents a huge tail due to energy gone with the SUSY particles produced.
α_T is mostly used in hadronic searches, however there exist a leptonic version of it[43].

Chapter 6

Search for SUSY in Events with Same-Sign Double Leptons

If SUSY exists it will be produced in the LHC collisions most likely in the form of gluinos and squarks, and in the case in which R-parity is conserved these particles will be produced in pairs: gluino-squark, gluino-gluino, and squark anti-squark. In some SUSY models, gluinos are expected to be Majorana particles. In this cases the gluinos will produce a decay chain that will lead to leptons of both signs with the same probability, therefore gluino pair production and gluino-squark production will produce same-sign double leptons fifty percent of the times, in the cases were the final states of both decay chains are leptonic.
The goal of the analysis presented in this thesis is to find signals of production of SUSY in the LHC data. To achieve this goal the same-sign double lepton channel is studied by searching for significant statistical differences from the standard model.
In the following sections the details of the analysis done in the same-sign double lepton channel are described.

6.1 Final State Signals

As it was mentioned before, if SUSY matter is produced its signature in the detector will be marked by the presence of large amounts of MET, large deposits of energy in the calorimeters that can be identified with a large H_T; and in the leptonic case, isolated leptons produced by charginos or

neutralinos.
As was discussed in the previous section, in fifty percent of the cases in which two leptons are present in the final state, these leptons will have the same sign. Since the leptons present in the final state could have any of the three possible flavours, all the combinations ee, $\mu\mu$, $\tau\tau$, $e\mu$, $e\tau$, and $\mu\tau$ are possible with the same probability. However reconstruction efficiency for each kind of lepton is different (the best one for the muons, a very good one for electrons, and less efficient in the case of taus since they quickly decay into other particles).

6.2 Trigger

In order to select the interesting events for a double-lepton-same-sign analysis, two trigger strategies have been used. The first option has been to use a leptonic trigger. In this case, events with either an electron, a muon, or a tau are accepted. Leptonic triggers allow the experimentalist to select events with low MET and H_T thresholds, however this type of analysis usually requires a cut in the lepton P_T higher than 20 GeV. Lower cuts are not allowed without a pre-scale factor because they will increment HLT rates beyond the acceptable limits.

The second trigger option for a same sign double lepton analysis, is the case in which events are selected using a hadronic trigger. This kind of trigger increases the acceptance of leptons with low P_T (as low as the reconstruction allows it to be). This quality can be used in the case in which charginos and neutralinos have a degenerate mass. In this case, leptons produced by the decay of a neutralino into another lighter neutralino are soft (they will present a low P_T spectrum). These leptons cannot be triggered with a lepton trigger due to its low momentum, therefore a hadronic approach is mandatory.
The analysis presented in this thesis is optimised to search for low P_T leptons, therefore the selected events are required to be triggered by an HLT H_T trigger. These triggers have been evolving in CMS due to the different luminosities the experiment has had, the thresholds used for them in the 2010 data have been moved from 100 GeV up to 200 GeV, this was done to keep the HLT rate inside the allowed limits each time the luminosity of the LHC has increased.
HLT H_T triggers are seeded by L1 triggers with lower thresholds, these triggers are based on the scalar sum of the transverse energy of the L1 identified jets. These jets are constructed from the energy sums computed with

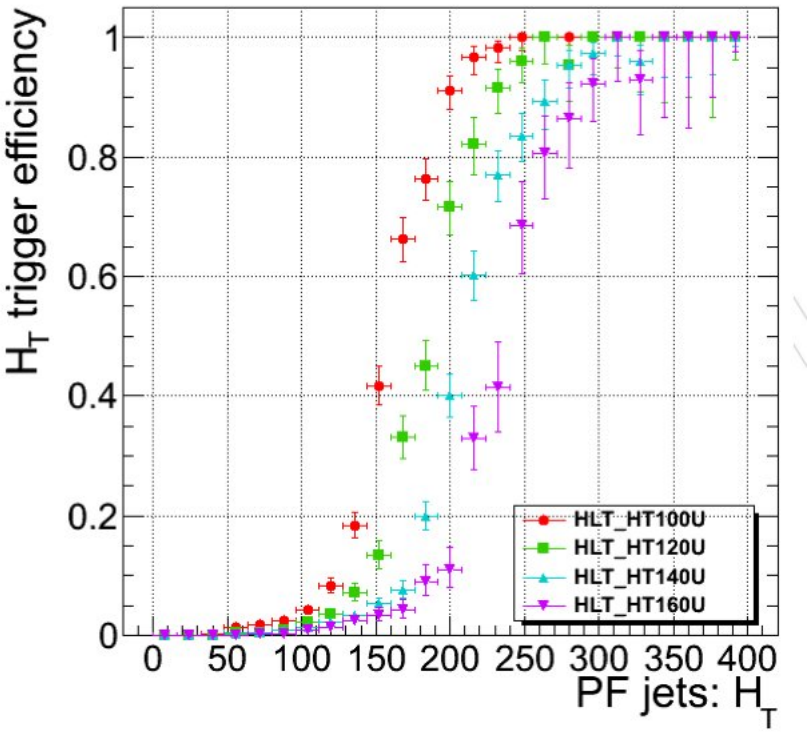

Figure 6.1: Turn on efficiency curve for the H_T HLT trigger. In this plot different H_T thresholds were considered, this triggers are presented as a function of the H_T reconstructed off line, using PF jets with $P_T > 30$ GeV.

the energy deposits in 12×12 tower windows in the calorimeters, these windows correspond to regions of approximately 1.0×1.0 in the (η, ϕ) space (a calorimetry tower is approximately 5×5 crystals in the ECAL, of dimensions $\Delta\eta$ =0.087 ×$\Delta\phi$ =0.087).
These triggers have no energy scale corrections applied, therefore a small difference between the object triggered and the reconstructed object may exist. To estimate the reconstructed H_T value at which these triggers become fully efficient, the trigger efficiency curve has been studied. At the HLT level the jets are reconstructed using the IC5 algorithm. All jets with a transverse energy above 20 GeV are used to calculate the H_T sum in the HLT. From figure 6.1 one can observe that the HLT_HT160U path, becomes fully efficient at a H_T bigger than about 340 GeV. This value suggested the cut used in the analysis.

6.3 Event Selection

In addition to the HLT H_T trigger, the events used in this analysis were required to have at least 50 GeV of MET, 350 GeV in H_T, and at least two leptons present.
The first two leptons ordered by P_T were required to have the same sign. In the case in which a third lepton was present, the invariant masses of all possible lepton pairs were calculated. If one of these invariant masses lay in the window between 76 GeV and 106 GeV, the event was rejected as coming from a Z boson decay. This procedure is called a "Z veto" for the third lepton. This kind of veto reduces the background coming from events with one Z and a fake lepton, and VV production with Z's present.
Jets are selected with a loose identification, requiring the jet P_T to be bigger than 30 GeV, and the jet $|\eta|$ to be less than 2,5. The P_T cut is applied to eliminate the jets produced by soft scattering during the bunch crossings. Usually high P_T jets are produced when a large part of the energy of the crossing protons is used in the interaction to create particles. On the other hand, the η cut guarantees that the jets are accepted in a high efficiency region of the calorimeters. It also helps to select jets that are not a product of soft scattering processes.

6.3.1 Lepton Selection

In order to sort the leptons depending on their origin, a classification was done. This classification is inspired in a comparison between simulated and

reconstructed data, were the generated and the reconstructed leptons are matched. Three kind of leptons were distinguished:

- *Prompt*: These are the leptons originated in the decay of a SUSY particle, a W/Z, or a τ.
- *Heavy-Flavour*: These leptons are originated in hadronic decays of heavy-flavour particles (b/c decays). These leptons are also called "fake" leptons for the analysis.
- *Fake*: These leptons are all those that do not have any generated match. In the case of muons this category includes in-flight decays of π/K mesons, as well as jet punch-throughs (jets in which the signals were beyond the HCAL into the muon system).

Basically two categories are widely used, they are: prompt leptons, or simply leptons; and fakes, which include fake as well as heavy-flavour leptons.

Electron selection

The electrons used were taken from the Particle Flow (PF) electron collection, this implies that the Gaussian Sum Filter algorithm was used to reconstruct the electron tracks, as was described in section 4.3.2.
From a PF collection of electrons, the particles that satisfy the following requirements were accepted:

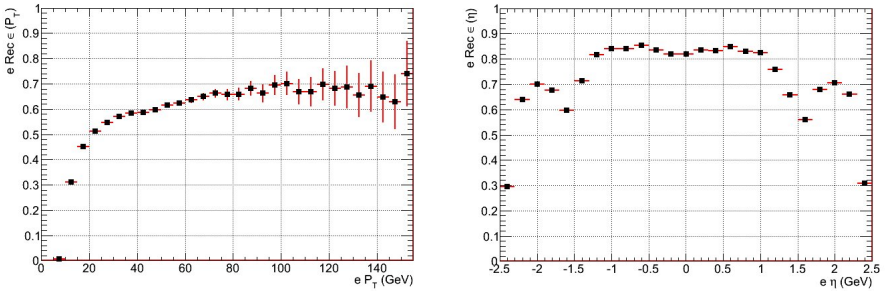

(a) (b)

Figure 6.2: The plots show the efficiency for the tight electron selection as a function of P_T in plot (a), and as a function of η in plot (b). This efficiency was calculated by matching the simulated muons with the reconstructed ones in a Z plus jets sample.

- $P_T > 10$ GeV: To ensure electron reconstruction with acceptable efficiencies.(see figure 6.2).
- $|\eta| < 2.4$: To guarantee that the electrons are in the region in which the calorimeters are efficient. Beyond this region the calorimeters are not anymore present (see figure 6.2).

Table 6.1: Electron cuts for a tight identification

	Barrel	End Caps
$\sigma_{i\eta i\eta}$	0.01	0.03
$\Delta\Phi$	0.06	0.03
$\Delta\eta$	0.004	0.007

- $\sigma_{i\eta i\eta}$: This variable is known as the cluster shape covariance, it quantifies the shape of the showers produced by the electrons in the calorimeters. Different cuts for this variable are applied in the barrel and the end-caps, the table 6.1 shows the maximum values allowed in each case (see figure 6.3).

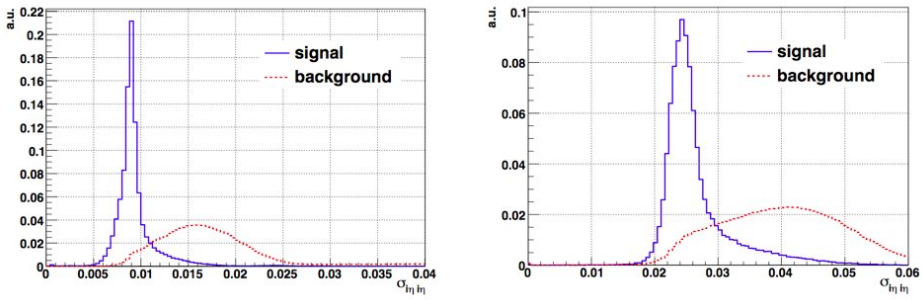

Figure 6.3: On the left the $\sigma_{i\eta i\eta}$ distribution is shown for the barrel case. On the right the same distribution is shown for the end-cap [44].

- $\Delta\phi, \Delta\eta$: These variables measure the difference between the ϕ or η of the track of the electron extrapolated to the calorimeter, and the ϕ or η of the clusters of energy deposited in the calorimeters. Different cuts are applied for the barrel and for the end-caps, the maximum values are listed in table 6.1 (see figures 6.4, and 6.5).
- $|D0| < 0.02$ cm: The impact parameter ($D0$) calculated with respect to the beam-spot, is the distance at which the electron track starts. A

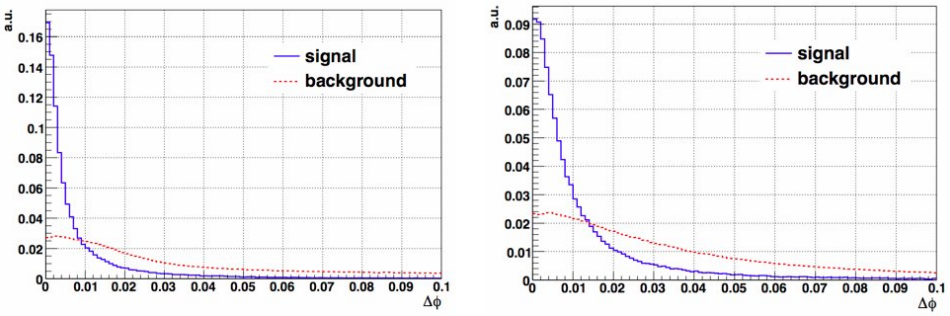

Figure 6.4: On the left the $\Delta\phi$ distribution is shown for the barrel case. On the right the same distribution is shown for the end-cap [44].

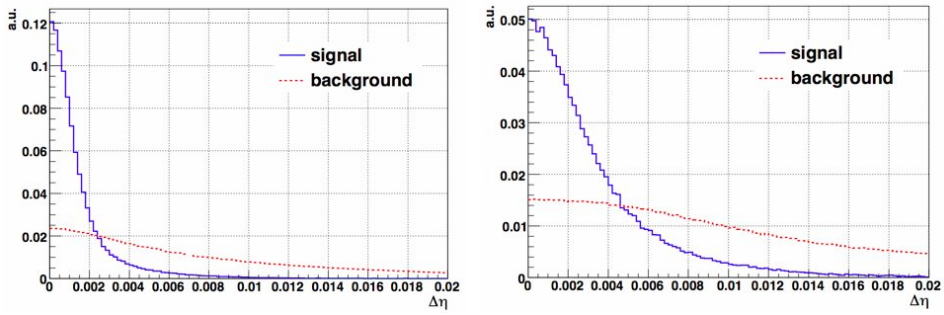

Figure 6.5: On the left the $\Delta\eta$ distribution is shown for the barrel case. On the right the same distribution is shown for the end-cap [44].

cut on this parameter guarantees that the electron being reconstructed was produced close to the beam-spot (see figure 6.6).

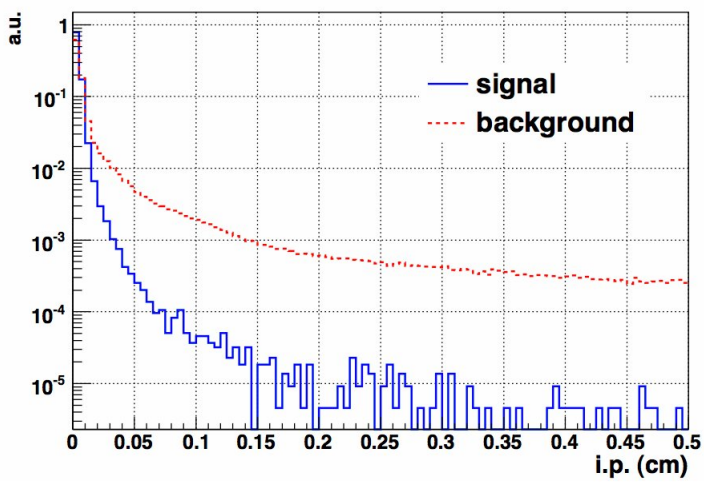

Figure 6.6: The $D0$ distribution is shown for both signal and background [44].

- Missing hits in the inner tracker: To identify the electrons coming from conversions, the number of expected missing hits in the inner tracker is required to be equal to 0. If a conversion happens, the resulting electron will leave no hits in the inner tracker, therefore if an extrapolation is done from the electron track into the inner tracker, there will be no inner hits. Electrons with no inner hits are rejected as conversion electrons.

- Conversion rejection: Requiring no missing hits in the inner tracker reduces the number of electrons coming from conversions. To reduce even more the number of electrons produced in conversions, two more cuts are implemented. If two electron tracks are close at a distance less than 0.02 cm, and the quantity $|Cot(\theta_1) - Cot(\theta_2)|$ is less than 0.02, then the electron is considered as a conversion and the electron is rejected.

- Charge consistency: There are three charges that can be computed for an electron candidate, these charges are: the charge assigned by the electron cluster together with the KF track, the charge assigned by

the GSF track, and the charge assigned by the super cluster object. If these three charges are not consistent the electron is rejected.

- Isolation: Leptons produced by the decay of vector bosons, are expected to be isolated. The same isolation is expected to be present in leptons produced by the decay of heavy s-particles such as neutralinos. An isolation study was done to optimise the cut applied on this variable, the details can be found in the appendix C.
  The isolation variable is computed for every electron by adding all the energy deposited by other particles in a cone around it. This cone was taken to be $\Delta R < 0.3$. The total sum of the P_T of the tracks inside that cone is called the "trackIso". The total sums of the energies deposited in the calorimeters inside that cone are called "ecalIso", and "hcalIso". To make the isolation relative to the electron, this sums were divided by the P_T of the electron being considered. Electrons with a relative isolation grater than 0.15 were rejected. Isolation was defined for the barrel and for the end-cap in slightly different ways as:

  $$RelIso_{\Delta R<0.3} = \frac{trackIso+ecalIso+hcalIso}{P_T} \text{ endcaps } (|\eta| > 1.56)$$
  $$RelIso_{\Delta R<0.3} = \frac{trackIso+max(0,ecalIso-1)+hcalIso}{P_T} \text{ barrel } (|\eta| < 1.56).$$

  When the ecalIso was computed for the barrel, the maximum between zero, and the ecalIso minus the electron P_T, was taken. This was done to account for the normal noise present in the ECAL.

All these requirements together conform the electron tight identification. A loose criteria was also defined by requiring all the cuts but the $\Delta\phi$, $\Delta\eta$, and $\sigma_{i\eta i\eta}$. The loose and tight identifications are used to estimate the number of fakes present in an event, this estimation is described later on in this chapter. From now on in this analysis, every time that there is a reference to an "electron", that will mean that it has passed all selection criteria.

Muon selection

In this analysis Particle Flow Muons were used, they were reconstructed as it is described in section 4.3.3. The muons selected satisfy the following requirements:

- $P_T > 5$ GeV: This cut was applied to go as low as possible in the reconstructed muon transverse momentum. The used P_T threshold lies in the limit in which the muons are reconstructed by CMS (see figure 6.7).

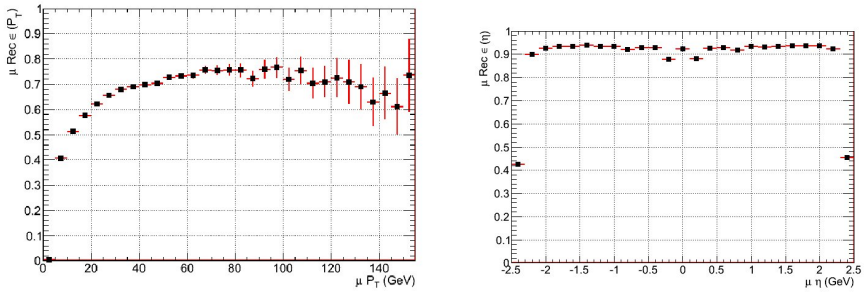

(a) (b)

Figure 6.7: The Plot shows the efficiency for the tight muon selection as a function of P_T (a), and η (b). This efficiency was calculated by matching the simulated muons with the reconstructed ones in a Z jet sample.

- $|\eta| < 2.4$: This cut guarantees that the reconstructed muons are inside the muon system acceptance region. It also grants a high efficiency in the muon reconstruction (see figure 6.7).

- Global track $\chi^2/n.d.f. < 10$: This cut guarantees the selection of a good fit of the tracker hits used to reconstruct the muon track.

- Number of Valid hits: The number of valid hits found in the tracker is requested to be at least 10, this threshold grants a good track-quality.

- $|D0| < 0.02$ cm: The $D0$ cut for muons is equivalent to the one used for the electrons (see section 6.3.1).

- Valid Stand alone hits > 0: There should be at least one hit in the muon chamber in order to have a valid muon, this selection is very loose from the muon-detector point view, but it is set in this analysis in order to accept soft muons (low P_T).

- Isolation: A very similar isolation study was done for both electron and muons (see section 6.3.1), the results can be found in the appendix C. The muon isolation is defined as:

  $$RelIso_{\Delta R<0.3} = \frac{trackIso+ecalIso+hcalIso}{P_T}.$$

  Muons were rejected if this value was bigger than 0.15.

- Global Muon: The selected muons are required to be Global, this implies that the muons are identified as such by both the tracker (tracker muons), and the muon chambers (Stand Alone Muon).

All aforementioned cuts are necessary to define a tight identification for muons. To define a loose identification, the isolation requirement was removed. From now on in this analysis, every time there is a reference to a "muon" it means it has passed all the cuts.

Tau selection

In this analysis the taus used were Particle Flow taus. The reconstruction of these particles is described in section 4.3.5. They were selected to satisfy the following requirements:

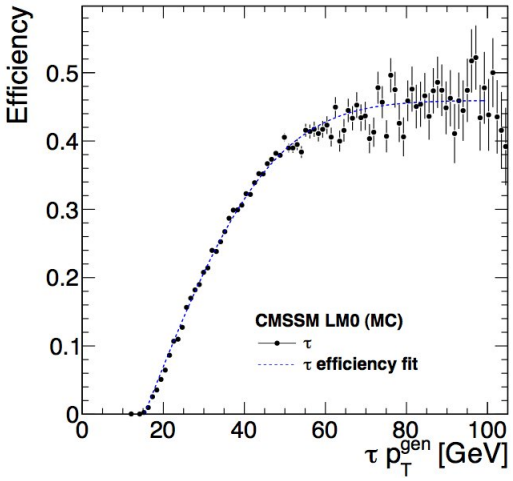

Figure 6.8: This plot shows the efficiency for the tightly identified taus, the efficiency was calculated from the comparison between reconstructed and simulated data [45].

- $P_T > 15$ GeV: This cut was applied to have a good acceptance for taus as a function of P_T (see figure 6.8).
- $|\eta| < 2.4$: This cut guarantees a good acceptance as a function of η for the tau leptons.
- Leading track finding: This algorithm was used to identify "loose" taus (see section 4.3.5).

- TaNC algorithm at half percent: This algorithm was used to identify "tight" taus (see section 4.3.5).

From now on, any reference to "taus", mean that the particle candidates have passed these requirements.

6.4 Backgrounds

In summary, the accepted events in this search were composed by at least two leptons of the same sign that comply with the requirements described in the previous sections. In addition to the leptons an HLT_HT trigger was required with a threshold of 160 GeV, together with a H_T threshold of 340 GeV. This H_T was calculated using PF jets with the $a\mathbf{K_T}$ algorithm presented in section 4.3.4. A MET value bigger than 50 GeV was also required, this MET was calculated with the PF algorithm.
The remanent background after applying the event selection is produced mostly by fake leptons. In the next sections a description and an estimation of the expected background is presented.

6.4.1 Standard Model Background

Same-sign double lepton signatures can be produced in significant quantities according to some SUSY model predictions. This is not the case for the SM in which same-sign double lepton events are unlikely to be produced. The possible SM background signals for same-sign double leptons that are significant for SUSY searches are:

- QCD: QCD processes are dominated by the production of jets. In this kind of physics no high amounts of MET, nor isolated leptons are expected to be produced. However MET can still be present produced by neutrinos and total energy miss-measurements. Leptons could be produced in the decay of heavy-flavour quarks. This leptons will not be isolated from jets, however they could still satisfy tight lepton identification cuts. This background becomes important due to its high production cross section.
  The kind of background expected from QCD can happen when: two or several high P_T jets are produced, leading to a large value of H_T; neutrinos are present in the final state, leading to a high MET when

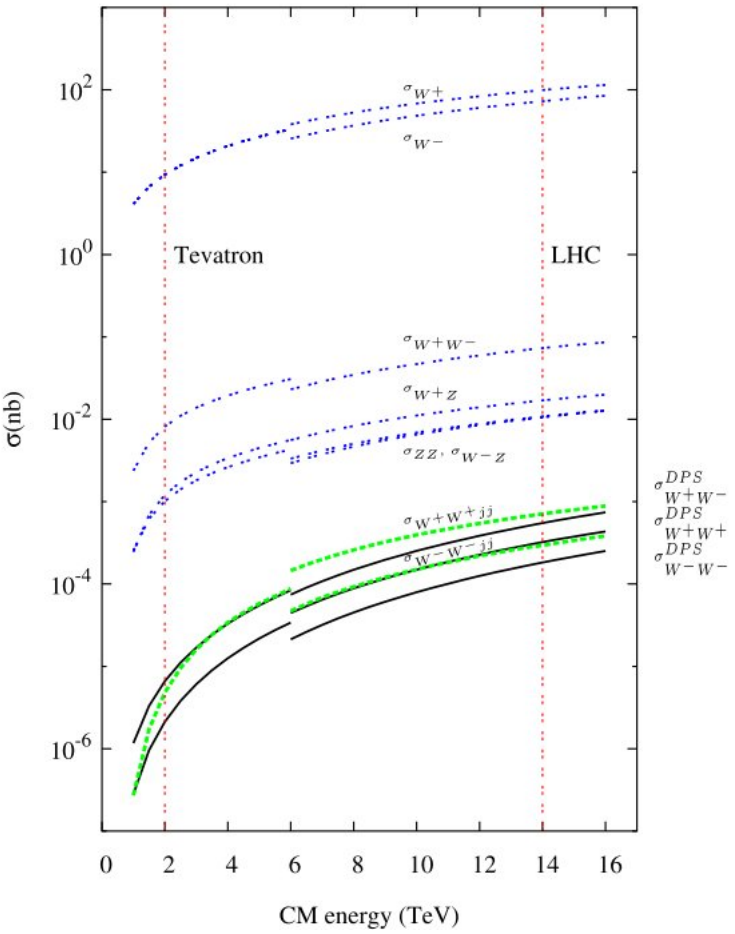

Figure 6.9: Production cross sections of vector bosons as a function of the LHC reachable energies [46]. DPS stands for Double Parton Scattering.

it is combined with energy miss-measurement effects; and two heavy-flavour leptons satisfy the tight-lepton identification. A data driven estimation of these cases is presented in the next sections.

- W plus jets: Processes with Ws can easily produce an isolated lepton and a neutrino. This two particles will result on one tight-lepton and some MET in the final topology. If there are jets present in the same event, these jets have a certain probability of having a non-isolated lepton on them, therefore one could have a signal with MET and two tight leptons that could be of the same sign (one of them being a

heavy-flavour fake).

- Z plus jets: Z bosons can easily decay into two isolated leptons. If the charge of one the leptons flips, the same-sign-double-lepton signal is easily produced. In this case, MET can come from the miss-measurement of the jet total energy, creating the necessary conditions to produce a background signal.

- TTbar: In the case in which a top anti-top pair is produced, followed by a semi-leptonic decay of one of them, a same-sign-double-lepton final state can be produced. In this case one of the leptons will be a prompt, and the other one will be a heavy-flavour fake that passes the tight identification. The required MET signal will come from neutrinos, and the H_T sum will be fulfilled due to the hadronic nature of the top anti-top pair.

- VV plus jets: VV processes are those in which two bosons are present, such as $W^{\pm}W^{\mp}$, ZZ, and $W^{\pm}Z$. This processes can easily produce a same-sign double lepton signal in the final state, however the production cross section for this processes is very low compared with the other backgrounds. From the cross sections in figure 6.9, one can see that the process with the highest cross section that could lead to a same-sign double lepton state is the $W^{+}Z$ production. This process can be highly suppresed by implementing a Z veto for the events that have more than two selected leptons. Therefore the real background coming from this kind of processes will be the production of jets associated with two same sign Ws.

- Same-Sign W bosons: Processes leading to the production of two W with the same sign can be classified in two groups: The production of two same sign Ws from a single parton interaction resulting from higher order electroweak processes, or from parton-parton interaction in the same proton-proton collision. These processes have smaller cross sections than the double-boson production mentioned above(see figure 6.9).
  At an integrated luminosity of 50 pb^{-1} one expects approximately 20 events for this process (N= $\sigma(\text{pb}) \times L(\text{pb}^{-1})$), but after all selection cuts almost nothing survives. The number of expected events for this channel was estimated from the simulated data, and therefore a conservative systematic error was assigned to it.

In the following section, a data-driven method to estimate the number of events coming from fake leptons background is presented.

6.4.2 Expected Events

The total number of events observed at the end of the analysis can be written as:

$$N_{Tot} = N_{Signal} + N_{Background}, \tag{6.1}$$

where N_{Signal} is the number of same-sign double lepton events produced by the decay of SUSY particles, and $N_{Background}$ is the number of events produced by the irreducible background. This background can be expressed as:

$$N_{Background} = N_{SM} + N_{Fakes}, \tag{6.2}$$

where N_{SM} is the background expected from the SM. This number is basically zero for the current luminosity as was already discussed. N_{Fakes} is the background produced by fake signals such as: a charge flip for one of the leptons, or non-prompt leptons that actually pass the tight selection cuts.
N_{Fakes} can be produced in three cases which are: two non-prompt leptons with the same sign; one non-prompt lepton, and one prompt lepton with the same sign; and no fake leptons, but a charge flip of one of the leptons from an opposite sign double lepton event. The cases can be summarised as:

$$N_{Fakes} = N_{2Fakes} + N_{1Fake} + N_{ChargeFlip}. \tag{6.3}$$

6.4.3 Fake Lepton Estimation

Non-prompt leptons are very often produced inside jets coming from heavy-flavour decays. These leptons could satisfy the loose selection requirement, and in some cases they could satisfy a more tight identification also. In the case in which a heavy flavour lepton satisfies the tight identification selection, a fake same-sign double lepton event can be accepted. An estimation of this kind of processes is therefore required.
Since a fake event contains loose objects that also satisfy the tight selection, the method consist in counting all events that have two loose leptons with the same-sign, or a loose and a tight lepton with the same-sign. For each loose lepton a probability to satisfy the tight identification was assigned (see figure 6.10, and 6.11), so that the probability of the entire event to be accepted was accounted for.
From the data and from simulation one can measure the probability of a loose lepton to be identified as a tight lepton, this can be done by simply

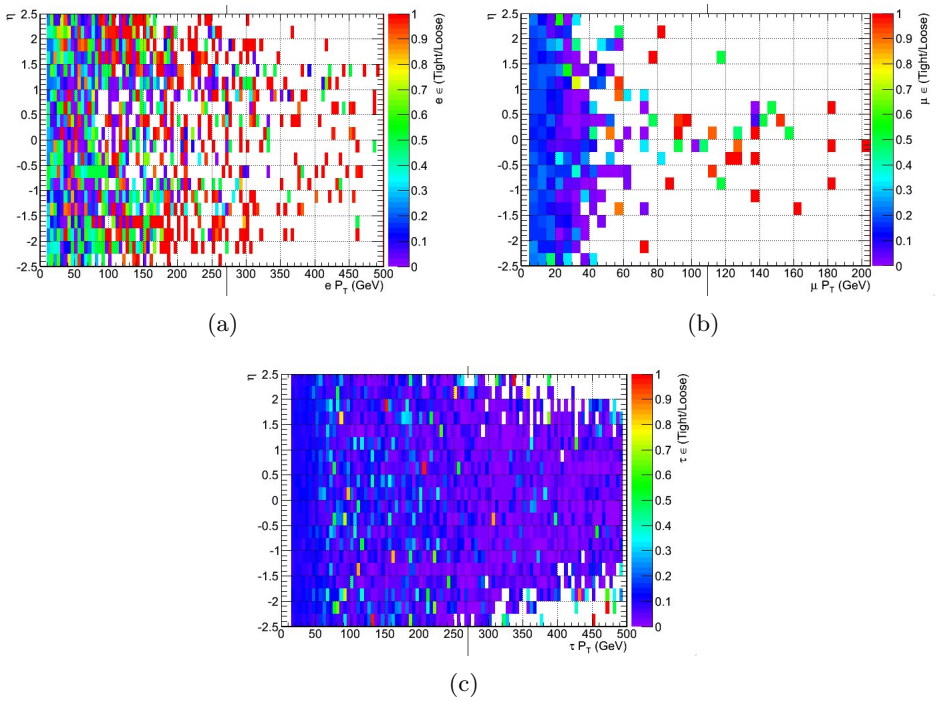

Figure 6.10: The following three plots present the probability of a loose lepton to fulfill the tight lepton selection. These probabilities were plotted for electrons (a), muons (b), and taus (c) as a function of the transverse momentum and η.

counting the number of loose leptons, and counting how many of them are identified as tight leptons as well. The ratio between the number of tights and the number of loose will be the probability of a loose lepton to be identified as a tight one:

$$\epsilon_{T/L}(\eta_i, P_{Ti}) = \frac{N_{Tight}}{N_{AllLoose}}, \tag{6.4}$$

This probability was tested to be invariant as well as constant in P_T for different simulated samples, this behaviour can be observed in figure 6.11. For the case of electrons and muons it can be seen that there is a bias in P_T around and beyond 50 GeV, this bias is produced by electroweak leptons.
Loose leptons can be sorted into two orthogonal sets which are: the loose leptons that are also tight, and the loose leptons that are not tight and that will be referred as L!T. This separation was used to make an unbiased measurement of the number of fake events expected.
The measurement was done by using the N_{Loose} leptons that are also tight, to estimate $\epsilon_{T/L}(\eta_i, P_{Ti})$, and the $N_{L!T}$ to estimate the number of fake events present in the final selection.
If one defines the total number of leptons as N_T (which is also equal to the total number of loose leptons), this number can be understood as the sum of the L!T, with the tight leptons that come from non-prompt leptons:

$$N_T = N_{L!T} + N_{Tight}. \tag{6.5}$$

From equation 6.5 together with the definition 6.4, one can see that the total number of leptons is given by:

$$N_{Tot} = \frac{N_{L!T}}{1 - \epsilon_{T/L}(\eta_i, P_{Ti})}. \tag{6.6}$$

Therefore the total number of events with one prompt lepton and one fake lepton can be estimated as the addition of the total number of leptons, multiplied by the probability of each lepton to be identified as a tight:

$$N_{1Fake}(\eta_i, P_{Ti}) = \sum_i N_{L!T}(\eta_i, P_{Ti}) \frac{\epsilon_{T/L}(\eta_i, P_{Ti})}{1 - \epsilon_{T/L}(\eta_i, P_{Ti})}. \tag{6.7}$$

The case in which zero prompt leptons are present (2 non-prompt leptons) can be written as:

$$N_{2Fake}(\eta_i, P_{Ti}; \eta_j, P_{Tj}) = \sum_i \sum_j \frac{N_{L!T}(\eta_i, P_{Ti}; \eta_j, P_{Tj}) \epsilon_{T/L}(\eta_i, P_{Ti}) \epsilon_{T/L}(\eta_j, P_{Tj})}{(1 - \epsilon_{T/L}(\eta_i, P_{Ti}))(1 - \epsilon_{T/L}(\eta_j, P_{Tj}))}. \tag{6.8}$$

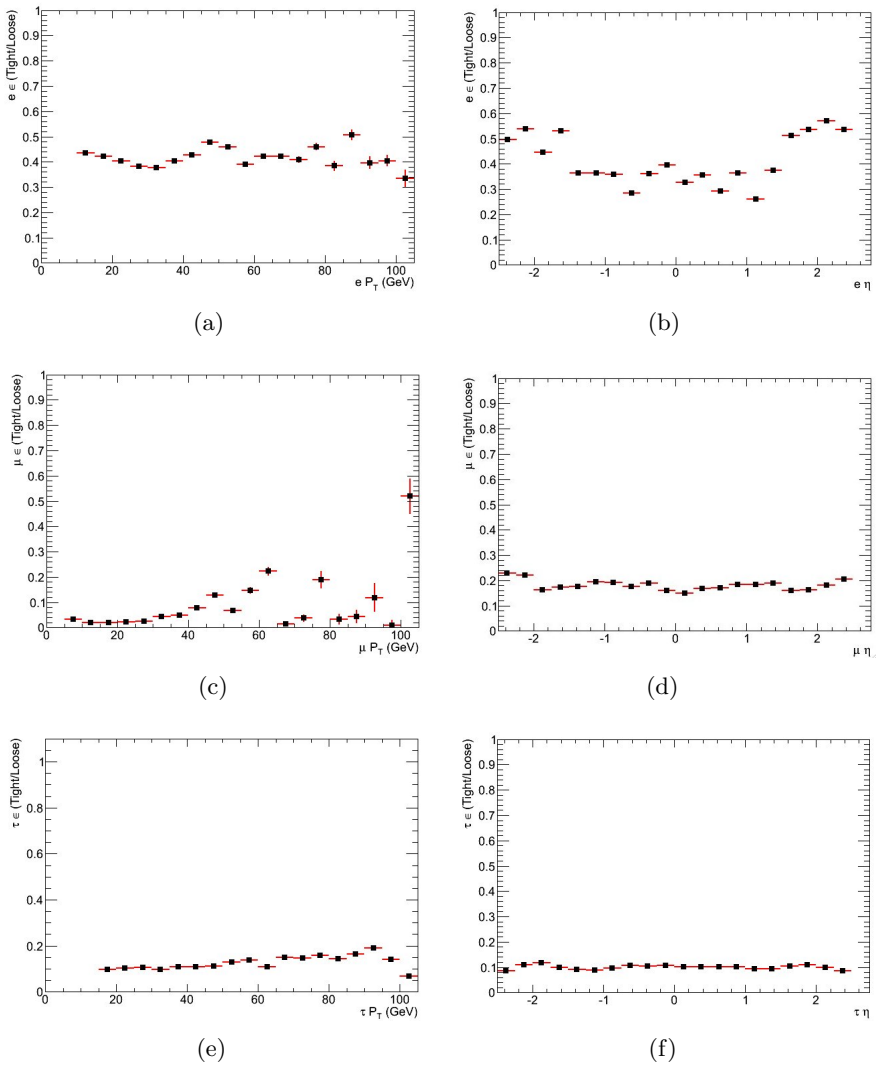

Figure 6.11: The following six plots present the probability of a loose lepton to fulfill the tight lepton selection. This probabilities are plotted as a function of P_T (left), and as a function of η (right) for: electrons (a) and (b); muons (c), and (d); and taus (e) , and (f).

This method was used to estimate the number of background events coming from: two fake leptons, and one fake and one prompt leptons. This method was tested with both simulated as well as collisions data, and that is its merit, it is a data-driven method.

6.4.4 Charge Flip

Besides the background produced by the presence of non-prompt leptons, SM processes with two prompt opposite-sign leptons can also be reconstructed as same-sign events. This can happen if a wrong charge is assigned to one of the leptons.
Such cases are very unlikely for muons (muon charge can be measured twice in the detector), however a careful study is needed to estimate this effect for electrons.
Electrons can emit radiation from bremsstrahlung producing photons. This photons can decay into electron pairs, leading to electrons of both signs close to the initial track. If one of the produced electrons (the one with the opposite charge with respect to the original) is mistaken to be the original electron, the reconstructed track will lead to the wrong assignment of electric charge. In these cases two opposite-sign electrons, can be easily mistaken with a same-sign event. This kind of effect can happen mostly in processes with two prompt opposite-sign leptons, mostly in: Drell-Yan production (Z^*/γ+jets), and top quark pair production.
To grant an electron selection free of this kind of effect, a match is expected between the charge of the electrons estimated by: the GSF track, the KF track, and the electron super cluster coming from the energy deposition in the calorimeters. This sole requirement should be enough to avoid accepting opposite-sign doble lepton events as same-sign events. However, considering the importance of the same-sign requirement for this analysis, two methods were implemented to estimate the rate at which electron-charge flips. The method descriptions follow.

Charge Flipping from Simulation-Reconstruction Comparison

The first method uses a matching between simulated and reconstructed electrons. A $\Delta R < 0.5$ is required between the electrons, where ΔR is given by:

$$\Delta R = \sqrt{(\eta_{Simulated} - \eta_{Reconstructed})^2 + (\phi_{Simulated} - \phi_{Reconstructed})^2}.$$

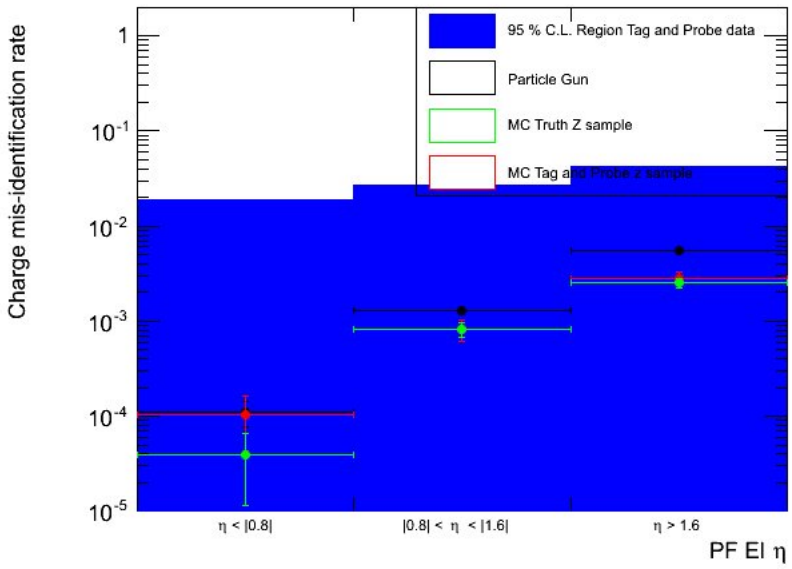

Figure 6.12: Charge Flip rate as a function of η. The comparison between the two methods used is shown. The blue zone shows the 95 % confidence level region in which the electron charge-flip probability lies as obtained from the data (approximately 3 pb^{-1} of data were used). The red data points represent the probability for an electron to flip its charge, as obtained from the tag-and-probe method with the simulated sample. The black data points represents the probability for an electron to flip its charge as calculated from a particle gun simulation.

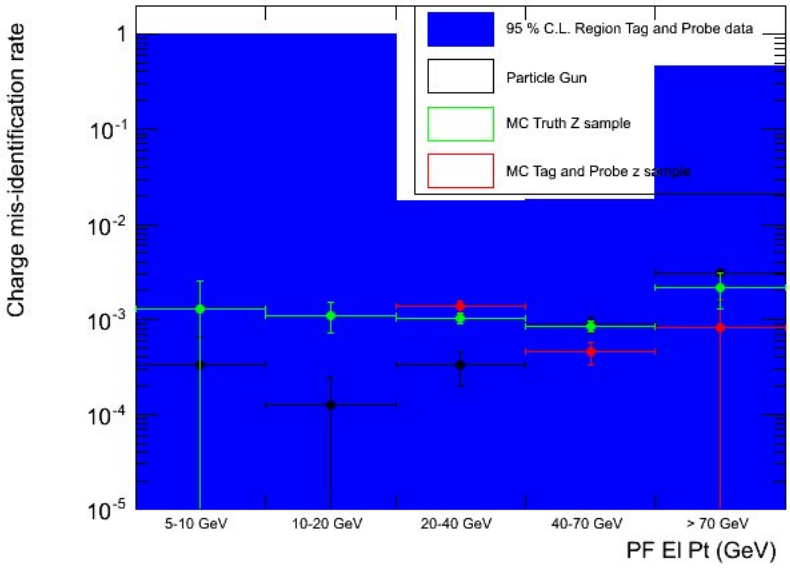

Figure 6.13: Charge Flip rate as a function of P_T. The comparison between the three methods used is shown (approximately 3 pb^{-1} of data were used). The conventions are the same as in figure 6.12.

If the reconstructed electrons have a different charge with respect to the simulated ones, the reconstructed electron is counted as a flip.
This method was used over two different simulated data samples which were a Z + jets sample, and a sample with only electrons, called a particle gun sample. The second sample used gives an unbiased measurement, since electrons are the sole particles present in these data.

Charge Flipping estimation using the Tag-and-Probe method

The details of the Tag-and-Probe method are presented in appendix D. The method consists on selecting events with a high quality electron which is called the "Tag", and a lesser quality electron candidate called probe. The invariant mass of these two particles is calculated, and if it is within a window around the Z peak, the electron pair is taken as coming from the decay of a Z. Therefore the charge of the probe should be opposite to the one of the tag. If the charge of the probe assigned by the reconstruction is the same as the charge of the tag, the event is identified as the result of a charge flip. By counting these events one can estimate the probability of an electron to "flip" its charge.
For the tag selection a well defined electron is chosen, this electron is matched with a low P_T non pre-scaled trigger. The electron charge is checked to be consistent for the three charge assignments: GSF track, KF track, and the electron super cluster. The tag is also required to have a GSF track with $|\eta| < 1$, and a $|\Delta\phi| < 0.01$.
In the case in which an electron super cluster is not present, the probe is defined as a GSF track with $E_T > 20$ GeV, and $|\eta| < 2.4$. In the case in which a super cluster is present, the probe is defined as a super cluster together with the track. It is rejected if its transverse energy $E_T < 20$ GeV, or if its $|\eta| > 2.4$. Electrons with super clusters in the region $1.44 < |\eta| < 1.56$ are rejected also (transition region).
The probes that are identified as coming from conversions are rejected. They should also have the same charge assigned for the GSF track, the KF track, and the electron super cluster.

Both methods were tested on a Z + jets simulated dataset. The tag-and-probe method was also run over the data. To study the flip rate as a function of P_T and η, both quantities were segmented into bins, 5 and 3 bins respectively. The P_T bins correspond to the ranges listed as 5-10 GeV, 10-20 GeV, 20-40 GeV, 40-70 GeV, and greater than 70 GeV. The η bins correspond to the regions $|\eta| < 0.8$, $0.8 < |\eta| < 1.6$, and $|\eta| > 1.6$. The results of the methods are compared in figures 6.12 and 6.13.

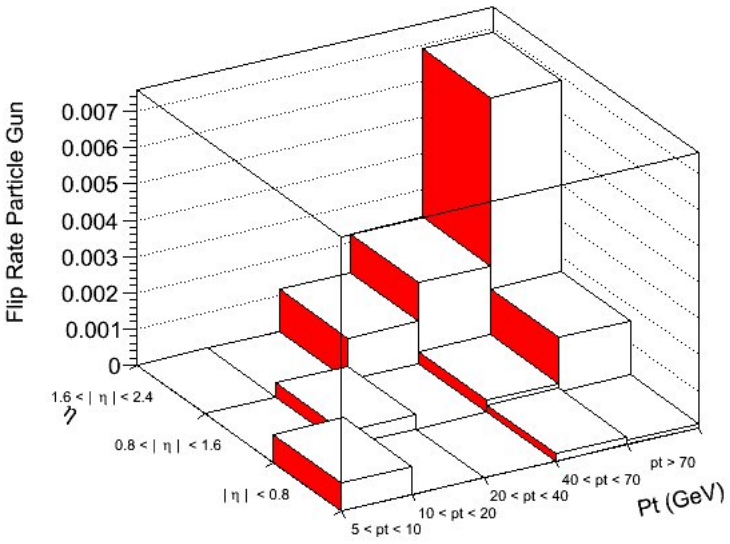

Figure 6.14: Charge Flip rate as a function of P_T and η.

The results obtained with the electron gun simulation, were interpreted as the probability of mis-measuring an electron charge as a function of P_T and η. This probability was used to estimate the number of same-sign double lepton events coming from charge-flips of opposite-sign double lepton events. As can be seen from the results (see figures 6.12 and 6.13) the two methods present a good agreement within statistical errors. The difference between the three results was used to calculate the systematic error of the probability measurement. This error was obtained to be of approximately 50 % of the particle gun sample results.

Electron Charge Flip Estimation

To estimate the number of fake events, a weight was assigned to every opposite-sign event. This weight was defined for as the sum of the charge-flip probabilities for every electron in the event. The probabilities were calculated as a function of P_T and η (see figures 6.12, 6.13,and 6.14). The case in which two electrons presented a charge-flip simultaneously was neglected. In the case of the muons, the charge flip probability is much lower because they do not present conversions, and because of the excellent reconstruction capabilities of the CMS. In the case of taus since the reconstruction efficiency is of the order of 40 % charge flipping was not considered, therefore muons

and taus were assigned a zero probability for charge-flip. The number of events accepted in the analysis produced by a charge flip was estimated as:

$$N_{CF} = \sum_{ij} N_{OS}(\eta_i, P_{Ti}, \eta_j, P_{Tj})(\epsilon_{CFi}(\eta_i, P_{Ti}) + \epsilon_{CFj}(\eta_j, P_{Tj})), \qquad (6.9)$$

where N_{OS} is the number of events with two leptons of opposite sign; i, j are the indices of these leptons, and $\epsilon_{CFi}(\eta_i, P_{Ti})$ is the probability of the lepton to flip its charge as a function of η, and P_T. A systematic uncertainty of 50 % of the estimated events was assigned to this measurement to account for the error in the charge flip probability estimation.

6.4.5 Signal to Background Studies

To validate the methods used to estimate the background, the aforementioned selection was applied in a set of simulated data samples. Pythia and Madgraph simulators were used to generate the data (produced during the spring of 2010). The conditions at which the simulation was done are collected in a tag called START3X_V26_S09-v1, this conditions are saved in a CMS database accesible by the CMSSW code.
The type of data used for these studies is of the type GEN-SIM-RECO, this means that the information from the generation, simulation, and reconstruction of the data was saved in the same file. QCD samples from both generators, pythia and madgraph were considered (pythia going from 15 to 1400 GeV, and madgraph going from 100 GeV to Inf). The list of the simulated data used is summarised in table 6.2.

The event selection was applied over all background samples assuming an integrated luminosity of 35 pb^{-1}, the obtained yield is summarised in table 6.4. The background was estimated with the methods described in section 6.4.3.
The probabilities for loose leptons to be identified as tight leptons were calculated using QCD madgraph samples. Two probabilities were calculated to study the systematic error of the method, the first one was obtained from a H_T cut of 350 GeV in the event selection, the second probability was calculated lowering that threshold to 150 GeV. The obtained probabilities are very similar and can be seen in figure 6.11.
The yield from which the systematics were calculated, are listed in table 6.3. The resulting yield after the entire selection, together with the corresponding systematic errors can be seen in table 6.4. The same table assumes a 50 % error added to every double-lepton channel in the observed column, this assumption was done to account for the simulation systematics in a very

Table 6.2: Simulated data samples used to study the event selection.

Type	Data sample	σ_s (pb)	Number of events
SUSY signal	LM0	38.93	$\approx$ 200000
QCD	P_T 15 GeV	8.76×10^8	$\approx$ 6000000
	P_T 30 GeV	6.04×10^7	$\approx$ 5000000
	P_T 80 GeV	923800	$\approx$ 3000000
	P_T 170 GeV	25470	$\approx$ 3000000
	P_T 300 GeV	1256	$\approx$ 3000000
	P_T 470 GeV	87.98	$\approx$ 2000000
	P_T 800 GeV	2.186	$\approx$ 2000000
	P_T 1400 GeV	0.0112	$\approx$ 1000000
	P_T 100-250 GeV	7000000	$\approx$ 10000000
	P_T 250-500 GeV	171000	$\approx$ 5000000
	P_T 500-1000 GeV	5200	$\approx$ 4000000
	P_T 1000-Inf GeV	83	$\approx$ 1600000
	Top anti-top	148.9	$\approx$ 1400000
Electroweak	W plus jets	24170	$\approx$ 10000000
	Z plus jets	2400	$\approx$ 1000000
Vector bosons	WW	28	$\approx$ 100000
	WZ	10.5	$\approx$ 100000
	ZZ	4.3	$\approx$ 100000

Table 6.3: Systematic calculation for the data-driven method using the simulated data.

	expected (H_T cut 150 GeV)	expected (H_T cut 300 GeV)	error %
ee	0.06 $\pm$ 0.04	0.06 $\pm$ 0.04	5 %
eμ	0.33 $\pm$ 0.01	0.29 $\pm$ 0.02	12 %
eτ	0.38 $\pm$ 0.04	0.36 $\pm$ 0.03	5 %
$\mu\mu$	0.54 $\pm$ 0.10	0.38 $\pm$ 0.05	30 %
$\mu\tau$	0.9 $\pm$ 0.07	0.80 $\pm$ 0.07	11 %
$\tau\tau$	0.37 $\pm$ 0.06	0.35 $\pm$ 0.06	5 %

Table 6.4: Background yield obtained for all the channels with the systematic errors included.

	observed	expected
ee	0.03 ± 0.01 (stat) ± 0.01 (sys)	0.06 ± 0.04 (stat) ± 0.01 (sys)
eμ	0.13 ± 0.02 (stat) ± 0.06 (sys)	0.29 ± 0.02 (stat) ± 0.03 (sys)
eτ	0.54 ± 0.13 (stat) ± 0.27 (sys)	0.36 ± 0.03 (stat) ± 0.02 (sys)
$\mu\mu$	0.11 ± 0.02 (stat) ± 0.05 (sys)	0.38 ± 0.05 (stat) ± 0.11 (sys)
$\mu\tau$	0.96 ± 0.20 (stat) ± 0.47 (sys)	0.80 ± 0.07 (stat) ± 0.08 (sys)
$\tau\tau$	0.33 ± 0.13 (stat) ± 0.16 (sys)	0.35 ± 0.06 (stat) ± 0.02 (sys)
Total	2.10 ± 0.24 (stat) ± 0.57 (sys)	2.23 ± 0.12 (stat) ± 0.14 (sys)
Tot (stat + sys)	2.1 ± 0.62	2.23 ± 0.18

conservative way.
The errors reported are added in quadrature as it is shown in table 6.4. The results between both columns are in good agreement within the statistical and systematical errors.
LM0 was used as a signal example, the yield produced by LM0 and the background samples can be found in table 6.5. A summary of this yield produced in every double-lepton channel can be found in table 6.6.
In the next chapter the same analysis is presented using the data taken by the CMS experiment.

Table 6.5: Yield observed after the entire selection is applied in the simulated data.

	ee	eμ	eτ
LM0	0.76 ± 0.07	2.35 ± 0.12	0.75 ± 0.07
QCD	0.00 ± 0.00	0.00 ± 0.00	0.05 ± 0.04
TTbar	0.02 ± 0.01	0.12 ± 0.02	0.3 ± 0.03
WJets	0.00 ± 0.00	0.00 ± 0.00	0.17 ± 0.12
ZJets	0.00 ± 0.00	0.00 ± 0.00	0.00 ± 0.00
WW	0.00 ± 0.00	0.00 ± 0.00	0.01 ± 0.01
WZ	0.00 ± 0.00	0.01 ± 0.01	0.01 ± 0.01
ZZ	0.00 ± 0.00	0.00 ± 0.00	0.00 ± 0.00
Back	0.02 ± 0.01	0.13 ± 0.02	0.54 ± 0.13
	$\mu\mu$	$\mu\tau$	$\tau\tau$
LM0	1.86 ± 0.11	1.04 ± 0.08	0.12 ± 0.03
QCD	0.00 ± 0.00	0.04 ± 0.04	0.04 ± 0.04
TTbar	0.1 ± 0.02	0.47 ± 0.04	0.1 ± 0.02
WJets	0.00 ± 0.00	0.43 ± 0.19	0.17 ± 0.12
ZJets	0.00 ± 0.00	0.00 ± 0.00	0.00 ± 0.00
WW	0.00 ± 0.00	0.00 ± 0.00	0.00 ± 0.00
WZ	0.01 ± 0.01	0.01 ± 0.01	0.00 ± 0.00
ZZ	0.00 ± 0.00	0.00 ± 0.00	0.00 ± 0.00
Back	0.11 ± 0.02	0.94 ± 0.19	0.31 ± 0.12

Table 6.6: Closure test for the simulated data, done with the background and LM0 as the signal sample.

	observed	expected
ee	0.78 ± 0.07 (stat) ± 0.39 (sys)	0.10 ± 0.04 (stat) ± 0.01 (sys)
eμ	2.48 ± 0.12 (stat) ± 1.24 (sys)	0.62 ± 0.03 (stat) ± 0.07 (sys)
eτ	1.29 ± 0.15 (stat) ± 0.64 (sys)	0.61 ± 0.04 (stat) ± 0.03 (sys)
$\mu\mu$	1.97 ± 0.11 (stat) ± 0.98 (sys)	0.61 ± 0.04 (stat) ± 0.18 (sys)
$\mu\tau$	2.00 ± 0.22 (stat) ± 1.00 (sys)	1.13 ± 0.07 (stat) ± 0.12 (sys)
$\tau\tau$	0.45 ± 0.13 (stat) ± 0.22 (sys)	0.41 ± 0.06 (stat) ± 0.02 (sys)
Total	8.97 ± 0.34 (stat) ± 2.03 (sys)	3.48 ± 0.12 (stat) ± 0.23 (sys)
Tot (stat+sys)	8.97 ± 2.03	3.48 ± 0.26

Chapter 7

Data Analysis

In the previous chapter the same-sign-double-lepton analysis performed with simulated samples was described. In the case in which supersymmetry does not exist, or it is not visible with the luminosity accumulated during 2010, approximately 2.1 $\pm$ 0.62 events of background are expected considering all double lepton channels. For the sake of comparison, the same yield was calculated for the mSUGRA benchmark LM0. In this case one expects 8.97 $\pm$ 2.03 events. In this chapter the same analysis is repeated using the data collected with the CMS experiment during the first run of the LHC.

7.1 LHC 2010 Data

As it was described in section 3.1, the LHC proton beams were changing during the entire year of 2010, therefore different instantaneous luminosities were delivered to CMS (see figure 7.1) depending on the continuing improvements of the LHC performance during the year. All these luminosity changes were reflected in the experiment, resulting in an evolution of the trigger menus available to collect data.
The saved events were sent to different datasets depending on the trigger that selected them (see section 3.3.5 and 3.3.6). In this thesis, the trigger used was based in H_T, this implies that all the events used in the analysis are present in the hadronic datasets listed in table 7.1. The H_T triggers used, present in each dataset, are listed in table 7.2.
Not all of the data collected with the CMS is good to perform physics analysis, this may happen because during the data taking periods either technical or human errors may be present. For this reason a Data Quality Monitoring (DQM) group was always tagging the data as good or bad for physics. In

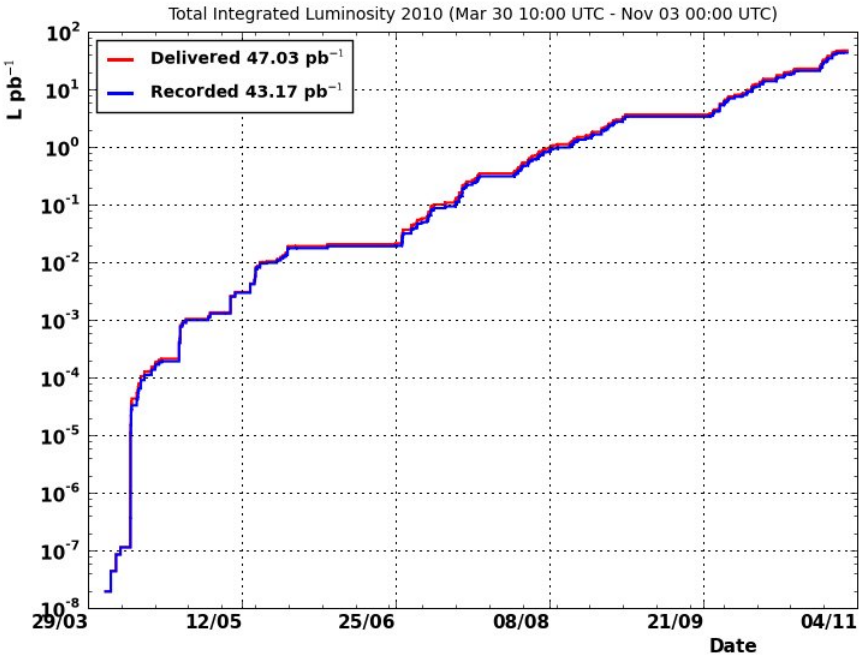

Figure 7.1: The plot shows the delivered and recorded integrated luminosity obtained at the CMS detector.

the particular case of CMS, 35 pb^{-1} were recorded and tagged as good for physics analysis.

Table 7.1: Names and number of events of the hadronic datasets used in this analysis. The names of the dataset point to a specific CMSSW version, a specific period of time, and specific triggers present in the trigger options.

Dataset	Number of events
/JetMET/Run2010A-Nov4ReReco_v1/RECO	24064576
/JetMETTau/Run2010A-Nov4ReReco_v1/RECO	15042368
/MultiJet/Run2010B-Nov4ReReco_v1/RECO	23315336

Table 7.2: Hadronic H_T triggers used and present in each dataset.

Dataset	H_T triggers
JetMET	HLT_HT100U
JetMETTau	HLT_HT100U
MultiJet	HLT_HT140U and HLT_HT160U

7.2 Data-Driven Studies

The datasets mentioned in table 7.1 were used to perform the analysis described in the previous chapter (see section 6.4.2 and on). In particular, the H_T trigger efficiency (see figure 6.1), and the probability of electron charge flipping when reconstructed (see figures 6.12, and 6.13), were both measured directly with collision data.

The probabilities for fake leptons to satisfy a tight identification were measured from simulated and collision data. These quantities are better estimated from a pure QCD sample (as is done in figure 6.11), because most leptons produced in QCD processes come from the decay of heavy quarks and are therefore considered as "fake". If the same quantity is estimated with collision data, a bias due to prompt leptons coming from electroweak bosons and top-antitop processes is going to be observed (see figure 7.2). This bias is due to the definition of tight and loose leptons (prompts and fakes), all tight leptons also meet the requirements for loose leptons, therefore a sample with a high amount of tights, will present a high probability of a loose leptons being identified as a tights. A fully data-driven method

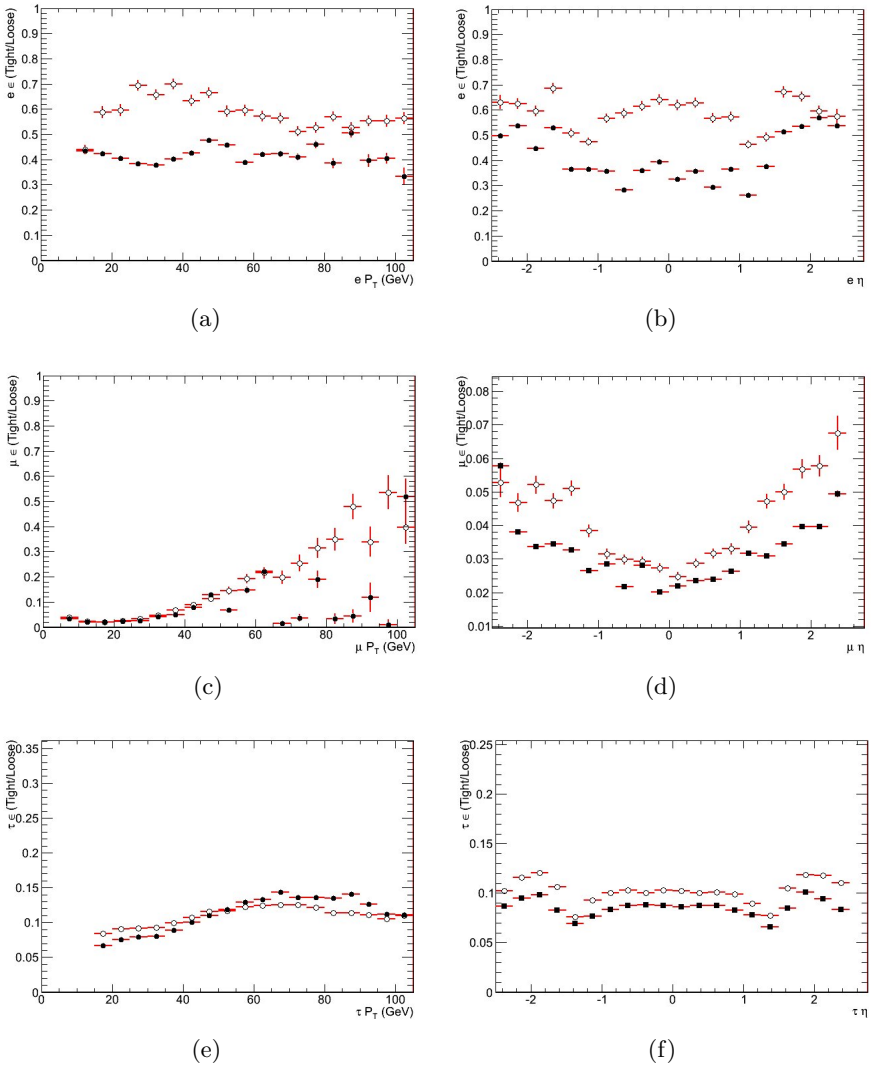

(a) (b) (c) (d) (e) (f)

Figure 7.2: The following six plots present the probability of a loose lepton to fulfill the tight lepton identification for, a simulated QCD sample (black points) and all collision data (open points). These probabilities are plotted as a function of η (right), and as a function of P_T (left) for: electrons in plots (a) and (b); muons in plots (c), and (d); and taus in plot (e), and (f). From the plots one can notice the bias produced by electroweak leptons.

would demand the selection a QCD control sample directly from the collision data; to get these samples one would have to set cuts to reduce most of the electroweak events such: an invariant mass veto for the Z, and a transverse mass veto for the W, etc. To obtain these control samples a large amount of data processes is required, however at this stage of the analysis we obtained the probabilities of fakes being identified as tights from the simulated QCD sample. Since the agreement between the CMS simulated samples and the collision data is very good, as will be presented in the next sections, the use of a QCD simulated sample to estimate the probabilities is justified. Therefore the yields presented in tables 6.4, 6.6, and 7.3; were calculated using the probabilities taken from the QCD simulated samples.

7.3 Data and MC Comparison

Collision and simulated data were compared after the trigger selection. This was done as a cross-check for the analysis cuts. The first objects to be compared were the leptons. Their multiplicities after the trigger selection, and the MET and the H_T cuts; are shown in figure 7.3.

The leptons were ordered by its transverse momentum, therefore a comparison of the P_T distributions for both, the first and the second lepton was possible. This comparison can be seen in figure 7.4.

The H_T and MET distributions were also compared as can be seen in figure 7.5. The MET signal was cleaned from beam halo events and known detector noise produced by the electronics of the calorimeters. The level of agreement after applying the cleaning procedure described in reference [47] for these two quantities is very good.

As a final extra-test, a search was done for the remanent events of Z boson production present after the H_T trigger and the H_T cut. Some events were found for both electrons and muons as can be seen in figure 7.6

7.4 Observed Events

After applying the event selection to the entire 35 pb^{-1} of data, only 3 $\pm$ 1.72 (stat) events passed the selection. This value is in agreement with the expected background yield of 3.91 $\pm$ 0.63 obtained from the collision data, and 2.1 $\pm$ 0.62 (stat) obtained from the simulated data.

From figure 6.1 one can see that the H_T HLT triggers used in this analysis are fully efficient at H_T values grater than or equal to 350 GeV. Sources of

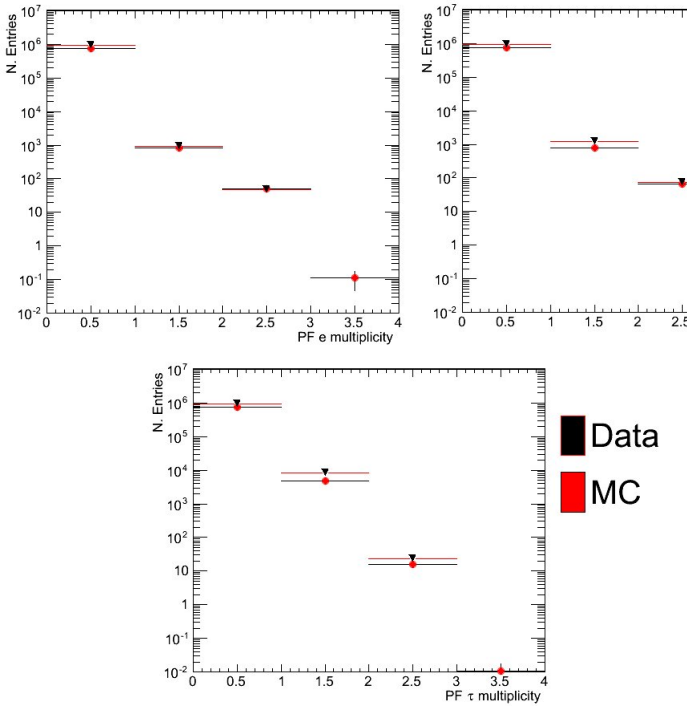

Figure 7.3: Lepton multiplicity for the electrons (top left), muons (top right), and taus (bottom) are shown after the H_T trigger and the H_T and MET cuts have been applied. A very good agreement between the collision and the simulated data can be observed.

Table 7.3: 2010 Run data yields.

	observed	expected	95 % C.L UL $\sigma \times B_R$ (pb)
ee	0 ± 0	$0.00 \pm 0.00 \pm 0.00$	0.38
eμ	0 ± 0	$0.39 \pm 0.11 \pm 0.05$	0.30
eτ	1 ± 1	$0.79 \pm 0.29 \pm 0.04$	0.96
$\mu\mu$	0 ± 0	$0.27 \pm 0.08 \pm 0.08$	0.21
$\mu\tau$	2 ± 1.41	$1.94 \pm 0.45 \pm 0.21$	0.91
$\tau\tau$	0 ± 0	$0.52 \pm 0.20 \pm 0.03$	1.21
Total	3 ± 1.72	$3.91 \pm 0.59 \pm 0.23$	
Total	3 ± 1.72	3.91 ± 0.63	

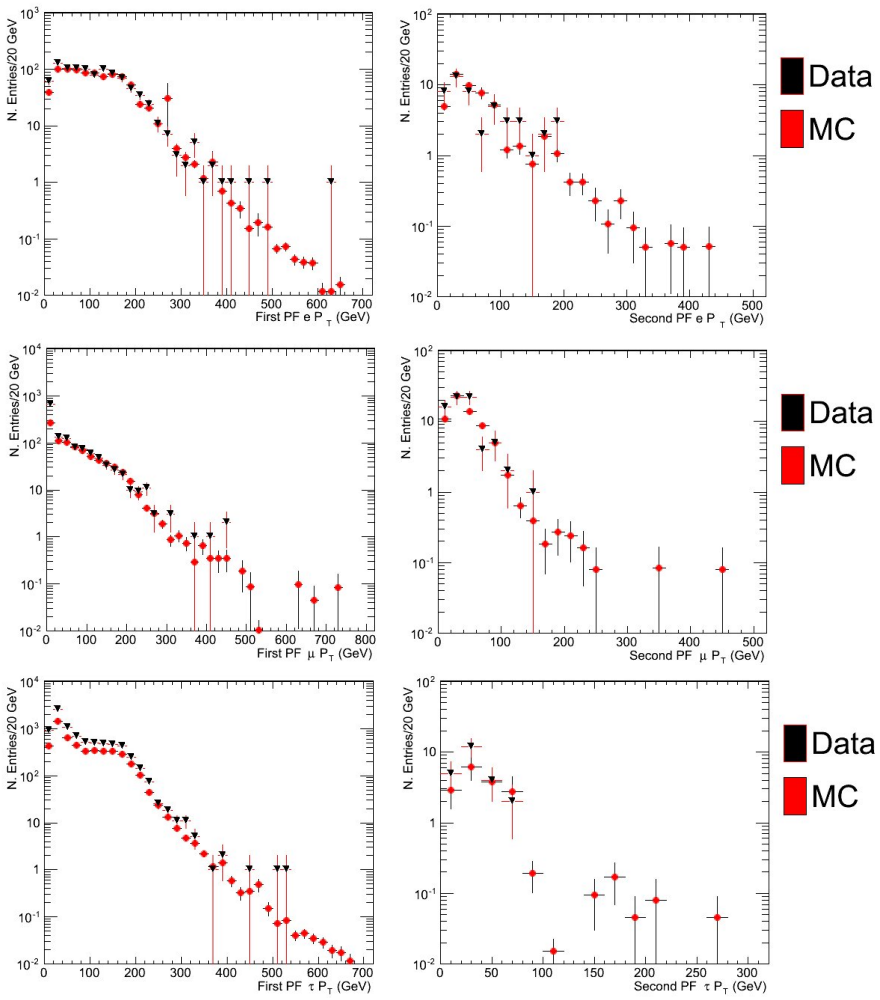

Figure 7.4: Lepton P_T distribution for the electrons (top), muons (middle), and taus (bottom) are shown after the H_T trigger and the H_T and MET cuts have been applied. A good agreement between the collision (black triangles) and the simulated (red points) data can be observed.

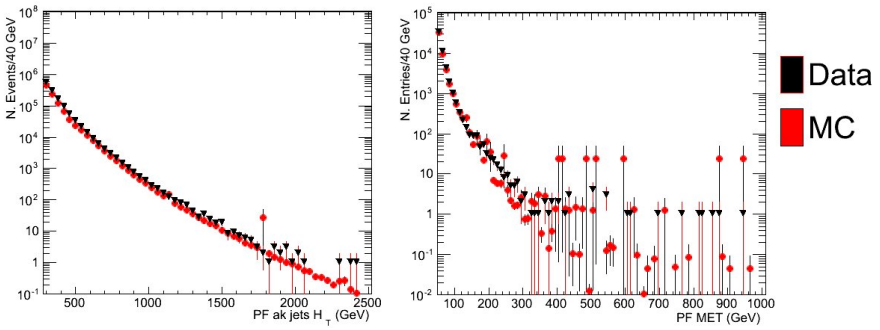

Figure 7.5: H_T (left) and MET (right) distributions for particle flow jets $a\mathbf{K_T}$ with r = 0.5. The agreement between simulated and collisions data is very good.

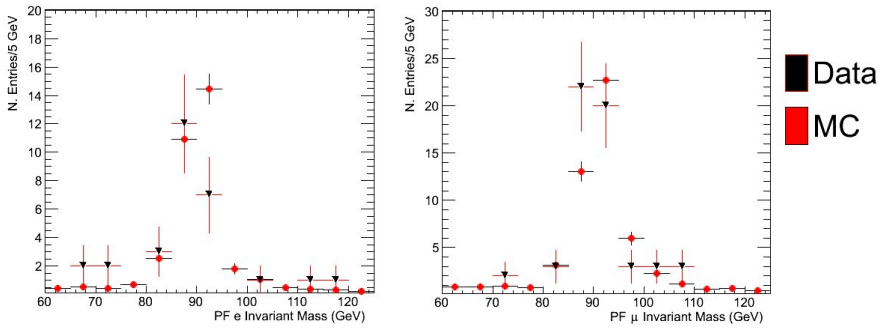

Figure 7.6: Double lepton invariant mass for both the electrons (left) and the muons (right) in the Z mass window. A few remanent events are still present after the H_T cuts.

inefficiency for the event selection related to H_T may be found by considering the jet energy resolution and therefore the H_T resolution.
The acceptance for the H_T and MET was studied with a LM0 sample. This dataset was selected to study the acceptance in a "signal-like" environment. The generated H_T was defined as the sum of the P_T of all the final generated jets with a 30 GeV threshold. The generated MET was defined as the sum of the P_T of all non-interacting particles present in the event, mostly neutrinos and LSPs. The ratio between the number of reconstructed events above the H_T and MET thresholds (350 and 50 GeV) and the number of simulated events over the same thresholds, gives an estimation of the detector acceptance for these two variables. From the LM0 sample this acceptance was estimated to be 0.94 $\pm$ 0.05 for H_T, and 0.95 $\pm$ 0.05 for MET. The errors and the inefficiency of these two numbers are dominated by the jet energy scale uncertainty, this uncertainty has already been estimated in CMS[48].
The electron efficiency was calculated using a Z + jets sample as can be seen in figure 6.2(a). From this calculation the fraction of electrons accepted was estimated to be (53.51 $\pm$ 0.04 (stat))%. The fraction of muons accepted was calculated using the same procedure with a result of (65.53 $\pm$ 0.04 (stat))% (see figure 6.7(a)). In the case of taus the fraction was (29.6 $\pm$ 0.01 (stat))% (see figure 6.8). A 30 % systematic error must be added to these numbers to account for the fact that simulated data were used to estimate them.
The observed number of events after the selection can be written as:

$$N_{events} = L\sigma_p B\epsilon_{tot},$$

where L is the integrated luminosity, σ_p is the production cross section, B is the branching ratio for the specific channel, and ϵ_{tot} is the total efficiency of the analysis, that includes the acceptance due to the applied cuts. This equation is valid for all channels shown in table 7.3, but the efficiency and branching ratios vary for each of them.
The efficiency for every channel was taken as the product of the acceptances in H_T, and MET, the two lepton efficiencies, and the efficiency of the trigger.
To obtain the upper limits of the production cross-sections for each channel, with a 95 % Confidence Level (C.L.), a likelihood function was used[49]. The likelihood method searches for the set of parameters in the distribution that maximises the probability of the observed result. Three different statistical distributions were used to calculate these values: Gaussian, Lognormal, and Gamma distributions. The results obtained with the Lognormal and the

Gamma distributions are in good agreement, on its side the Gaussian distribution gives different results in some cases as expected according to the reference [50].
The complete set of limits can be seen in table 7.4. The numbers listed in table 7.3 correspond to the lognormal distribution. These numbers can be interpreted as the maximum value of the cross section multiplied by branching ratios at which new signal would have leaved the observed yield with 95 % C.L..

Table 7.4: 95 % Confidence Level Upper Limit for the cross-sections (pb) times the branching ratio for two same-sign leptons in the final state, calculated from different probability density functions.

	Gaussian	Lognormal	Gamma
ee	0.58	0.38	0.37
eμ	0.30	0.30	0.30
eτ	0.81	0.96	0.96
$\mu\mu$	0.21	0.21	0.21
$\mu\tau$	0.89	0.91	0.91
$\tau\tau$	1.21	1.21	1.21

The analysis presented in this work, is a little bit less sensitive to a mSUGRA scan than the analysis done with the lepton triggers, this is because there is an improvement in the lepton efficiency due to the higher P_T cuts, therefore the plot presented here (see figure 7.7) corresponds to the official result of the CMS collaboration for the same-sign-double-lepton exclusion limit in the mSUGRA plane, which has been done with the lepton triggers rather than with the hadronic triggers. In this plot, the blue line shows the event yield upper limit obtained with a 95 % C.L., the red region besides it shows the uncertainties in the measurement obtained by considering the theoretical cross section uncertainty. The shape of the blue line is defined by the topological final states present in each of the mSUGRA points analysed, in this case the curve follows a constant value (the observed upper yield) for the final state in which two leptons have the same charge. All points below that curve are now excluded since they have all bigger expected yields than the one observed.
The mSUGRA plane exclusion plot was done by scanning, point by point in the mSUGRA plane, the final number of events resulting after all selection cuts have been applied. To calculate the NLO cross section limit, all LO

cross sections were rescaled to the NLO cross section process by process (squark production, gluino production, etc...). The uncertainties of these production cross sections were calculated using the recommendations listed in reference [51]. Leptonic topologies are less frequent than purely hadronic final states, therefore leptonic channels are less sensitive to some points than purely hadronic anaylises. This implies that better limits have been set by CMS using purely hadronic channels [52].

To summarise, in this chapter a brief description of the hadronic data

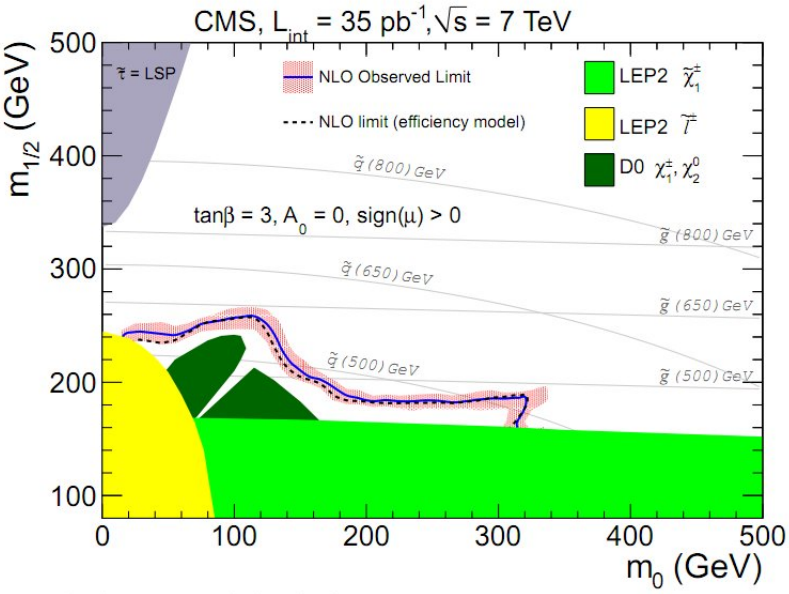

Figure 7.7: Exclusion plot obtained with the leptonic trigger analysis for the mSUGRA plane m_0, $m_{1/2}$, with $\tan\beta = 3$, $A_0 = 0$, and $\text{sign}(\mu) > 0$.

samples used was presented. This description, together with the information given in section 3.1, gives a simple complete picture of the LHC data used for this analysis. Following the description, a summary of the data-driven methods used, and a discussion of their results was presented. Later on, a few plots showing a comparison between interesting quantities using simulated and collision data was shown, these plots were meant to prove a good agreement between simulated and collision data. As a final section, a description of the observed events, the efficiencies of the analysis, the errors involved, and the limits found; was presented. In the following chapter, all these results will be analysed, and a final discussion about it will be

presented.

Chapter 8

Conclusions

The work presented in this thesis was done with the data taken during the first LHC physics run, a period during which the accelerator was performing all kinds of tests and operations to improve its quality and luminosity, and therefore it was not working at its complete capabilities. There were 35 pb^{-1} of data collected and certified by the CMS Experiment as good for physics analysis. This early data was enough to perform physics analyses with results that were already improving the measurements done in previous accelerators. A clear example are the exclusion limits obtained in the mSUGRA parameter space, they were extended beyond what had been achieved by LEP and Tevatron.
In the present work some SUSY benchmark points were excluded (see figure 7.7). In general, any model that predicts a bigger yield than the one observed in the 95 % C.L. upper limit set by this plot, is excluded. However, this is just one of the objectives of this work. The main scientific goal was to perform a scan at the new energies reached by the LHC, using the luminosity taken during the year 2010. As a conclusion it can be said that in this new kinematical region no evidences of new physics consistent with Supersymmetry were found so far. For the 35 pb^{-1} dataset no signal was found that increments the number of events expected from the Standard Model (based on calculations and measurements already performed at these energies), in the channel with at least two same-sign leptons in the final state, were found in the 35 pb^{-1}-integrated-luminosity dataset. It may still happen that at higher luminosities something pops out at the same energies, but this will be part of the continuous search that CMS is, and will be, performing with the data from the current run of the LHC (that is expected to keep on going until the end of 2012).

The results of this thesis do not deny nor confirm the existence of SUSY, they only state that models that predict, for the channel analysed (same-sign double lepton), with an integrated luminosity of 35 pb^{-1}, significantly higher number of events than the ones stablished in the 95 % C.L. upper limit, are ruled out with a 95 % C.L.
By the end of the current run the LHC is expected to collect an integrated luminosity of the order of fb^{-1}. At this luminosity the searches will be sensible to SUSY models with much smaller production cross sections. These data will give a more complete picture of the physics at 7 TeV, giving us a better idea of the kind of phenomena that lies at higher energies. However, this early results, although not conclusive, give us an idea of the impressive potential of the LHC and its experiments to search for new physics, and in particular of the high sensitivity and performance of the CMS Detector.
All scientific goals of the CMS collaboration rely on the performance of the LHC and the detector. The performance of both machines has been remarkable. In the case of the CMS, the collaboration has proven the readiness of all subdetectors involved, and its excellent performance during the data taking periods. This readiness has been reflected in several publications with results obtained during the cosmic-ray-data-taking period, the commissioning period (2008 and 2009), and with the collision data at 7 TeV. In general, the most clear example of the CMS performance can be seen when one considers that in this very short period CMS has remapped the SM at 7 TeV as can be seen in all publications done so far by CMS[53].
The CMS software has shown also a very good behaviour, from the DAQ, through the reconstruction, all the way to the simulation. This can be appreciated specially when one considers the level of agreement between collision and simulated data. Not only the simulation of the data has played an important role, but also all pieces of code that allow the experiment to run smoothly have been proven to work very well.
As it was already mentioned, the SM was remapped by the CMS collaboration at 7 TeV. This is already a very remarkable issue since all results shown were obtained almost "out of the box". Previously this results have been the scientific goal of other experiments, but in CMS they were obtained to confirm that the entire machine and software were ready to be used in the search for new physics. This remapping of the SM is very important when one considers searches for new physics, because a very good knowledge of the SM improves the sensitivity when looking for deviations that point to new phenomena.
Since I joined the CMS Collaboration as a graduate student in 2007, I had the experience of working with the muon detectors, particularly with the

RPCs. My contributions in this regard helped to achieve the level of performance of this subdetector, that has been very good in both, triggering, and reconstruction of muon tracks (see appendices A). My work with the SUSY Analysis Group, and with the SUSY-Leptonic subgroup, studying the same-sign double lepton channel, contributed to the obtention of the early results made public by CMS, and summarised in the exclusion-limit plot discussed previously. Physics-wise this exclusion limit is the result of this work, however, when looking at the goals achieved during these years, from a wider perspective, one must add that the other very important result was to demonstrate the readiness of the LHC and CMS to fulfill the scientific goal of performing the search for new physics in the energy range extending up to 14 TeV. The research presented in this work also contributed in this regard.

Appendix A

Commissioning of the RPC system

As part of the service work that every university involved in the CMS collaboration has to do, the CMS Uniandes group is involved with the RPC detector performance group (RPC-DPG). As a student of the university I was working for this group writing code needed to analyse the RPC data.
The data analysed was collected in the commissioning period of the detector, where mostly cosmic rays were taken. The contributions done were focused in the data analysis of the CRAFT08, and CRAFT09 (Cosmis Rays At Full Tesla) exercises. To analyse these data, tools to monitor the detector performance were created and extensively tested. These tools were written and used by the RPC collaboration in CMS.
The principal contribution I did for the RPC was the detailed study of the noise in the detector. The details of these contributions are presented in the following sections.

A.1 Noise Studies

At the beginning of the CMS commissioning period, cosmic rays were used to calibrate the detector and study its performance. Cosmic rays were collected and stored by using the detector on a special trigger configuration. The data was divided into runs depending on the configuration of the detector and in any issue related with the data acquisition configuration.

A.1.1 Coherent Noise

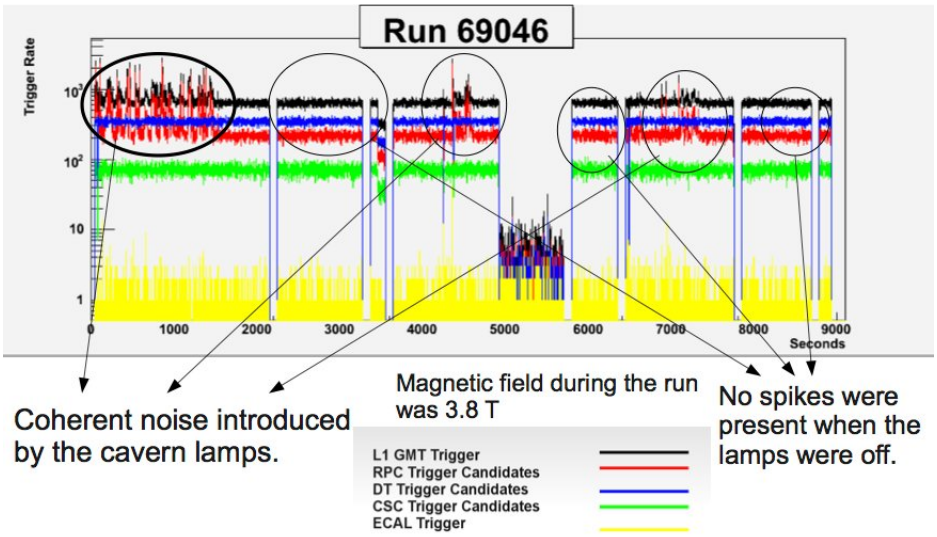

Figure A.1: The plot shows the trigger rate for several sub-detector trigger systems. Some spikes can be seen in the RPC trigger rate, they were affecting the L1 GMT cosmic trigger and therefore creating noise in the data collected by the detector.

During this period some runs presented spikes in the trigger rate profiles that were at the moment not understood (See figure A.1). These spikes were later understood as electronic noise coming from some lamps located inside the cavern.

The off line study done to understand this problem lead to the creation of a tool able to detect the source of any RPC noise. This tool was able to identify a noise peak from the trigger profile, once the peak was located the tool searched for the detector wheel or end-cap that was producing the signal. Located signals could be studied at the level of sectors, chambers, rolls, or even strips depending on the specific case (see figure A.2).
This tool was widely used in the RPC community to spot noisy chambers and noise problems in the detectors. With the use of this tool, noise was classified as coherent noise, like the one produced by lamps and hardware problems; and non-coherent noise produced normally in the detector operation. Besides the lamp problem, there was another case of coherent noise in which a piece of hardware was malfunctioning (see figure A.3); this case was spotted with the tool and its origin was also traced. Further hardware

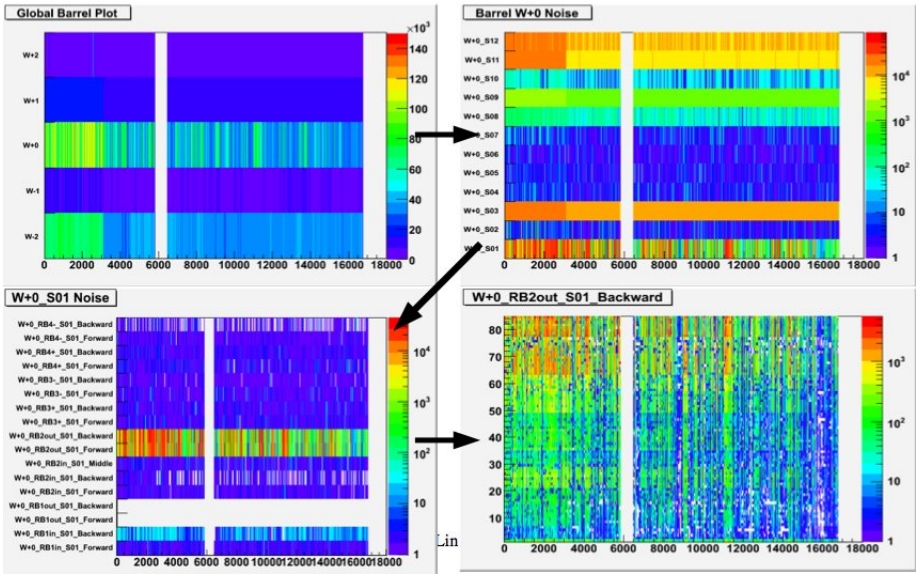

Figure A.2: The pictures show the sequence that was followed to identify the noisy places inside the detector. In this case the upper left plot shows how the barrel occupancy per second was changing in time. On the upper right plot the same time period is shown for one of the wheels that shows high trigger rates. Once the noisy sectors were identified, they pointed easily to the chamber occupancy in which the rates were not normal, identifying therefore the rolls being affected by noise as can be seen in the left lower corner plot. The right lower corner plot shows the same noise at the strip levels which is the lowest level that could be reached.

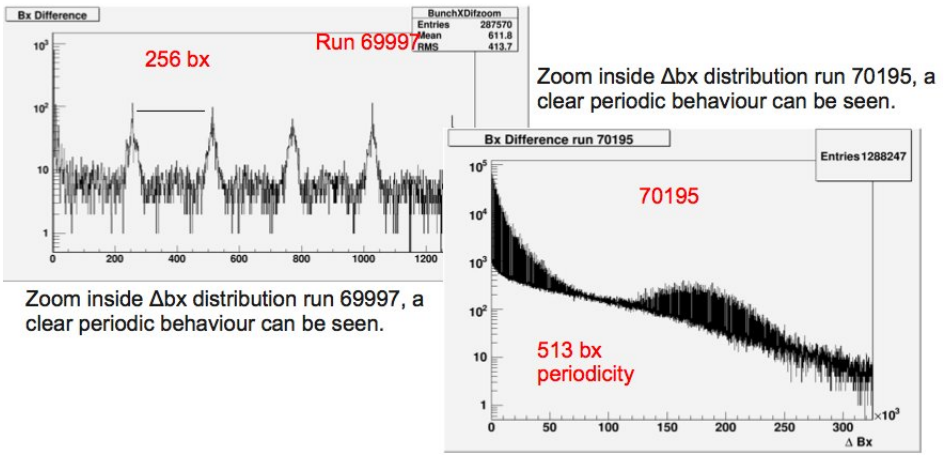

Figure A.3: The plot shows a hardware problem that was spotted with the off-line noise analysis. In the plots the bunch crossing difference between two consecutive events is plotted for both cases. This distribution is expected to have a maximum near to zero and to be spike free, however two cases were observed in which the distributions were not as expected.

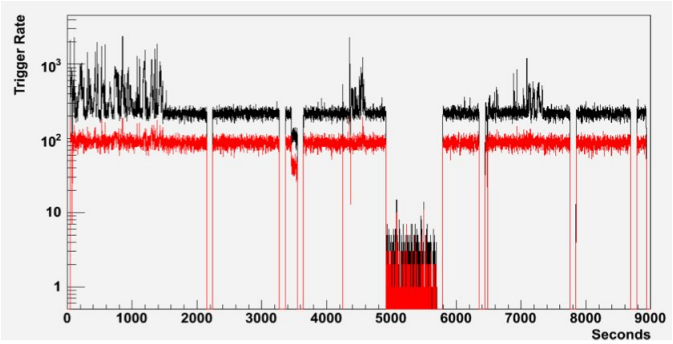

Figure A.4: In this plot, the trigger rate observed for a cosmic ray run in which spikes were present (black line) is shown together with the rate for the same data but this time using the RPC collision trigger emulator (red line). A significant reduction in the spikes can be seen just by the use of the collision patter emulator.

and on-line studies found the reason for these behaviour and solved it.
The general concern in the collaboration at the moment was how much would these noise affect the trigger for physics analysis, therefore a study was done using the L1 RPC trigger emulator with the data affected by the presence of spikes. The results showed that the trigger spikes were highly rejected using a collision trigger instead of a cosmic ray trigger (see figure A.4).

A.1.2 Non-Coherent Noise

The other kind of noise present in the RPC system is due to the normal electronic activity of the detector. This noise does not represent a problem for the physics goals of CMS at all, but is still important to measure it, so that it is permanently controlled. This noise is basically measured by roll as the number of hits that are fired per second without any physical signal as input (no muons in the detector).

The noise distribution done by putting together all the noise rates of every roll into a histogram gives a measurement of the mean noise rate in the detector. These measurements were done for several interesting cases and were compared in different time periods (see figure A.5).
For some non-coherent noise cases several strips can be fired at the same time without a muon passing through them. The number contiguous strips fired in one roll is usually called the cluster size, high cluster size values in different rolls increase the probability of producing a fake trigger. To calculate the probability of this effect a study was done.
Seven different cases were defined: the first one is the case in which all the rolls involved in a muon reconstruction have a small cluster size (less than ten hits); the second case includes a roll with at least ten hits; the third case includes two rolls with three hits; the following cases continue the patter until the sixth case in which the six possible rolls included in a muon reconstruction have cluster sizes bigger than ten. The results show that less than two percent of the signatures could result in a trigger caused by three or more rolls with cluster size bigger than 10 hits (see figure A.6 and table A.1), this implies that more than 98 percent of the triggers are actually good. An internal note to summarise this work was written by the RPC people involved, more complementary information can be found on it [54].

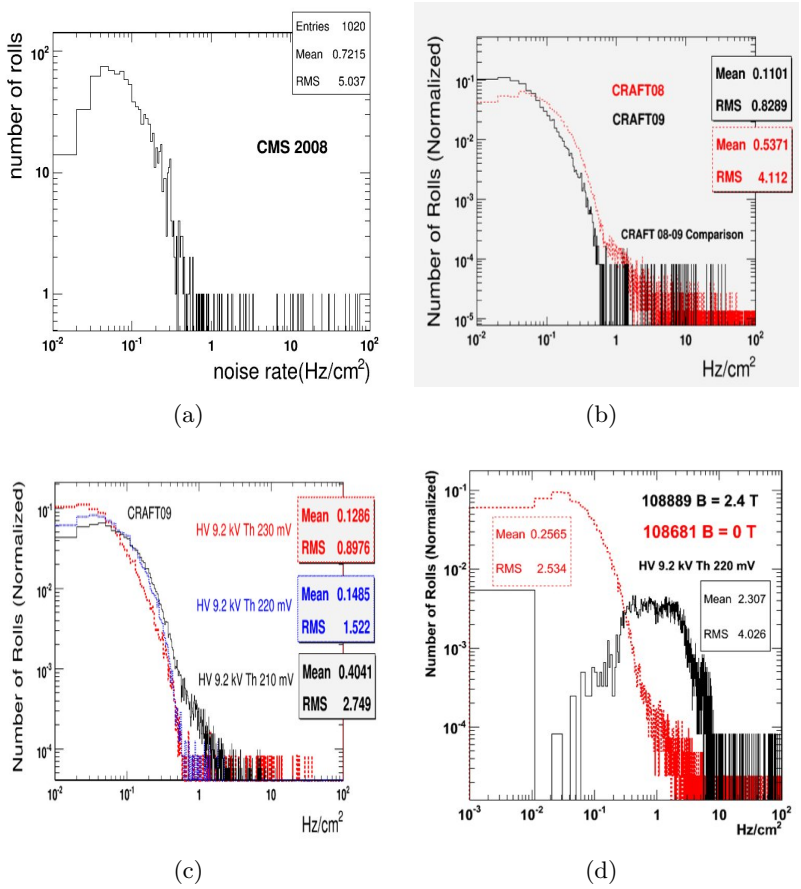

Figure A.5: Plot A.5(a) shows the noise distribution per roll for the barrel for a good run in the cosmic ray exercise CRAFT 08. In Plot A.5(b) the comparison between two runs that have the same conditions is shown, these runs were taken during different CRAFT periods. Plot A.5(c) shows the comparison between different conditions of the threshold for the same high voltage applied. Plot A.5(d) shows how the noise produced in the chambers increases when the magnetic field is ramped in the CMS magnet.

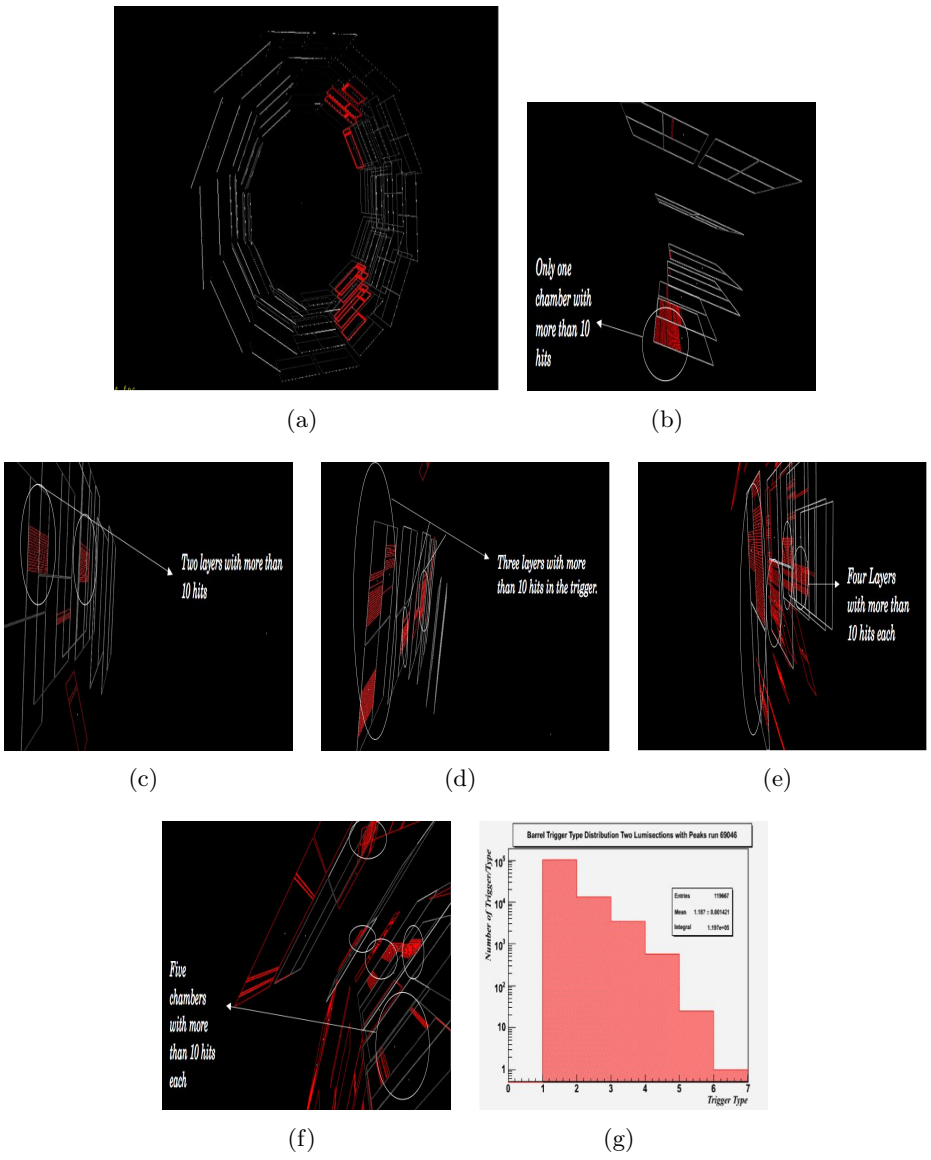

(a) (b) (c) (d) (e) (f) (g)

Figure A.6: Figure A.6(a) shows the type 1 muon signature, figure A.6(b) to A.6(f) show the types 2 to 6. Figure A.6(g) shows the number of times each case was present during a cosmic ray run. From these plot one can conclude that less than 2% of the muons are produced by pure-noise-big-cluster-size cases.

Table A.1: This table shows the percentage of muons of type 1 to 6 present in a cosmic run.

Type of muon	Percentage in the sample
1	80.69 %
2	13.85 %
3	4.6 %
4	0.8 %
5	0.036 %
6	0.0014 %

A.2 RPC prompt analysis tool

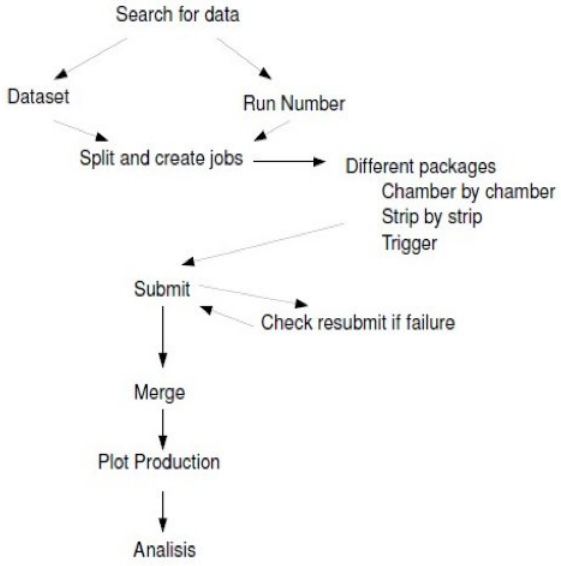

Figure A.7: The sketch shows the workflow for the RPC prompt analysis tool.

To have a complete picture of the performance of the RPC detectors, an analysis tool able to spot any change in the normal operation conditions was designed. This tool was called RPC Prompt Analysis Tool (RPC PAT), it was developed in C++, and python, within the software framework of CMS (CMSSW). It was able to create, submit, merge, and analyse jobs that run over data taken by the RPC system (see figure A.7). The tool was designed to monitor the performance of parameters such as: cluster

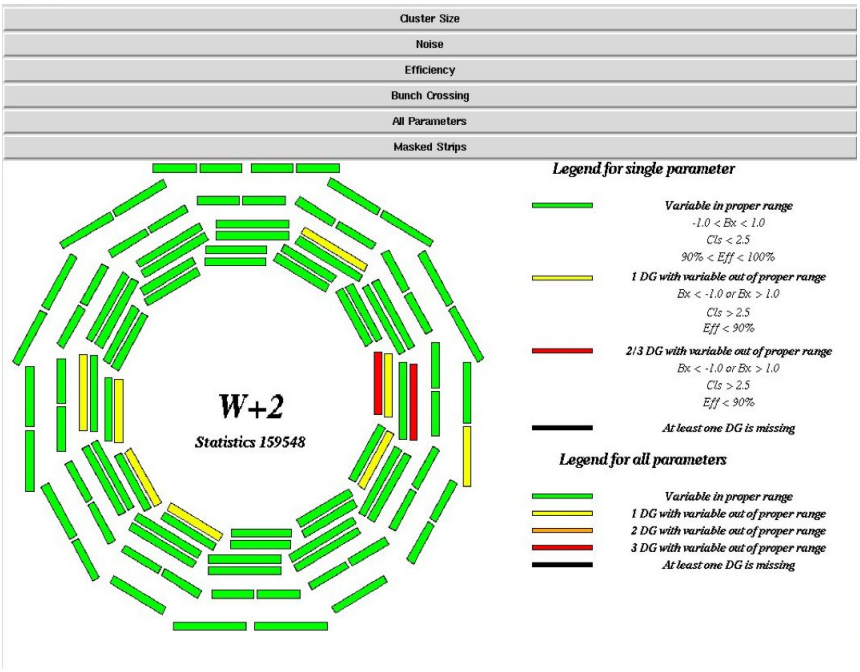

(a)

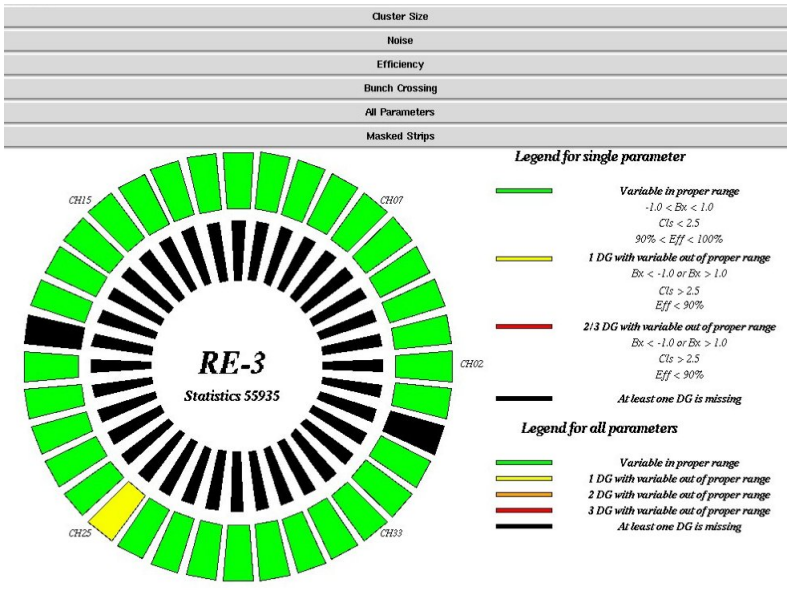

(b)

Figure A.8: Plot A.8(a) and A.8(b) show and example of how the information of the wheels, and disks of the RPC system was displayed in the RPC Prompt Analysis Tool.

size, efficiency, noise rate, bunch crossing, and the occupancy of every roll in the detector (see figure A.8). All these parameters were later combined into more complex analysis such as: high voltage scans for efficiency and noise, and historical plots produced with previous data. An analysis note to describe the functionalities of this tool was written as reference for the RPC collaboration[55]. Examples of the physic analysis that could be done with the RPC PAT can be seen in figure A.9.

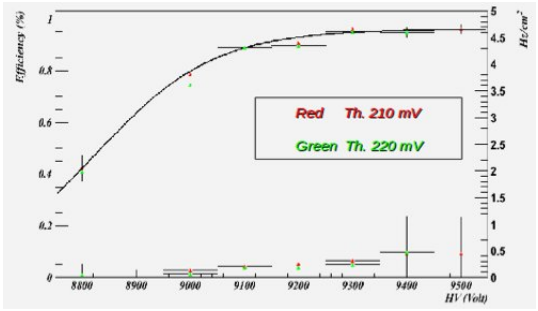

(a)

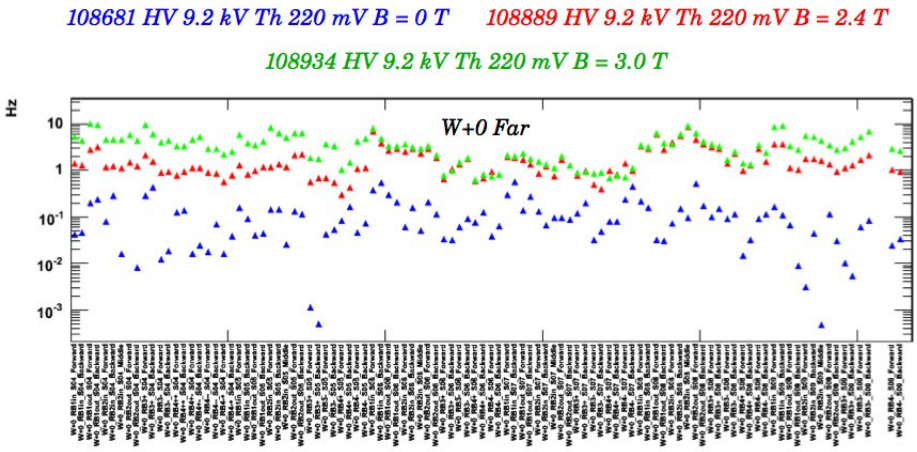

(b)

Figure A.9: Plot A.9(a) shows a high voltage scan example of one roll made on efficiency and noise for different threshold conditions. Plot A.9(b) shows all the rolls for one half of the wheel 0 comparing the noise rate for different magnetic fields when the magnet was "ramping up" (magnetic field being increased).

Appendix B

Publications, Presentations and Software Developed

B.1 Publications

Two internal notes were published in the CMS collaboration. The first note was a description of the on-line and off-line noise tools for the RPC, the second publication described the RPC PAT tool created to monitor the performance of the RPC detector system. Both tools were integrated in a single framework. The internal notes can be found in the references [54, 55].
Based on the results obtained with the analysis coming from some of these tools, and on further studies done by the RPC collaboration three more publications were done, two of them at Nuclear Instrumental Methods journal [56, 57], and one at the AIP conference procedures [58].
On the SUSY group I have been collaborating with the researchers from the Imperial College of London, as part of the CMS SUSY leptonic group, specifically with Dr. Michele Pioppi who is in charge of the same-sign double-lepton inclusive supersymmetric search. Together with Dr. Marcello Maggi, and Dr. Pioppi, I published an internal note based on an Isolation study done as a comparison between the Particle Flow and the Standard Reconstruction inside CMS (see chapter 4)[59]. A second note describing the analysis presented in the same-sign double-lepton search was written and published in collaboration with them [60], this note reported one of the several supporting studies for the official CMS paper on same sign double lepton searches which is in the process of being submitted to a scientific journal[45]. These results together with all the other SUSY searches done at CMS were presented at the Moriond QCD and High Energy interactions

2011 conference[61].
Besides the previous seven publications in which I am one of the main authors, there are about 50 more CMS publications in which I am one of the authors. As member of CMS collaboration performing service work as well as physics research durin during 4 years I am in the author list of the collaboration and my name appears in all the publications.

B.2 Presentations

There are over 30 internal presentations done in the CMS collaboration as part of CMS weeks, RPC DPG meetings, CMS weeks, CMS Jamborees, and SUSY meetings. And three external presentations done on behalf of the CMS collaboration. Two presentations were done in Italy, one in the CMS Cosmic Workshop done at Torino in March 2009 [62], and one done at Ischia for the RPC Italy group on September 2009 [63], both talks were about the RPC performance and the noise present on the RPC chambers. The third talk was done in the *Congreso Nacional de Física de Colombia* in October of 2009[64]. This talk was about the tools designed for the RPCs in the CMS experiment. In this occasion the meeting took place at Santa Marta and the talk was presented by Dr Bernardo Gomez on my behalf. Also a poster was presented in that meeting about the measurement of the L1 trigger efficiency using a tag-and-probe method in which muons identified by the calorimeter were used as tags.
A complete list of the presentations can be found in the twiki page https://twiki.cern.ch/twiki/bin/view/Sandbox/AlbertoOcampoPresentaciones.

B.3 Software Developed

All the code that I have written for CMS is located in either the CVS CMSSW repository in the UserCode/Aocampor area (see figure B.1), or in the SVN CMSuniandes repository located in the Analysis, or in the Users/aocampor Area (see figure B.2). This code have been developed during the entire duration of my PhD research and can be divided into RPC code and SUSY code.
For RPC two big packages were written, one for the RPC Prompt Analysis Tool, and another one for the RPC noise analysis. This code has several packages written for filtering, analysing, or creating data.
For the SUSY analysis a similar amount of code was written, this code is

located mostly in the SVN CMSuniandes repository.

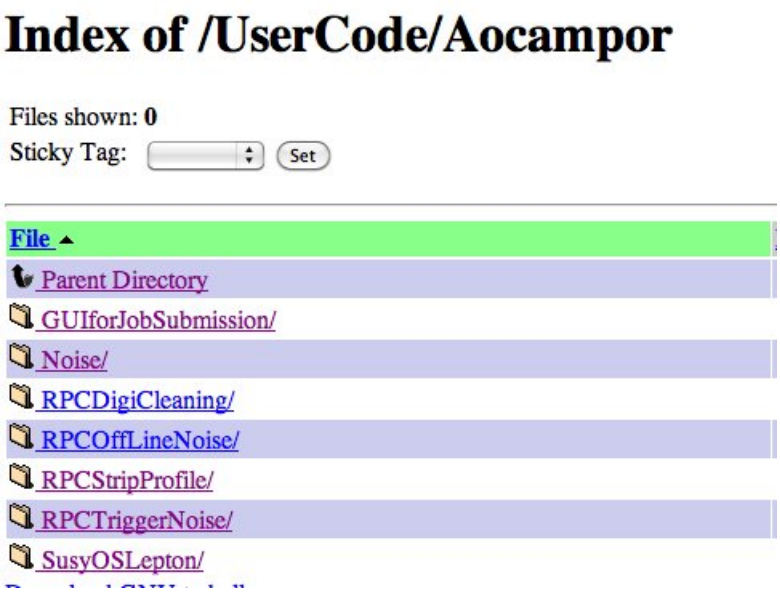

Figure B.1: Snapshot of part of the CVS repository, with a fraction of the code written for the same-sign analysis, and the RPC noise analysis.

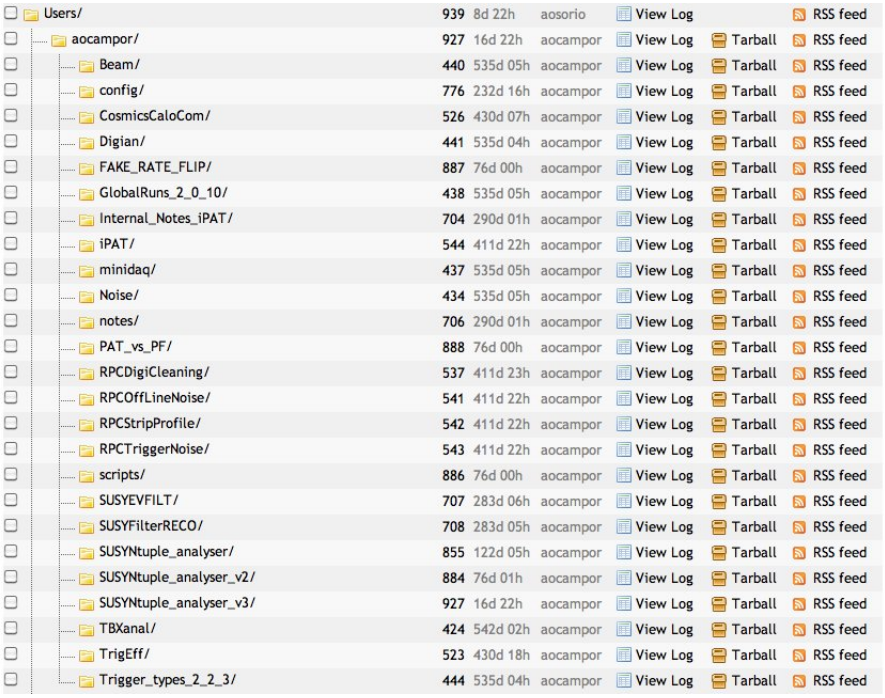

Users/	939	8d 22h	aosorio	View Log			RSS feed
aocampor/	927	16d 22h	aocampor	View Log	Tarball		RSS feed
Beam/	440	535d 05h	aocampor	View Log	Tarball		RSS feed
config/	776	232d 16h	aocampor	View Log	Tarball		RSS feed
CosmicsCaloCom/	526	430d 07h	aocampor	View Log	Tarball		RSS feed
Digian/	441	535d 04h	aocampor	View Log	Tarball		RSS feed
FAKE_RATE_FLIP/	887	76d 00h	aocampor	View Log	Tarball		RSS feed
GlobalRuns_2_0_10/	438	535d 05h	aocampor	View Log	Tarball		RSS feed
Internal_Notes_iPAT/	704	290d 01h	aocampor	View Log	Tarball		RSS feed
iPAT/	544	411d 22h	aocampor	View Log	Tarball		RSS feed
minidaq/	437	535d 05h	aocampor	View Log	Tarball		RSS feed
Noise/	434	535d 05h	aocampor	View Log	Tarball		RSS feed
notes/	706	290d 01h	aocampor	View Log	Tarball		RSS feed
PAT_vs_PF/	888	76d 00h	aocampor	View Log	Tarball		RSS feed
RPCDigiCleaning/	537	411d 23h	aocampor	View Log	Tarball		RSS feed
RPCOffLineNoise/	541	411d 22h	aocampor	View Log	Tarball		RSS feed
RPCStripProfile/	542	411d 22h	aocampor	View Log	Tarball		RSS feed
RPCTriggerNoise/	543	411d 22h	aocampor	View Log	Tarball		RSS feed
scripts/	886	76d 00h	aocampor	View Log	Tarball		RSS feed
SUSYEVFILT/	707	283d 06h	aocampor	View Log	Tarball		RSS feed
SUSYFilterRECO/	708	283d 05h	aocampor	View Log	Tarball		RSS feed
SUSYNtuple_analyser/	855	122d 05h	aocampor	View Log	Tarball		RSS feed
SUSYNtuple_analyser_v2/	884	76d 01h	aocampor	View Log	Tarball		RSS feed
SUSYNtuple_analyser_v3/	927	16d 22h	aocampor	View Log	Tarball		RSS feed
TBXanal/	424	542d 02h	aocampor	View Log	Tarball		RSS feed
TrigEff/	523	430d 18h	aocampor	View Log	Tarball		RSS feed
Trigger_types_2_2_3/	444	535d 04h	aocampor	View Log	Tarball		RSS feed

Figure B.2: Snapshot of part of the SVN repository, with a fraction of the code written for the same-sign analysis, and the RPC noise analysis.

Appendix C

Isolation studies

Events with leptons in the final state will play a significant role in SUSY searches at initial LHC luminosities. It is expected that the leptons produced in SUSY decays have a soft energy spectrum, especially in cases predicted by models where the mass difference between the initial SUSY particle and the lightest SUSY particle is small. An optimisation study of the isolation cuts was done for electrons in the range of $2 < P_T < 30\ GeV$, and for muons in the range of $3 < P_T < 30\ GeV$. The results are presented in terms of SUSY lepton reconstruction efficiency; and rejection of fake and heavy quark leptons.
The primary sources for lepton production in SUSY are the neutralinos, charginos, and sleptons. We expect those particles to decay as:

$$\tilde{\chi}_2^0 \to l^{\pm} + \tilde{l}^{\mp}$$

$$\tilde{\chi}_1^{\pm} \to l^{\pm} + \tilde{\nu}_l$$

$$\tilde{l}^{\pm} \to l^{\pm} + \tilde{\chi}_1^0$$

C.1 Lepton reconstruction and isolation requirements

Leptons were reconstructed as it is described in chapter 4. A comparison between normal Standard Reconstructed (SR) objects and Particle Flow (PF) objects was performed for the isolation study. The following identification cuts were applied.
For SR electrons:

- Loose id was required,

- $p_T > 5\ GeV$,
- $|\ \eta\ | < 2.5$,

for SR Muons:

- Tight id was required,
- $p_T > 3\ GeV$,
- $|\ \eta\ | < 2.4$,

for PF electrons the cuts are:

- MVA id > 0.6,
- Hadronic energy over the Electromagnetic energy was required to be < 0.06,
- $p_T > 2\ GeV$,
- $|\ \eta\ | < 2.5$,

and finally for PF muons:

- $p_T > 3\ GeV$,
- $|\ \eta\ | < 2.4$.

SR particle isolation was studied with the following variables:

$$
\begin{aligned}
iso_{abs}^{track} &= \sum_{\Delta R<0.3} p_T^{track}, \\
iso_{abs}^{ECAL} &= \sum_{\Delta R<x} E_T^{ECAL}, \\
iso_{abs}^{HCAL} &= \sum_{\Delta R<x} E_T^{HCAL}, \\
iso_{abs}^{comb} &= \sum_{\Delta R<0.3} p_T^{track} + \sum_{\Delta R<x} E_T^{ECAL+HCAL}.
\end{aligned}
$$

In the PF case the isolation is slightly different:

$$
\begin{aligned}
iso_{abs}^{gamma} &= \sum_{\Delta R<0.3} p_T^{gamma}, \\
iso_{abs}^{chargedHadrons} &= \sum_{\Delta R<0.3} p_T^{chargedHadrons}, \\
iso_{abs}^{neutralHadrons} &= \sum_{\Delta R<0.3} p_T^{neutralHadrons}, \\
iso_{abs}^{comb} &= \sum_{\Delta R<0.3} p_T^{gamma} + \sum_{\Delta R<0.3} p_T^{chargedHadrons} \\
&\quad + \frac{1}{3} \sum_{\Delta R<0.3} p_T^{neutralHadrons}.
\end{aligned}
$$

Where P_T is the transverse momentum of the particle-tracks inside a cone around the lepton being consider. This cone was taken as $\Delta R < 0.3$ in almost all the cases, with the exceptions of SR electrons. In that case a cone of $\Delta R < 0.4$ was considered to add up the transverse energy (E_T) deposits. Only tracks with P_T grater than 1 GeV were used to compute iso_{abs}^{track} for the electron isolation. In the case of muons, a threshold of $200MeV$ was used. Electrons with a P_T bigger than 2 GeV were accepted in the PF case. In the SR case the threshold was 5 GeV. For muons the PF and SR lower limit was set to 3 GeV.

A comparison between PF and SR relative Isolation was done for prompt,

Table C.1: Simulated data samples used in the optimisation excersice. Two of the important backgrounds for SUSY searches and a mSUGRA LM0 point were considered. The data was produced during the summer of 2009 with the CMS global tag Summer09-MC_31X_V3_7TeV-v1.

Sample	Number of Events	σ (pb)
LM0	208629	38.93
QCD_Pt1000toInf-madgraph	1664384	83
TTbar	632010	94

heavy-flavour, and fake leptons. The datasets used are listed in table C.1. Relative isolation was defined by dividing the SR and PF isolation variables by the P_T of the lepton being considered. Very similar behaviours can be seen for all PF and SR cases (figures C.1, and C.2).

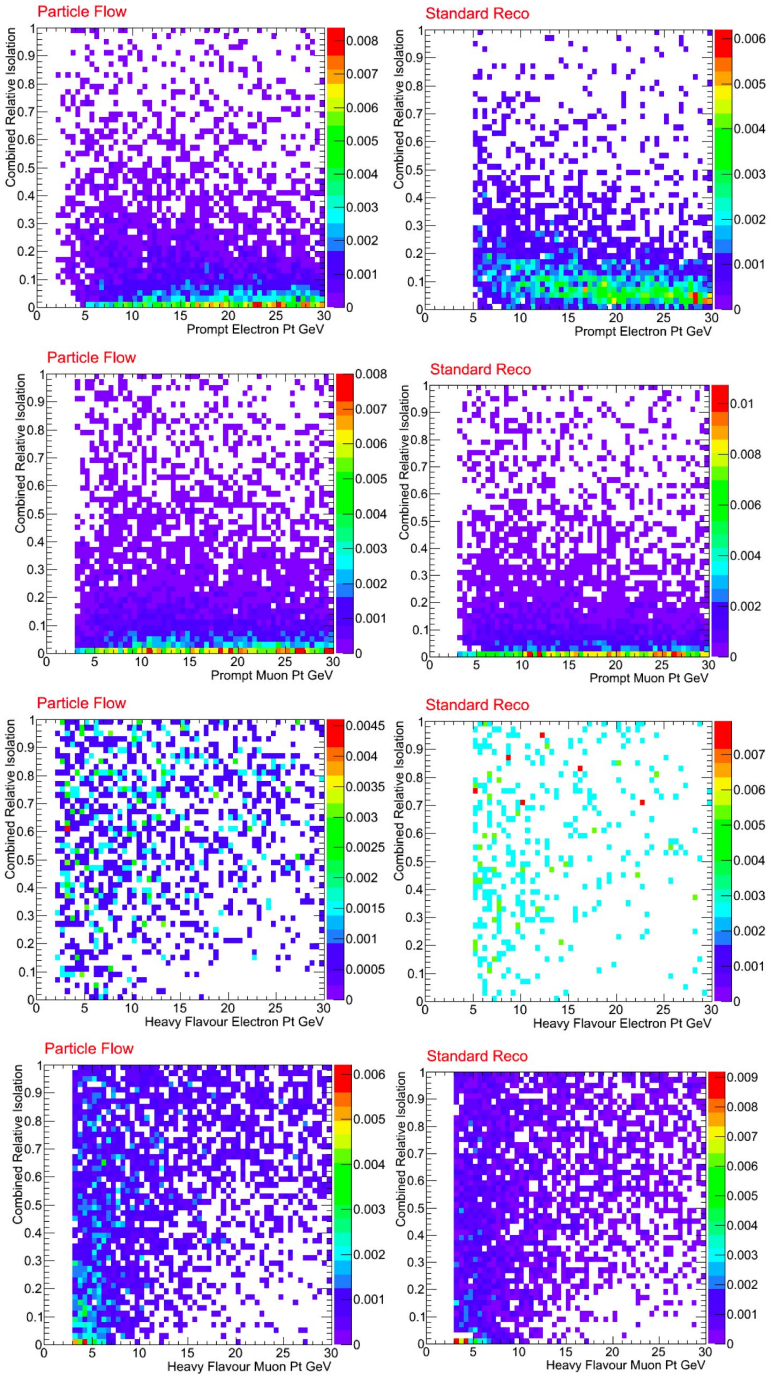

Figure C.1: Combined relative isolation vs. transverse momentum for prompt and heavy-flavour leptons.

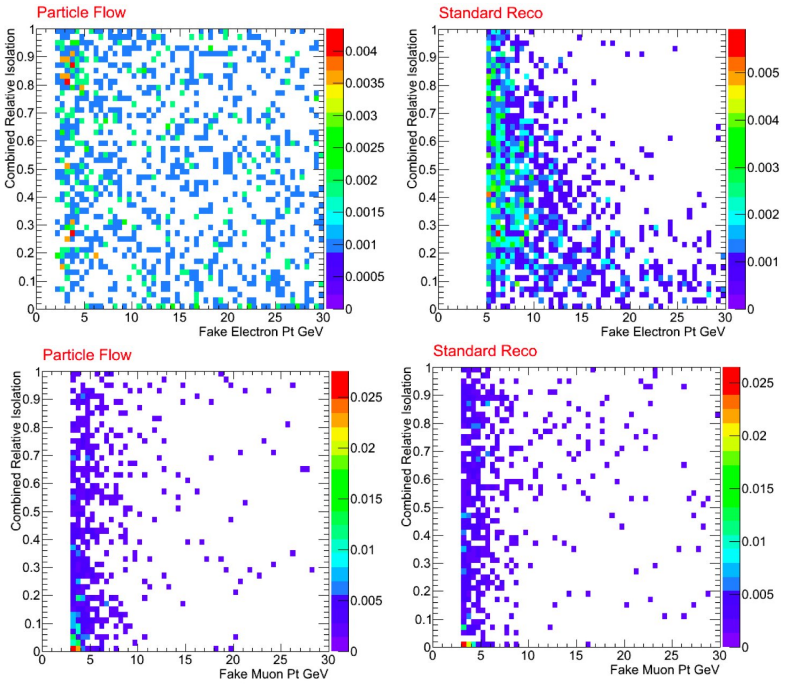

Figure C.2: Combined relative isolation vs. transverse momentum for fake leptons.

C.2 Optimisation of Isolation requirements for low P_T leptons

In order to select prompt leptons, reducing fake and heavy-flavour backgrounds at low P_T, a further optimisation was done.

C.2.1 Optimisation procedure

Ten P_T bins were considered, those bins were equally taken for electrons and muons from 0 - 3 GeV, 3 - 6 GeV, ..., and 27 - 30 GeV. For each of the bins the multiplicity of leptons as a function of isolation was calculated. This procedure was applied to prompt, heavy-flavour, and fake leptons.
The lepton efficiency as a function of isolation was defined as: the ratio between the number of leptons in a certain P_T range before a given isolation cut divided by the total number of leptons being considered in that P_T range. This efficiency was calculated for prompt, heavy-flavour, and fake leptons. The Rejection was defined as the additive inverse of the efficiency. This quantity was relevant when fakes and heavy-flavour leptons were considered as background for prompt leptons.

$$eff(x) = \frac{\text{Number of leptons below a certain x value in isolation}}{\text{total number of leptons}}$$

$$rej(x) = 1 - eff(x)$$

Prompt efficiency for electrons and muons as a function of heavy-flavour and fake rejection was studied (figure C.3).
In order to obtain a SUSY like environment, in which a large multiplicity of high P_T jets is present, a cut in $H_T = (\sum_{jets} P_T + \sum_{lep} P_T) > 300$ GeV was applied. The first sum runs over all reconstructed jets with $P_T > 50$ GeV, and the second sum runs over all the accepted leptons.
Starting from the efficiencies and rejections calculated in the previous section, four different criteria were considered in order to optimise the lepton isolation cuts.
The optimisation criteria are:

- **Pure Heavy Flavour**:
  The heavy flavour rejection is required to be ≥ 0.9. The highest cut on isolation satisfying this condition was taken.

- **Pure Fake**:
  The fake rejection is required to be ≥ 0.9. The highest cut on isolation satisfying this condition was taken.

- **Optimal**:
  The Efficiency of the fake leptons, and the rejection of the prompt leptons were minimised by finding the lowest value for:
  $x = \sqrt{(1-eff)^2 + (1-rej_{fake})^2}$

- **Efficient**:
  Prompt leptons efficiency was required to be ≥ 0.9. The lowest cut on isolation satisfying this condition was taken.

Tables with the complete list of cuts for both PF and SR isolation variables were produced, these tables summarise the cuts for all leptons and they can be found in the reference [59]. Results for the PF combined isolation optimisation procedures can be seen in figure C.4.

C.3 Collision Data Studies

To study the performance from real data, the J/Ψ resonance was to select prompt leptons. Heavy flavour leptons were selected using b-tagged jets, and fake leptons were selected depending on the flavour; for electrons by asking a MVA < -1, and for muons requiring a match with a calorimeter muon. A minimum bias trigger was used for the very early 2010 data using only 7.9 nb^{-1}. The results obtained by removing the H_T threshold are summarised in figure C.5.

An isolation template was calculated for both electrons and muons for the three kind of leptons (see figure C.6)

C.4 Low-P_T Isolation for SUSY analysis

The results of the isolation studies were used in three SUSY simple selections, the cases considered were: the Single Lepton selection or SL, the Same Sign Double Lepton selection or SSDL, and the Opposite Sign Double Lepton selection or OSDL. For all the cases, only electrons and muons were considered.

For all the event selections, a comparison between four isolation scenarios was done. The first case considered was the case in which a combined relative isolation of < 0.1, and a $P_T > 10$ GeV were required. The second case used the **efficient** cut at a P_T bigger than 10 GeV. The other two cases also used the **efficient** cut, but different P_T thresholds were set for them (2 GeV, and 5 GeV). In all cases SR performance and PF performance was compared.

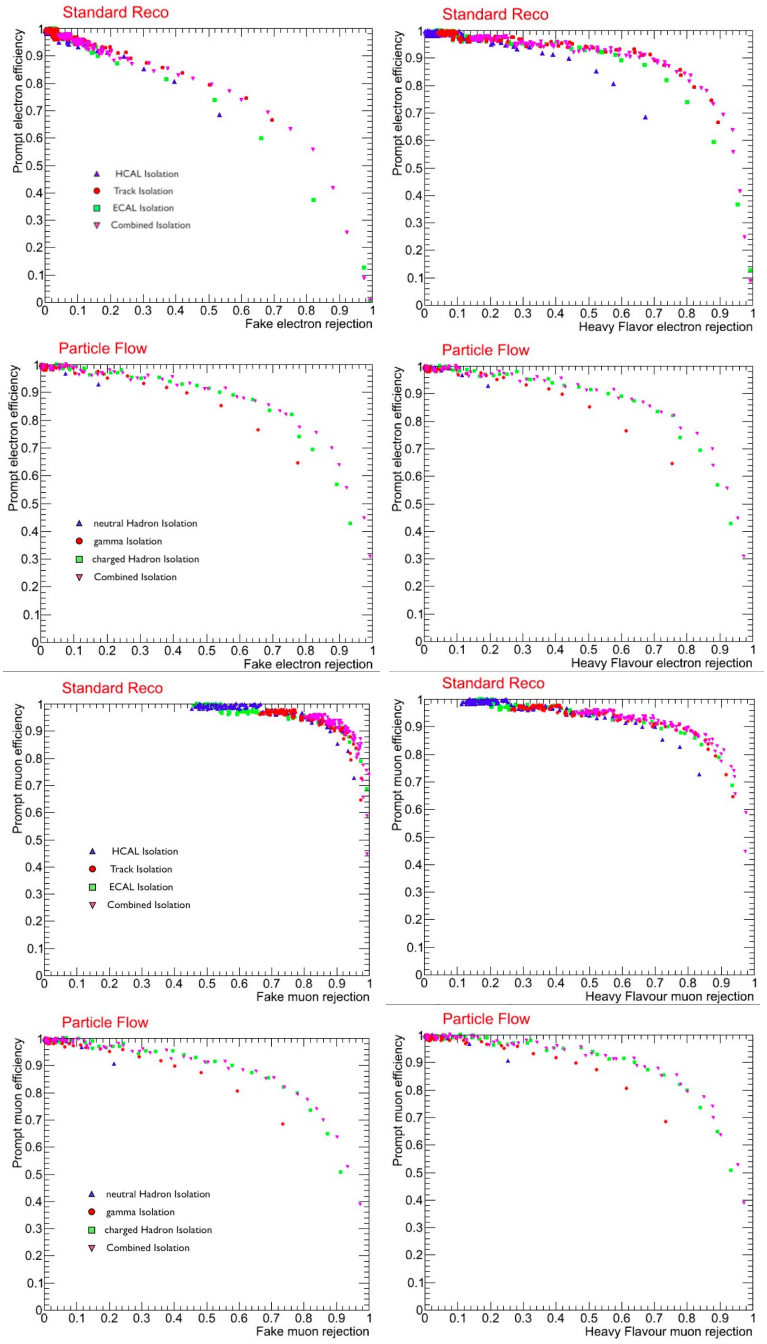

Figure C.3: Efficiency vs. rejection plots for SR and PF leptons. PF electron P_T is in the range $2 - 10\ GeV$, SR electron P_T is in the range $5 - 10\ GeV$, PF and SR muons have P_T in the range $3 - 10\ GeV$.

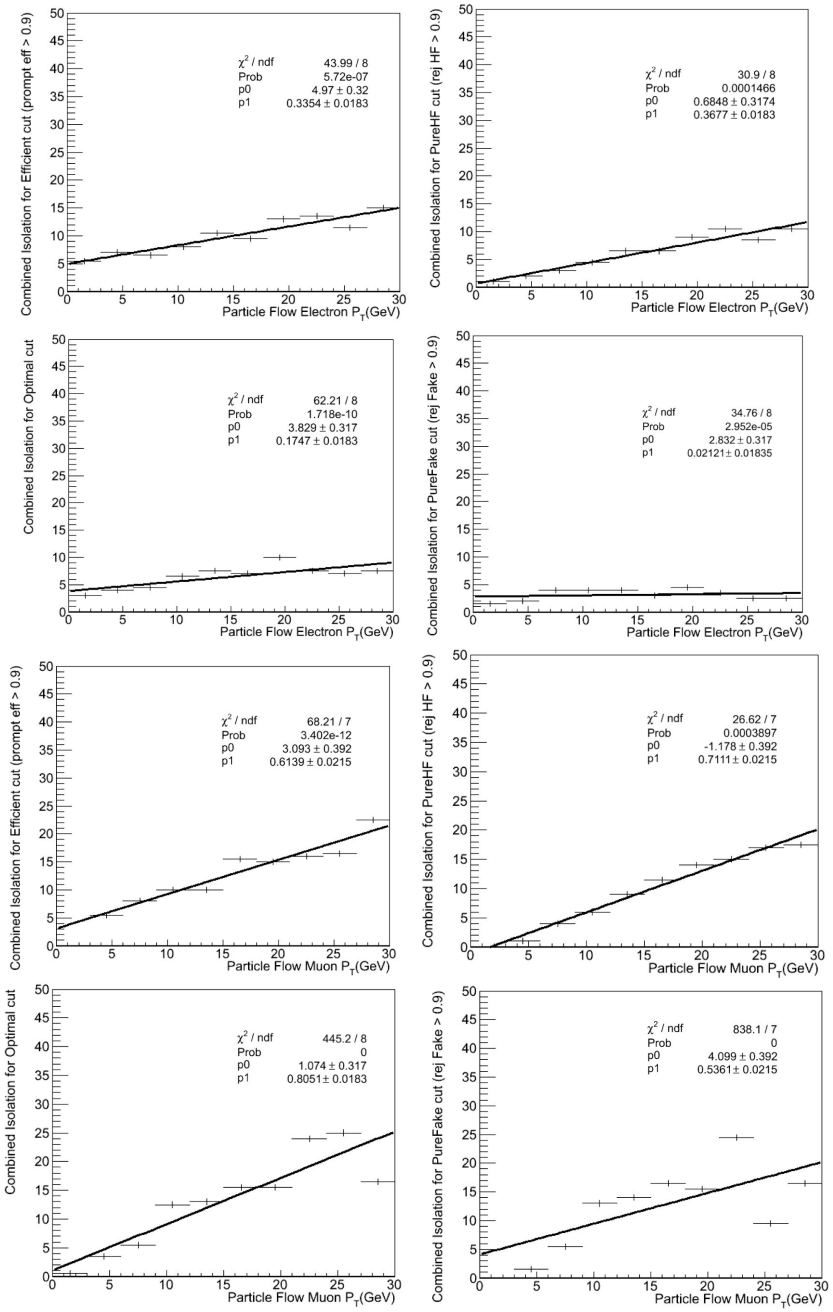

Figure C.4: PF lepton isolation cuts as a function of P_T. The four optimisation scenarios are shown for both, electrons and muons. The line showed in the pictures corresponds to a linear fit to the data.

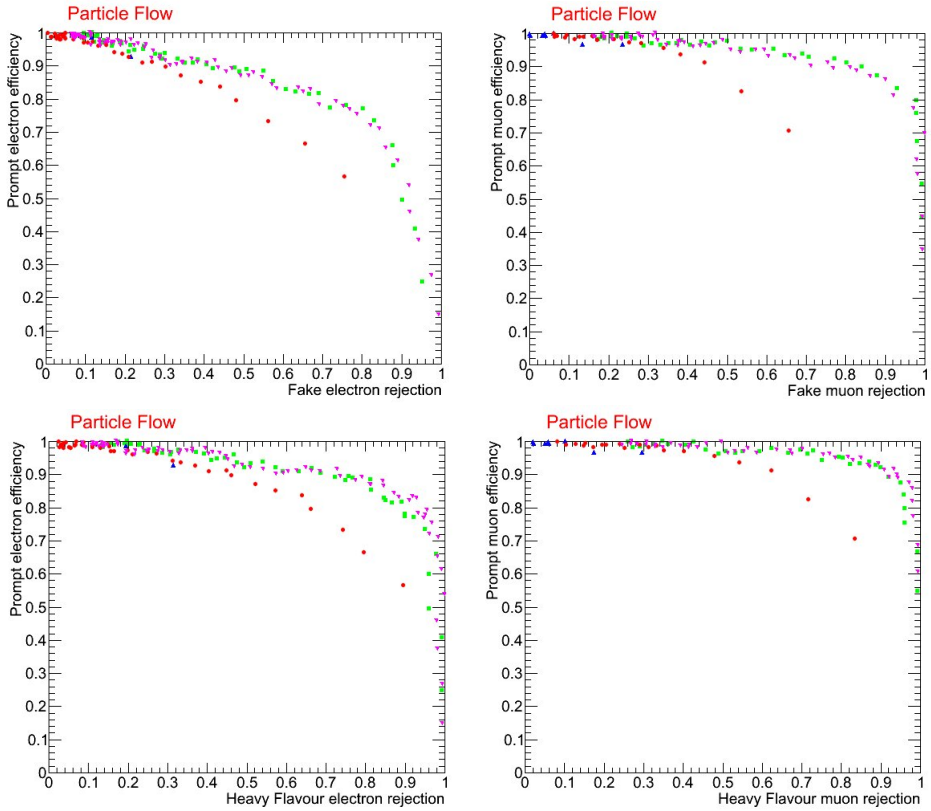

Figure C.5: Efficiency vs. rejection plots for PF leptons. PF electron P_T is in the range $2 - 10\ GeV$, SR electron P_T is in the range $5 - 10\ GeV$, PF and SR muons have P_T in the range $3 - 10\ GeV$.

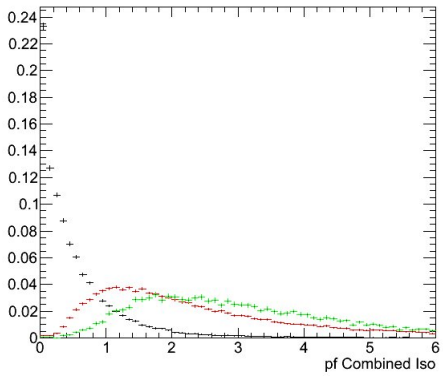

Figure C.6: Combined isolation template calculated for prompt muons (black), heavy flavour muons (red), and fake muons (green) using a J/Ψ trigger. The plot is normalised to the unity to make the distributions comparable, from the firsts bins one can see the reason to cut on a low isolation value to select prompt muons.

In order to isolate the contribution of the cuts over the leptons, also the case in which the standard jets and MET objects were reconstructed without PF but with PF leptons was considered, as well as the opposite case. Standard reconstructed jets were checked to be clean from electrons to avoid double counting or repeated objects.
All the previous consideration were done in order to study the performance of PF leptons vs SR leptons in lower P_T regions. The data used is summarised in table C.2.

C.4.1 Single Lepton Analysis

In the SUSY single-lepton analysis events containing one lepton, multiple jets, and large missing transverse energy are searched for. The CMS SUSY group provides a baseline for the analysis summarised in the Single-Lepton Reference Analysis (RA4) webpage. The trigger requirements of this analysis were deliberately omited in order to study leptons with low P_T.
The following cuts were applied:

- $N_{leptons} = 1$
- $N_{Jets} \geq 3$, with $E_T^{j_3} > 50\ GeV$
- $CaloMET > 100\ GeV$

Table C.2: Data samples used in the SL, SSDL, and OSDL selections. The datasets were of the type GEN-SIM-RECO, produced with the CMS global tag Summer09-MC_31X_V3_7TeV-v1.

Sample	N. Events	σ (pb)
LM0	208629	38.93
LM1	215853	4.88
QCD_Pt250to500-madgraph	4868809	171000
QCD_Pt500to1000-madgraph	4235979	5200
QCD_Pt1000toInf-madgraph	1664384	83
TTbar	632010	94
WJets-sherpa	10980000	30379
InclusiveBB_Pt30	1080358	6.04×10^7

Table C.3 shows the results of applying the four isolation scenarios considered. This table compares PF and SR frameworks. The four columns correspond respectively to the electron cases in which: an isolation ≥ 0.1, together with a $P_T \geq 10$ GeV are required; the **efficient** cut was applied with a P_T cut of 10 GeV; the case where the same scenario was applied with a P_T cut of 5 GeV; and the same scenario but this time with a P_T cut of 2 GeV.
The last two rows report the significance for LM0 and LM1 benchmarks. An improvement in the significance can be seen for the PF framework when jets and missing energy are fixed. A more complete list of the results is summarised in the reference [59].

C.4.2 Same Sign Double Lepton

To select the events the following basic cuts were applied:

- $MET > 50\ GeV$
- $MH_T > 50\ GeV$
- $H_T > 350\ GeV$
- $N_{leptons} = 2$
- Both leptons should have the same charge

The samples used for the single lepton selection where also used for the double lepton selection. In the same-sign double-lepton case, an increase in

Table C.3: Single lepton selection for PF and SR electrons. SR P_T was lowered to 2 GeV just for the sake of comparison.

Samples	Standard Reco			
	$V + j_{pT>10}$	Eff_{pT10}	Eff_{pT5}	Eff_{pT2}
LM0	94.67	156.43	192.58	225.02
LM1	11.77	20.23	27.00	31.68
QCD 250-500	0	0	0	0
QCD 500-1000	1.15	7.36	14.72	27.99
QCD 1000-Inf	2.05	3.25	6.46	12.76
BB	0	0	0	0
WJets	182.45	230.7	265.79	280.7
TT Bar Jets	34.23	46.12	51.64	54.83
Sig LM0	6.38	9.22	10.46	11.6
Sig LM1	0.79	1.19	1.46	1.63
Samples	Particle Flow			
	$V + j_{pT10}$	Eff_{pT10}	Eff_{pT5}	Eff_{pT2}
LM0	126.47	180.09	213.92	239.57
LM1	15.06	20.88	27.17	30.69
QCD 250-500	0	0	0	0
QCD 500-1000	0.14	1.01	2.59	5.77
QCD 1000-Inf	0.14	0.68	1.53	3.72
BB	0	0	0	0
WJets	341.22	391.22	414.91	420.17
TT Bar Jets	34.52	44.96	47.29	49.03
Sig LM0	6.52	8.6	9.9	10.9
Sig LM1	0.77	0.99	1.25	1.4

the PF significance was observed. The results are presented in table C.4.2.

C.4.3 Opposite Sign Double Lepton

To select the events the following basic cuts were applied:

- $MET > 50\ GeV$
- $MH_T > 50\ GeV$
- $H_T > 350\ GeV$
- $N_{leptons} = 2$

Table C.4: Same Sign Double Lepton selection for PF and SR electron-electron, SR P_T was lowered to 2 GeV just for the sake of comparison.

Samples	Standard Reco			
	$V + j_{pT>10}$	Eff_{pT10}	Eff_{pT5}	Eff_{pT2}
LM0	2.88	7.86	13.41	20.35
LM1	0.43	1.21	2.1	3.08
QCD 250-500	0	0	0	0
QCD 500-1000	0	0.86	4.32	13.56
QCD 1000-Inf	0	0.14	0.4	1.32
BB	0	0	0	8000
WJets	12.28	50.0	89.47	134.21
TT Bar Jets	0	2.61	4.06	6.96
Sig LM0	0.82	1.07	1.35	0.21
Sig LM1	0.12	0.16	0.21	0.03
Samples	Particle Flow			
	$V + j_{pT10}$	Eff_{pT10}	Eff_{pT5}	Eff_{pT2}
LM0	2.49	6.68	10.24	13.16
LM1	0.38	0.81	1.43	1.97
QCD 250-500	0	0	0	0
QCD 500-1000	0	0.14	0.57	1.15
QCD 1000-Inf	0	0.02	0.07	0.25
BB	0	0	0	0
WJets	1.75	8.77	10.52	18.42
TT Bar Jets	0	1.16	1.45	1.74
Sig LM0	1.88	2.10	2.88	2.83
Sig LM1	0.29	0.25	0.4	0.42

- Leptons should have opposite charge

In the opposite-sign double-lepton case, an increase in the PF significance was observed, the results can be seen in table C.4.3.
The results for PF and SR lepton isolation comparison show the impact that they both have in a SUSY analysis and are presented in figure C.7.

C.5 Summary

A comparison between particle-flow and standard-reco low P_T lepton isolation was done. Both isolations were optimised to obtain cuts that improve

Table C.5: Opposite Sign Double Lepton selection for PF and SR electron-electron. SR P_T was lowered to 2 GeV just for the sake of comparison.

Samples	Standard Reco			
	$V + j_{pT>10}$	Eff_{pT10}	Eff_{pT5}	Eff_{pT2}
LM0	14.94	29.67	39.56	48.24
LM1	3.42	6.14	8.16	9.56
QCD 250-500	0	0	0	0
QCD 500-1000	0	1.01	4.9	15.87
QCD 1000-Inf	0.04	0.11	0.37	1.48
BB	0	0	8989	8989
WJets	6.14	45.61	85.08	137.72
TT Bar Jets	8.41	17.4	21.75	25.24
Sig LM0	3.91	3.7	0.41	0.5
Sig LM1	0.89	0.76	0.08	0.09
Samples	Particle Flow			
	$V + j_{pT10}$	Eff_{pT10}	Eff_{pT5}	Eff_{pT2}
LM0	15.15	25.68	32.37	37.78
LM1	3.89	5.47	6.9	7.74
QCD 250-500	0	0	0	0
QCD 500-1000	0	0.14	1.01	3.03
QCD 1000-Inf	0	0	0.14	0.35
BB	0	0	0	0
WJets	1.75	7.01	10.52	16.6
TT Bar Jets	3.48	6.38	7.54	9.86
Sig LM0	6.62	6.97	7.38	6.9
Sig LM1	1.7	1.48	1.57	1.41

lepton selections. The cuts were chosen to increase the heavy-flavour and fake lepton rejections, and increase the prompt lepton efficiency acceptance. Four isolation cut-cases were proposed, the isolation cuts were optimised for each of these cases.
The optimisation was checked in the **efficient** scenario in which the prompt-lepton efficiency is required to be more than 90%. For this case a simple selection was done for each of the considered SUSY analyses (SL, OSDL, and SSDL). An increase in the particle-flow significance compared with the standard-reco significance for the same samples was observed, specially in the low P_T region where particle-flow performance was optimal.

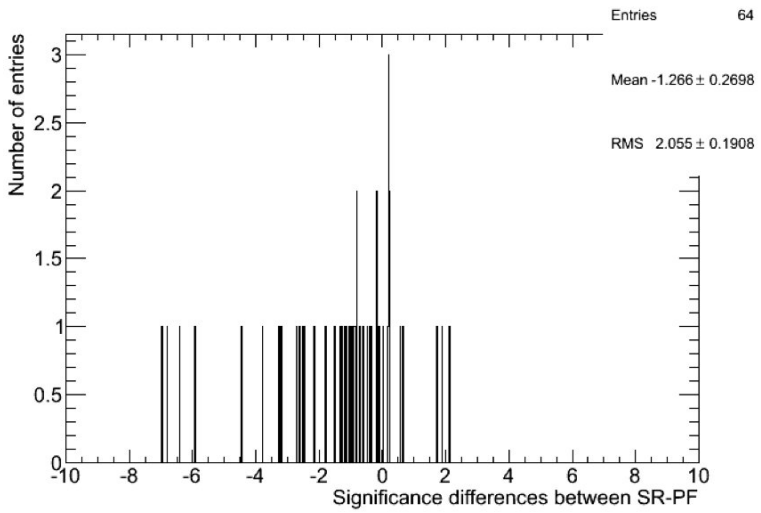

Figure C.7: Significance difference between SR and PF for SL, SSDL, and OSDL for all the comparables significances.

Appendix D

Tag and Probe Method

A data driven method widely used to study electron and muon properties is called Tag and Probe. This method profits the fact that in some cases such as the decay of a Z boson, or the decay of prompt J/Ψs, there are two opposite sign leptons produced. During my PhD work I used this method to study the L1 μ trigger efficiency. This method was also used in the thesis to measure the probability of an electron to have a charge miss-reconstructed (Flip Charge).
The method consist in identifying a good lepton candidate that will be called "Tag". The tag definition changes depending on the lepton being used, however it is common to require that it matches with a triggered candidate.

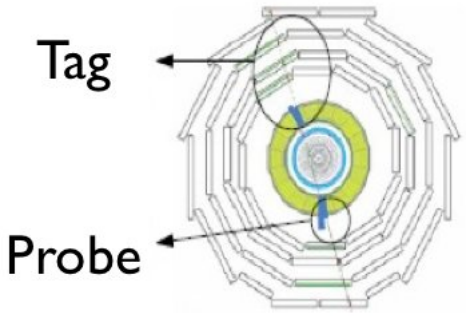

Figure D.1: Tag and probe schematic.

Once the tag has been selected, one has to find a "Probe". The probe is defined as the same kind of lepton candidate, but it is usually required to

have a very loose identification. If several probe candidates are present in an event, this event is not considered (see figure D.1)
To identify the probe one tries to reconstruct a resonance (commonly the Z peak), usually one requires the tag and the probe candidate to have an invariant mass inside a window from 80 to 110 GeV approximately. Besides the invariant mass, another requirements are done to help identify the probe, this selection usually depend on the type of lepton being studied.
The identified probe is then interpreted as a good lepton and is used to estimate the lepton efficiency for some process.
All the selected events reconstruct a peak over an irreducible background pool made out by more opposite-sign leptons not related to the resonance, therefor a background must be subtracted to obtain pure probes. This background is usually estimated by a method called side-band subtraction.
The method consist on counting the number of events that are in a window before and after the resonance peak. With this number, it is possible to estimate the number of background events under the signal peak.
For example, in the case in which one wants to know the P_T distribution of the leptons coming from the Z, one can plot the P_T of the leptons in the sidebands. This distribution will be $\frac{dN}{dP_T}(B)$ for the background in the sidebands. The same plot for the signal region will give a mixture of signal plus background as $\frac{dN}{dP_T}(S)+(1-f)\frac{dN}{dP_T}(B)$, where f is the ratio $f = S/(S+B)$. If one integrates the sidebands in the signal region, and then divide the signal yield by the background yield, one has a multiplicative factor called signal-to-sideband ratio. This factor multiplied by $\frac{dN}{dP_T}(B)$ gives an estimation of the amount of background under the peak. This estimation is subtracted to the signal region to estimate the number of pure signal events[65].
This method was used in the early stage of my PhD to study the L1 RPC

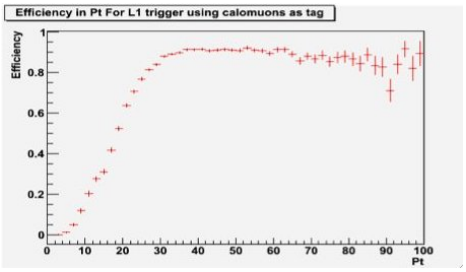

Figure D.2: Tag-and-Probe L1 RPC μ trigger using calorimeter muons as probes.

trigger muon efficiency as can be seen in figure D.2, and the probability for

an electron to flip its charge as can be seen in section 6.4.4.
For the case of the L1 RPC μ trigger efficiency, the tag was selected as a muon that matches a trigger. The probe was selected as a a calorimeter muon reconstructed from the tracks, this muon was reconstructed by selecting those tracks that were at a $\Delta\phi > 2.5$ to ensure that the probe was back to back to the tag.
In the case of the charge flip study, the tag was a triggered electron with a tight selection. The probe was defined as a super cluster, this super cluster was checked to have a charge assignment in agreement with the Kalman filter track, and the Gaussian Sum Filter track.

Bibliography

[1] Stephen P. Martin. A supersymmetry primer. *Advanced Series on Directions in High Energy Physics. PERSPECTIVES ON SUPERSYMMETRY*, 18:1–98, 1997.

[2] Manuel Drees. An introduction to supersymmetry. In *APCTP-96-05, KEK-TH-501*, 1996. arXiv:hep-ph/9611409v1.

[3] Wim de Boer. University personal web page. http://www-ekp.physik.uni-karlsruhe.de/∼deboer/html/Forschung/unification_eng.eps.

[4] Emilian Dudas. Supersymmetry breaking. *Pramana journal of physics.*, 72(1):131–141, Jan 2009.

[5] G. F. Giudice and R. Rattazzi. Theories with gauge-mediated supersymmetry breaking. *Physics Reports*, 322(6):419 – 499, 1999. ISSN 0370-1573.

[6] LEP SUSY Collaboration. Lep 2 joint susy working group web page. http://lepsusy.web.cern.ch/lepsusy/.

[7] T. Adams on behalf of CDF and D0 collaborations. Susy searches at tevatron. In *Hadron Collider Physics symposium, HCP 2008*, 2008. arxiv:hep-ex/0808.0728v1.

[8] CDF collaboration. Search for scalar top decaying into charm and neutralino in the met + jets samples. CDF Note 9834, http://www-cdf.fnal.gov/physics/exotic/exotics_published.html.

[9] CDF collaboration. Search for the production of scalar bottom quarks in $p\bar{p}$ collisions at $\sqrt{s} = 1.96$ tev. *Phys. Rev. Lett.*, 105(8):081802, Aug 2010.

[10] T. Aaltonen et al. Inclusive Search for Squark and Gluino Production in $p\bar{p}$ Collisions at $\sqrt{s} = 1.96$ TeV. *Phys. Rev. Lett.*, 102:121801, 2009.

[11] Aafke Christine Kraan. SUSY searches at LEP. arxiv:hep-ex/0505002, 2005.

[12] D0 Collaboration. Search for associated production of charginos and neutralinos in the trilepton final state using 2.3 fb-1 of data. *Physics Letters B*, 680(1):34 – 43, 2009. ISSN 0370-2693.

[13] A. Heister et al. Search for stable hadronizing squarks and gluinos in e+ e- collisions up to $\sqrt{s} = 209$ GeV. *Eur. Phys. J.*, C31:327–342, 2003.

[14] CDF collaboration. Search for supersymmetry with gauge-mediated breaking in diphoton events with missing transverse energy at cdf ii. *Phys. Rev. Lett.*, 104(1):011801, Jan 2010.

[15] CDF Collaboration. Search for r-parity violating decays of sneutrinos to $e\mu$, $\mu\tau$, and $e\tau$ pairs in $p\bar{p}$ collisions at $\sqrt{s} = 1.96$ tev. *Phys. Rev. Lett.*, 105(19):191801, Nov 2010.

[16] Oliver Sim Bruening, Paul Collier, P Lebrun, Stephen Myers, Ranko Ostojic, John Poole, and Paul Proudlock. *LHC Design Report*. CERN, CERN Geneva, 2004.

[17] CMS Collaboration. Operation, calibration and performance of the cms silicon tracker. In *35th International Conference of High Energy Physics - ICHEP2010*, 2010. CMS CR-2010/258.

[18] CMS Collaboration. The cms collaboration web page. http://cms.web.cern.ch/cms/Detector/.

[19] CMS collaboration. *The Tracker System Project Technical Design Report*. CERN/LHCC 98-6, CERN Geneva, 1998.

[20] CMS Collaboration. Cms silicon strip tracker operation. In *Symposium on Radiation Measurement and Applications, SORMA XII*, 2010. CMS CR-2010/081.

[21] CMS collaboration. *The HCAL Technical Design Report*. CERN/LHCC 97-31, CERN Geneva, 1997.

[22] CMS Collaboration. Performance of the cms drift tube chambers with cosmic rays. *Journal of Instrumentation*, 5(T03015), March 2010.

[23] CMS Collaboration. Performance of the cms cathode strip chambers chambers with cosmic rays. *Journal of Instrumentation*, 5(T03018), March 2010.

[24] CMS collaboration. *Technical Design Report Volume 1: The Trigger System*. CERN/LHC 2000-38, CERN Geneva, 2000.

[25] CMS Collaboration. The gmt web page. http://cms-global-muon-trigger.web.cern.ch/cms-global-muon-trigger/.

[26] CMS Collaboration. Performance of the cms global calorimeter trigger. In *Technology and Instrumentation in particle physics, Tsukuba Japan*, 2009. CMS CR-2009/125.

[27] CMS Collaboration. The austrian global trigger web page. http://wwwhephy.oeaw.ac.at/p3w/electronic1/GlobalTrigger/Global Trigger.htm.

[28] W. Adam et al. The CMS high level trigger. *Eur. Phys. J.*, C46: 605–667, 2006.

[29] Floarian Beaudette. Performance of the particle flow algorithm in CMS. *35th. ICHEP 2010 Proc.*, 2010.

[30] CMS collaboration. Photon reconstruction and identification at $\sqrt{s} = 7$ tev. CMS PAS EGM-10-005.

[31] CMS collaboration. Electron reconstruction within the particle flow algorithm. CMS AN 2010/034.

[32] CMS collaboration. Track and vertex reconstruction with the cms detector at lhc. CMS CR-2005-021.

[33] CMS collaboration. Electron reconstruction in cms. CMS AN 2009/164.

[34] Andreas Hoecker, Peter Speckmayer, Joerg Stelzer, Jan Therhaag, Eckhard von Toerne, and Helge Voss. TMVA: Toolkit for Multivariate Data Analysis. *PoS*, ACAT:040, 2007.

[35] CMS collaboration. Muon reconstruction in the cms detector. CMS AN 2008/097.

[36] CMS Collaboration. Underlying event and jet reconstruction in cms. In *International workshop on interplay between soft and hard interactions*

in particle production at ultra-relativistic energies, WISH 2010, 2010. CMS CR-2011/012.

[37] Grégory Soyez Gavin P. Salam. A practical seedless infrared-safe cone jet algorithm. *Journal of High Energy Physics*, 2007(05), May 2007.

[38] Davison E. Soper Stephen D. Ellis. Succesive combination jet algorithm for hadron collisions. *Phys.Rev.D*, 48(7), October 1993.

[39] CMS collaboration. Performance of jet algorithms in cms. CMS PAS JME-07-003, 2009.

[40] CMS collaboration. Study of tau reconstruction algorithms using pp collisions data collected at $\sqrt{s} = 7$ tev. CMS AN 2010-207, 2010.

[41] CMS Collaboration. Performance of tau reconstruction algorithms in 2010 data collected with cms. CMS PAS TAU 11/001.

[42] CMS Collaboration. Leptons, b-tagging and met reconstruction at cms after the first data. In *3rd International workshop on Top Quark Physics, TOP2010*, 2010. CMS CR-2011/105.

[43] CMS collaboration. Performance of methods for data-driven background estimation in susy searches. CADI:SUS-10-001.

[44] CMS collaboration. Electron identification in cms. CMS AN 2009/187.

[45] CMS collaboration. Search for new physics with same-sign isolated dilepton events with jets and missing transverse energy at the lhc. CMS PAPER SUS-10-004.

[46] Jonathan Gaunt, Chun-Hay Kom, Anna Kulesza, and W. Stirling. Same-sign w pair production as a probe of double-parton scattering at the lhc. *The European Physical Journal C - Particles and Fields*, 69:53–65, 2010. ISSN 1434-6044. URL `http://dx.doi.org/10.1140/epjc/s10052-010-1362-y`. 10.1140/epjc/s10052-010-1362-y.

[47] CMS collaboration. Met performance in pp collisions at $\sqrt{s} = 7$ tev. CMS PAPER JME-10-009.

[48] CMS collaboration. Jet energy calibration and transverse momentum resolution in cms. CMS PAPER JME-10-011.

[49] K. Nakamura et al. Statistics and Probability. *J. Phys. G.*, 37, 2010.

[50] CMS Statistics Committe. Probability density functions for positive nuisance parameters. http://www.physics.ucla.edu/∼cousins/stats/cousins_lognormal_prior.pdf.

[51] PDF4LHC group. Pdf recomendations. http://www.hep.ucl.ac.uk/pdf4lhc/PDF4LHCrecom.pdf.

[52] CMS collaboration. Search for supersymmetry in pp collisions at 7 tev in events with jets and missing transverse energy. *Physics Letters B*, 698:196–218, 2011.

[53] CMS collaboration. Cern document server cms papers. http://cdsweb.cern.ch/collection/CMS%20Papers?ln=en.

[54] S. Constantini A. Ocampo D. Piccolo and R. Trentadue. Noise monitoring tools with rpc online and offline data. CMS IN-2010/002.

[55] R. Trentadue S. Lee, A. Ocampo. Rpc prompt analysis tool description. CMS IN-2010/009.

[56] D. Piccolo et al. Resistive plate chambers performance with cosmic rays in the CMS experiment. *Nucl. Instrum. Meth.*, A617:180–182, 2010.

[57] G. Roselli et al. Resistive plate chamber commissioning and performance in CMS. *Nucl. Instrum. Meth.*, A602:696–699, 2009.

[58] N. Darmenov et al. The CMS RPC system overview. *AIP Conf. Proc.*, 1203:43–48, 2010.

[59] M. Maggi A. Ocampo M. Pioppi. Study of isolation properties of susy low-pt leptons using particle flow. CMS IN-2010/224.

[60] A. Guneratne A. Ocampo M. Pioppi A. Savin R. Volpe and M. Weinberg. Inclusive search for supersymmetry in same-sign dilepton final state at $\sqrt{s} = 7$ tev with full 2010 dataset. CMS AN-2010/300.

[61] CMS Collaboration. Susy searches in cms. In *Recontres de Moriond*, 2011. http://moriond.in2p3.fr/.

[62] CMS Collaboration. Rpc noise studies. In *International CMS Workshop on cosmic ray data analysis, 11-13 March, Turin*, 2009. http://cms-torino-2009.to.infn.it/index.html.

[63] CMS Collaboration. Rpc noise studies update. In *RPC Italy workshop, 20-22 September, Ischia*, 2009.

[64] CMS Collaboration. Tool for monitoring the rpc sub-detector in the cms collaboration. In *XXIII Congreso Nacional de Fsica de Colombia, 5-9 octubre*, 2009. http://www.sociedadcolombianadefisica.org.co/pag/eventos2009.php.

[65] CMS Collaboration. Physics tool, side-band subtraction. https://twiki.cern.ch/twiki/bin/view/CMSPublic/SWGuidePhysicsToolsSideBandSubtraction.